Analysis of effect of using estimated shear wave data as compared to measured compressional and shear wave sonic log

Felix Onovughe Oghenekohwo

A thesis submitted in fulfilment of the requirements

for the degree of Master of Science

in the Department of Geological Sciences

University of CapeTown

May, 2010

Abstract

This study is aimed at developing a workflow, and ultimately a model, for quantitative interpretation of sonic and seismic data. Measured data collected at the point of logging can be fraught with errors that can lead to wrong interpretation. One of such data is the shear wave velocity which in most cases is collected with the compressional wave velocity.

The measured shear wave velocity log may contain errors that are due to drilling conditions, mud invasion etc. It may also contain cycle skips and might contain a lot of missing data and information. It is because of the poor quality of this type of log that has often made well log analysis companies and log interpreters neglect the measured shear wave log and subsequently generate or create an estimated shear wave log which they use for interpretation and modeling to check how the amplitudes vary with increasing offsets, among other uses.

The workflow presented in this study considers the effect of working with the measured data, a reprocessed shear wave log and a locally estimated shear wave log. Specific correction procedures for invasion of the logs was done and synthetic seismograms were created for each type after correction for comparison to a 3D seismic data.

The results of this study suggest that oil based mud invasion can cause significant problems to sonic logs especially the shear wave log. It also suggests that, if a shear wave log is of low or bad quality, a reprocessed shear wave log would be better for interpretation and modeling rather than a locally calibrated shear wave log or an estimated shear wave log using global predictions. The conclusion is evident from the synthetics generated using the measured shear wave data and the estimated shear wave data.

Acknowledgements

I wish to thank and extend my sincere appreciations to the following people and institutions:

- Tullow South Africa (Pty) Limited for providing the funding for this research and also for providing the data used for the research
- African Institute for Mathematical Sciences in Cape Town for providing partial funding for this project
- George Smith, who as my supervisor, was always available for guidance, discussion and all forms of assistance and support
- Robin Sutherland, Keith Barton and Tobias Tönsing of Tullow Oil for their useful suggestions in the course of the study
- My parents and family for their moral and unending support from a distance
- Friends and well wishers for prayers, advice and general support

and finally, to the ancient of days, who has kept and preserved me all through my study at the University of Cape Town and in South Africa.

List of Figures

Contents

1. Borehole Geophysics and Well Logging

1.1 Borehole Geophysics

Borehole geophysics is basically the application of geophysical exploration techniques in a borehole. Some of these exploration methods, such as resistivity or self potential, can be applied deep in a borehole to obtain very useful information about the nature of the subsurface.

Borehole geophysics has been defined as "the science of recording and analyzing measurements of physical properties made in wells or test holes"(From Wikipedia, the free encyclopaedia). Borehole geophysics is used for example in ground-water and environmental investigations to obtain information on well construction, rock lithology and fractures, permeability and porosity, and water quality.

It is very important that maximum advantage be taken of geophysical methods to evaluate apparently non-productive ground (i.e. a "dry hole") in order to increase the probability of success during subsequent drilling of boreholes.

When a hole is drilled, it is hoped that the hole will intersect some amount of the commodity being sought, and that the quantity of that commodity can be measured. Other information about the geological environment is also expected to be obtained. The process of obtaining the geological information, which is by measurement of certain parameters along the borehole, is what is referred to as borehole geophysical logging or well logging. These measurements are often a valuable component of subsurface characterization, providing in situ property measurements.

More details on what borehole geophysical logging entails is discussed in the next section.

1.2 Well Logging

Geophysical borehole logging or well logging involves measuring geophysical properties of rocks and soils surrounding boreholes. The continuous recording of these properties along the boreholes produces what is known as "borehole logs" or "well logs". A well log is a continuous plot of the variation of a physical property e.g. resistivity, against depth in the well (see Figure 1.1 for an example of a resistivity log). The curve shows varying resistivity of a formation across the entire depth of the borehole; notice that the resistivity is maximum (greater than 15ohm m) around a depth of 175m, and this might be a feature sought for by well log interpreters.

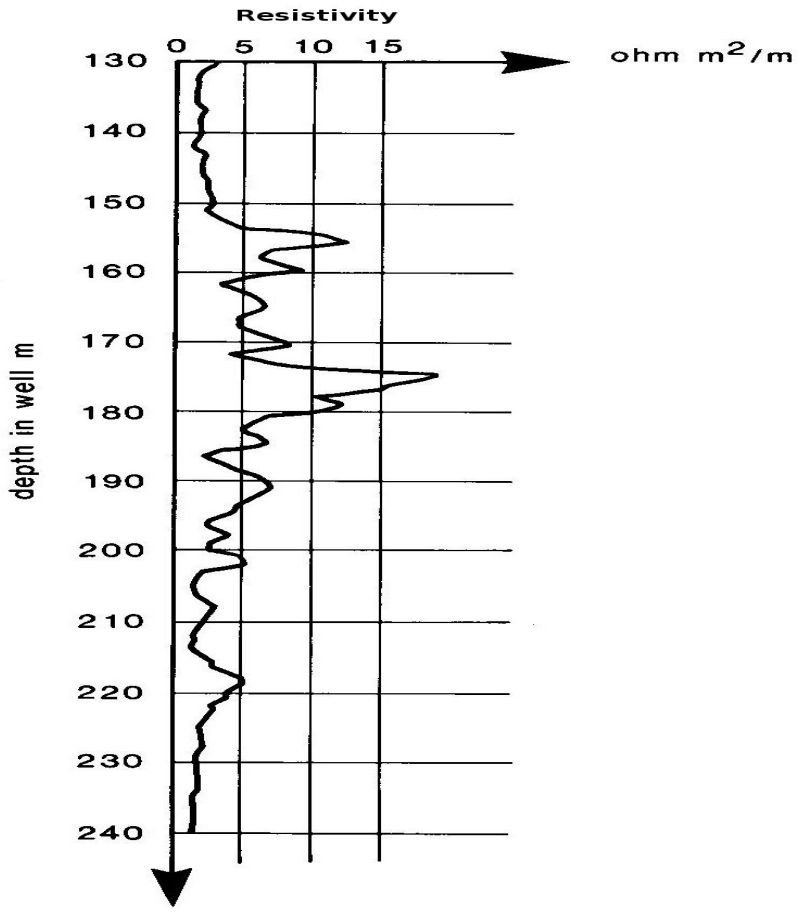

Figure 1.1: An example of a resistivity log. Representation of the first "log" made at Pechelbronn, Alsace, France, in 1927 by H. Doll. (From Allaud and Martin, 1976)[picture copied from Rider (2000)]

It is important to distinguish between two types of logs, namely, geological logs and geophysical

logs. A geological log is one which is based on visual inspection or analysis of samples brought to the surface, while a geophysical log is based on physical measurements made by instruments lowered into the hole. A geophysical log is sometimes referred to as a wireline geophysical log (Wikipedia-well logging).

The history of well logging dates back to 1912 when Conrad Schlumberger thought of the idea of making electrical measurements down a hole in order to map subsurface bodies. He worked with his brother Marcel and in 1927, the first electrical resistivity well log was taken using an instrument known as the sonde. Resistivity logging paved the way for other types of logs.

In geophysical well logging, many different physical properties can be used to characterize the geology surrounding a borehole. Properties such as formation thickness, lithology, porosity, formation fluid content, permeability, temperature, are obtained by one or several complementary geophysical methods.

Borehole geophysical logging involves recording of quantitative measurements which provide a reliable means to correlate and compare borehole conditions and to monitor changes within the borehole over time.

An example of complementary data which may be obtained during logging of a well could be, for instance, when a porous gravel bed containing some magnetic minerals exhibits low density, low sonic velocity and low natural gamma signal, but high magnetic susceptibility and neutron porosity.

1.2.1 Advantage of logs

In order to have better knowledge of subsurface conditions, for example in ground-water and environmental studies, borehole geophysical logging may be an essential requirement. It affords one the opportunity of determining the constituents, variability and physical properties of the rocks around the borehole. The advantages of logging are summarized in the points below:

- It is an inexpensive method of collecting subsurface data that may be unknown. e.g. water-producing and receiving zones, information which is usually sparse.

- Well logging is necessary because geological samples obtained during drilling leaves a very imprecise record of the formations encountered.
- Geophysical logs provide unbiased continuous and in-situ data and generally sample a larger volume than drilling samples.
- The determination of well construction and conditions, such as the location and condition of casing, can be easily done with geophysical logging.
- Also for ground-water studies, a combination of borehole geophysical logging and water-quality sampling provides a clear picture of what may be responsible for the contamination of ground water.
- Logs help match and calibrate certain surface geophysical exploration techniques. e.g. a sonic log could be used to calibrate seismic data.
- Geophysical logging enhances depth control.

1.2.2 Making of logs

Logs could either be taken onshore or offshore. In the latter, the logging system is mounted on the rig. Any simple borehole logging system consists of:

- Set of downhole tools (sondes and cartridges)
- A multicore cable
- A winch system to raise and lower the cable in the well
- A probe-control module
- A set of surface control panels
- A source of power supply
- A digital recording unit

The most common way of recording wireline geophysical well logs is when the drilling tools are no longer in the hole. A hole could either be "open" when the formation forms the wall of the well, or "cased" when there is a tube of metal casing lining the well. The cased holes are used to prevent cave-ins and contamination of the formation fluids. A major difference between both systems is that while most borehole methods can be used in open holes, only radiometric logs (gamma, density, and neutron) can be used in cased holes.

In order to run a wireline log, the downhole tools are lowered into the hole by means of the logging cable which is also the channel for transmission of data from the hole to the surface. The sondes contain sensors used in making the measurement, while the cartridges contain the electronic equipment which powers the sensors, processes the resulting measurement signals, and transmits the signals via the cable, up to the surface. Most logs are recorded during the ascent of the tool up the well to assure a taut cable and better depth control. The cable is also used to transmit electrical power from the surface to the downhole tools.

Most modern logging tools are readily combinable, where the sensors of several tools are combined in a single sonde. Thus many measurements are made at once while pulling the sonde out of the hole, which is less expensive and faster.

Finally, the signals which are received from the downhole tools, at the surface are processed and analyzed as necessary. The needed signals are sent to a magnetic tape in digital format (for future purpose) and to a paper display.

1.2.3 Log presentation and Log runs

A "log run" is the term used to describe the process of collecting a suite of logs at one time. It is generally made just before the hole is cased. The choice of logs depends on what it is hoped to find. Also, it makes sense to run many logs over intervals containing reservoirs or zones showing interesting features.

In some cases, a well may be logged while drilling is in progress. The type of log produced in this process is called a LWD log where LWD means logging while drilling. In this case, instead of

sensors being lowered into the well at the end of a logging cable, the sensors are integrated into the drill string and are active in the hole during drilling. Since there are no wires to the surface, the sensor signals are transmitted to the surface, generally in digital format, by pulse telemetry through the drilling mud and collected by surface receivers. The signals are then processed and a continuous log is formed as drilling progresses.

Whether a well is logged while drilling or after drilling, the end product is a log. There is a standard format for presenting a log which is given by the API (American Petroleum Institute). The format is such that, there are three tracks of 6.4cm width; tracks 1 and 2 being separated by a column of 1.9cm in which the depths are printed in metres or feet.

1.2.4 Log interpretation and uses

The interpretation of logs depends solely on the types of log collected and what information it is desired to extract from the logs. A typical well log is of more use to the petrophysicist whose interest is quantitative. The main objective of quantitative electric log interpretation is for instance to determine the nature and amounts of the fluids which fill the pore spaces of a rock. Another objective may be to determine which beds are permeable and thus possibly productive. Logs are also used to correlate geologic formations.

In the interpretation of logs, some features which may be sought for are the effects of salinity and temperature on rock resistivity, the effect of rock texture on resistivity, the effect of oil and gas on rock resistivity, and the effect of clay on rock resistivity.

In summary, the main parameters, which are calculated from a log, needed to evaluate a reservoir, are porosity, hydrocarbon saturation, and permeability. Knowledge of the thickness and area of the reservoir is also needed for calculation of the volume of the reservoir in order to estimate the total reserves.

Quantitative log interpretation provides the equations and techniques with which petrophysical parameters can be derived from the log. For instance, water and hydrocarbon saturation can be calculated from the resistivity log, while porosity can be deduced from the density log, and in

some cases, from the acoustic or sonic log.

Other log interpretation objectives include lithology determination, mapping of reservoir parameters, well to well correlation, stratigraphic correlation and fracture delineation.

1.2.5 Logging Environment

The act of drilling a borehole can alter the physical properties of the rocks that have been drilled. This implies that a logging tool may not be giving the true reading of the subsurface formation, since by drilling a well, the formation environment has been disturbed. Apart from the disturbances, the logging method itself may be responsible for a logging tool not being able to make a true, repeatable geophysical measurement of a formation.

In order to keep a state of equilibrium during drilling, it is important to maintain a balance between the formation pressure, which is the pressure under which the subsurface formation fluids are confined, and the drilling-mud column pressure, which is the pressure the mud exerts. The pressure of the mud column depends on the height of the mud column and its density. During drilling, it is necessary to maintain the drilling-mud column pressure at just a little above the formation pressure.

One source of disturbance is the fluids and drilling additives. These can invade the surrounding formations changing resistivities, densities, and electric potentials. This often occurs in a porous and permeable formation where the drilling mud pressure is higher than that of the formation encountered (Figure 1.2). This process causes a replacement of formation fluids by the drilling mud filtrate, leaving a deposit (mud cake) around the borehole wall once the drilling bit has passed.

The temperature of the subsurface is another factor which is disturbed during drilling, when cold mud is introduced into a hot formation. However, while drilling is in progress, the circulating cold mud is cooled slightly and gets heated up to a point where it approaches the temperature of the surrounding formation.

As mentioned above, the logging method employed affects the quality of measurement recorded

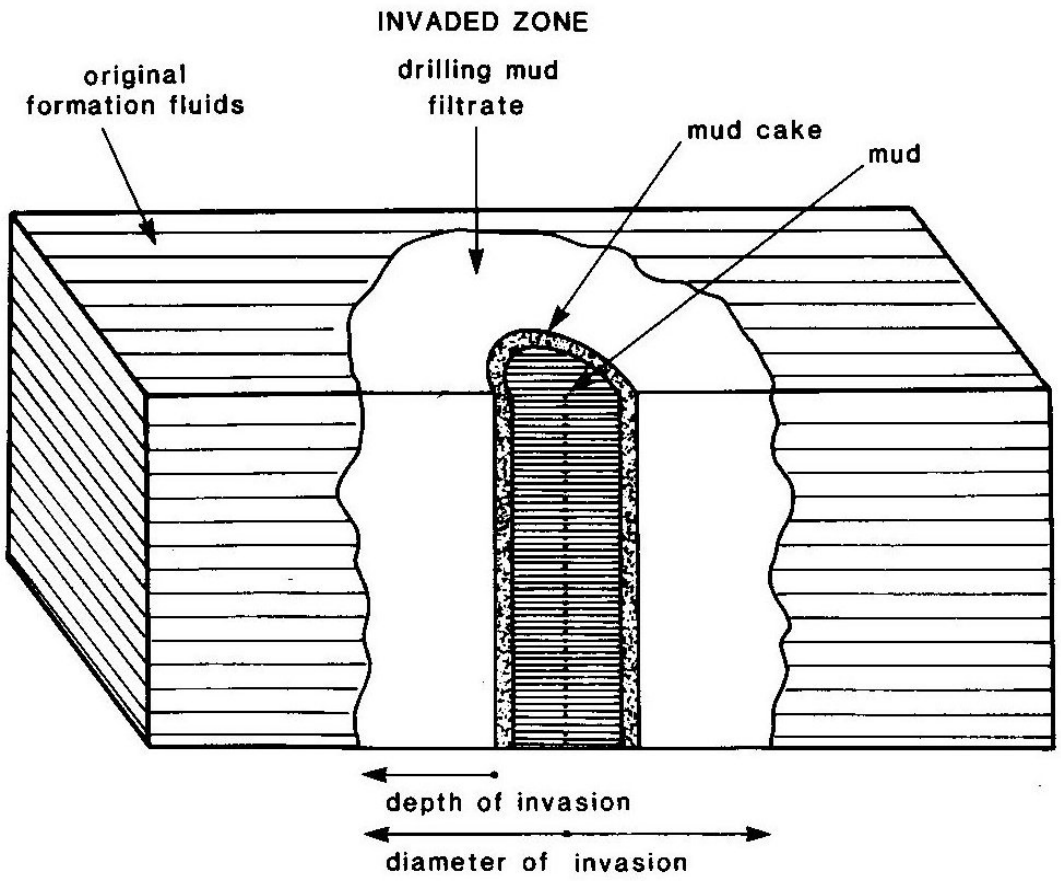

Figure 1.2: Invasion: simple representation of the effect of drilling on fluids in a porous and permeable formation. (Rider, 2000)

by a logging tool. For instance, logging tools are generally designed to sense and measure properties of undisturbed formations, and measurements will be adversely affected in an invaded zone.

The "depth of investigation" varies from one tool to another. Often, it depends on the transmitter-receiver separation for tools which use the principle of transmission and reception. Depth of invasion depends on the susceptibility of a formation to penetration, so that a high permeability bed may result in a greater depth of penetration of invading fluid.

1.3 Types of Logs

Geophysical logs, as briefly described in the previous sections, are obtained when a continuous measurement is made of formation properties. Measurements include electrical properties, sonic properties, dimensions of the well bore, formation fluid sampling, formation pressure measurement, etc. The logs could either be wireline logs, where measurement is made on ascent of the logging tool from the bottom of the well, or LWD logs where measurement is made from top to the bottom as the drilling is in progress. The logs collected using both methods are very similar. In this section, we shall be considering several types of wireline logs which are commonly used in the oil industry. Geological logs, on the other hand, use data collected at the surface, rather than by downhole instruments. These logs include

- Drilling time logs which record the time required to drill a given thickness of rock formation. A change in the rate of drilling implies a change in the rock type penetrated by the drilling bit.
- Sample logs which are made by examining bits of rock brought up to the surface by the drilling mud in rotary drilling. This sampling is made at regular depth intervals.
- Mud logs are obtained to provide information on the formation gas. A typical mud log normally includes drilling parameters such as rate of penetration, lithology, gas hydrocarbons, mud weight, and estimated pore pressure.

Based on the physical principle involved, or the method, geophysical logs can be put into several classes. Measurements could either be mechanical, spontaneous or induced. Logs can also be classified based on their principal uses so that we have logs which are solely for general geology uses, reservoir geology use, geochemistry, petrophysics and seismic application.

1.3.1 Temperature Logging

Temperature logs provide a continuous record of vertical variations in the water temperature in a well. The temperature measured in boreholes is not the formation temperature; it is the

temperature of the mud in the borehole. While drilling, the mud is consistently much cooler than the formation's temperature, and it would take some standing time before equilibrium would be attained. Temperature logs are generally taken several times during a logging run, so that the rise in mud temperatutes can be extrapolated to formation temperature. Temperature logs are:

- used to identify water-producing and water-receiving zones.
- used to determine zones of vertical borehole flow, where there is little or no vertical temperature gradient.
- used for environmental corrections as some logging tool sensors are sensitive to temperature. For example, temperature log measurements are used to calibrate resistivity logs to standard temperature conditions.
- used to calculate organic matter maturity.
- used for identification of zones of overpressure.

1.3.2 Caliper Logging

The caliper log is used to measure the size (diameter) and shape of the borehole. This is done with the aid of a mechanical caliper. A caliper tool may have two arms or more, the simplest being the two-arm caliper. The tool measures the diameter of the borehole by using one or more pairs of its arms, which are pressed against the borehole wall as the tool is raised from the bottom of the borehole. Multi-arm tools give better resolution of the borehole shape than a two-arm tool.

A very important application of the caliper log, using the four-arm caliper tool, is the definition of the shape of a hole. A hole could either be "on gauge" and round, or oval and "washed out" or enlarged by a "key seat" as shown in Figure 1.3. Both washouts and keyseats are generally caused during drilling and can be identified from the log. In both cases, the measured diameters are larger than the drill bit size with one caliper pair being larger than the other.

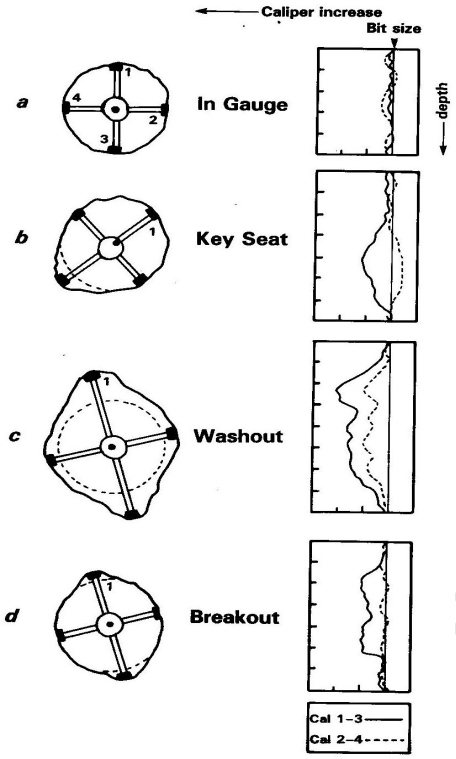

Figure 1.3: Diagrammatic representation of types of borehole shape and profile as identified on the two-arm caliper. *a*. Round, in-gauge hole. *b*. Key seat hole enlargement at a dogleg. *c*. Washout hole enlargement due to general drilling wear. *d*. Breakout, showing characteristic oval hole with abrupt vertical limits (Rider, 2000)

It is also used to identify possible water-bearing fractures and to adjust responses of other logs to changes in well diameter. Because borehole diameter commonly affects log response, the caliper log is also useful in the analysis of other geophysical logs. It is also used to identify mud-cake, which indicates invasion, when the borehole diameter is less than the bit-size.

The caliper log, which is usually plotted in track 1 of a standard well log sheet, shows continuous value(s) of the hole's diameter with depth. It is plotted along side the Bit size in dashed lines.

1.3.3 Sonic or Acoustic Logging

The basic principle of P-wave sonic logging tools is transmission and reception. The tools work by transmitting P-waves through the rocks of the borehole wall. The speed of these waves will vary

depending on the lithology encountered during passage of the waves. The transmitted signals are then received by an array of receivers also located at some distance along the tool from the transmitter or emitter. What the receivers actually measure is the interval transit time between when the source is fired and when it reaches them. The fastest arrival will generally be through the rocks near the borehole wall. This interval transit time can later be converted to velocity. Figure 1.4 shows a plot of the transit time logs where the vertical axis is in μs/ft. Since the

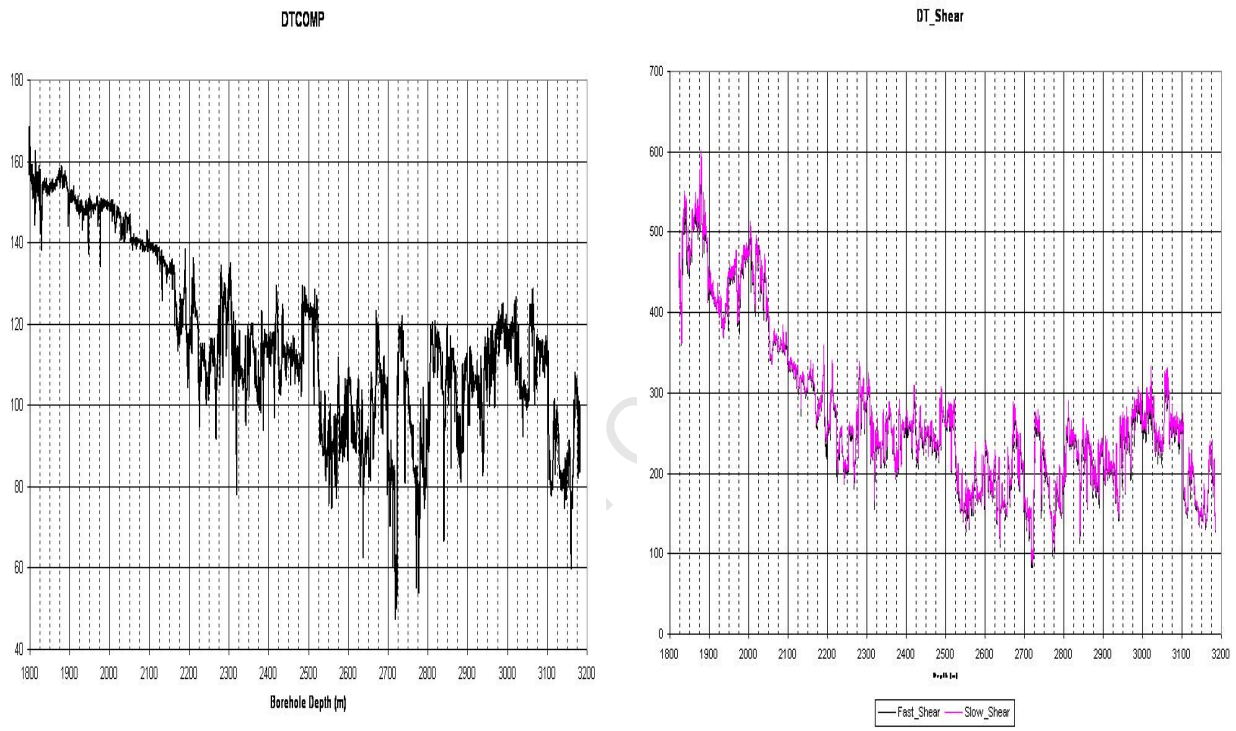

Figure 1.4: Compressional and Shear Transit time

interval time is dependent on the porosity of consolidated formations, it can be used to calculate the porosity of the rocks through which the signal passes.

In the porous zones, the travel time of sound waves is greater, while in compact zone, the sound waves travel faster. Where the hole size is large due to caving, the density tool cannot read the actual density of rock because of the nature of the tool. In such zones, a sonic log may be the best tool for porosity and lithology determination.

Other applications of a sonic log include lithology determination, well correlation, fracture detection, over-pressure detection, and in the calculation of acoustic impedance and other mechanical

properties when it is combined with other logs such as the density log.

A very clear detail on sonic logging which includes the acquisition, the tools used for acquisition, processing of a full waveform sonic, interpretation of a sonic log and the seismic applications, will be discussed in a later chapter.

1.3.4 Resistivity Logging

Resistivity logs display measurements of a formations resistivity, which is its resistance to the flow of an electric current. Its unit is the ohm-meter. Resistivity is the inverse of conductivity. A formation having more hydrocarbons will exhibit a higher resistivity than a formation containing water. The resistivity of a formation largely depends on the volume of water present, the temperature of the formation and the salinity of the formation. A resistivity log is measured by resistivity tools. If the rock has low porosity or is compact, then the resistivity of the formation is high. The resistivity tool is made up of a reference electrode and a measurement electrode, which are variably spaced on the logging tool. A typical spacing for potential electrodes is 16 inches for short-normal resistivity and 64 inches for long-normal resistivity (Survey). The greater the electrode separation, the greater the depth of penetration of the current and hence, the greater the depth of measurement.

Depending on the configuration of the tool, the resistivity can be measured at various distances from the tool in the borehole. This implies that resistivity measurements can be made in invaded zones, close to the borehole, and in the hydrocarbon zone, far away from the borehole. Therefore a combination of shallow and deep resistivity values can reveal the possible zones of hydrocarbon saturation (see Figure 1.5, where the numbers AT10, AT60 and AT90, indicate how deep in inches the tool penetrates the borehole formation). Normally, depth is plotted along the vertical axis with resistivity values on the horizontal axis. The referenced figure does not show this. Again, the unit of resistivity is not shown in the figure. We shall see a better example of such a log in a later chapter when we analyse the logs provided for the study.

Fluid resistivity logs are also used to identify water-producing and water-receiving zones and to determine intervals of vertical borehole flow. These zones are usually identified by distinct

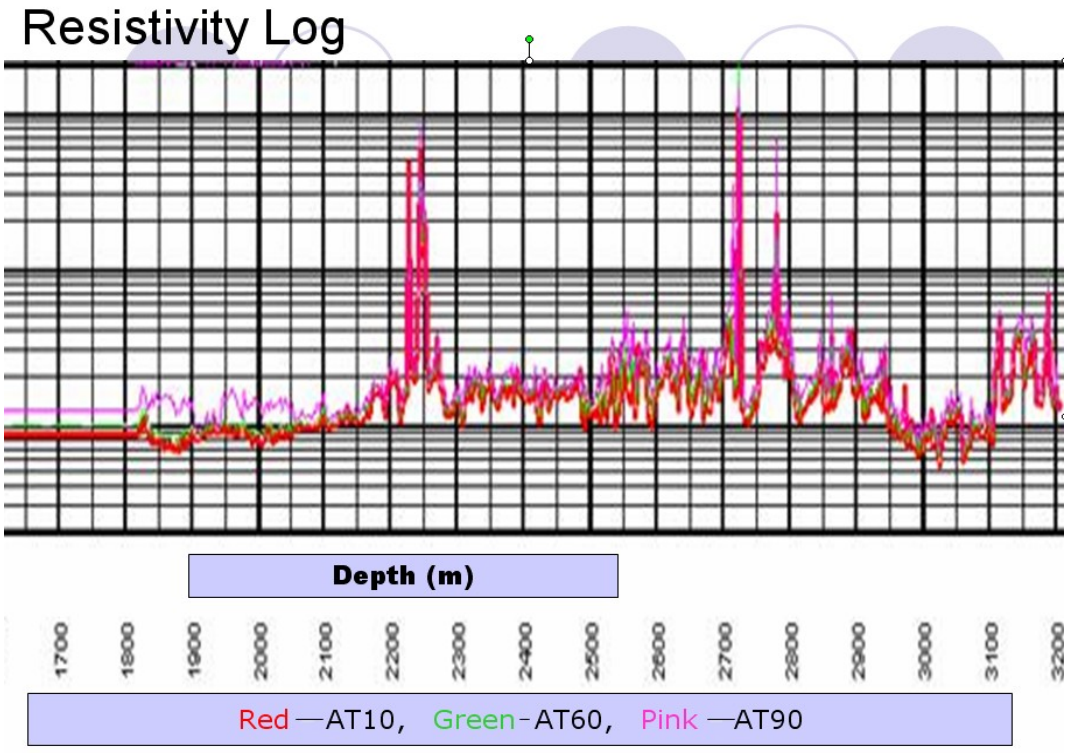

Figure 1.5: Resistivity log

changes in resistivity.

The principal quantitative use of the resistivity log is to locate and quantify oil and gas. It is used to determine water saturation and thus hydrocarbon saturation. A formation's resistivity also aids the understanding of the lithology, texture, facies, overpressure and source rock identification in geochemistry. In the determination of water saturation from the resistivity log, several equations can be used but one of the most fundamental equations is that of Archie stated in 1942. For a given rock with porosity ϕ, in order to be a able to find the level of water saturation S_w, the resistivity of the saturated water ρ_w and the true or measured resistivity ρ must be known. Equation 1.1 gives Archie's law which states that (Archie, 1942)

$$\rho = a\rho_w\phi^{-m}S_w^{-n} \tag{1.1}$$

where $0 < \phi < 1$; $0 < S_w < 1$; $0.5 < a < 2.5$; $n \approx 2$ while m varies between 1.3 and 2.5. ρ_w varies according to the type and quantity of the dissolved minerals and salts in the water.

1.3.5 Self Potential Logs

The Self Potential log is a measurement of the natural potential differences or self-potentials between an electrode in the borehole and a reference electrode at the surface. In this case, no artificial currents are applied unlike in the case of the resistivity log. These naturally occurring potentials are produced by the interaction of formation connate water, conductive drilling fluid, and shale. The potentials arise from electrochemical processes such as the diffusion and absorption of ions (cations and anions) through clays. For example, saline groundwater which is in contact with clay-rich materials often develops potentials as a result of fluid flow (Rider, 2000). In a nutshell, the measurement of a self potential log involves the evaluation of streaming potentials. Just like the resistivity log, self potential logs are limited to water or mud-filled holes.

A common feature normally sought for in a self potential log or curve is a deflection which indicates a permeable zone. The principal uses of the self potential log is to calculate formation water resistivity and to indicate permeability. It has other uses as well such as :

- Estimation of shale volume.
- Facies indication.
- Mineral identification
- Correlation of wells.

On a standard well log sheet, the SP log is usually run in track 1 with a gamma ray or caliper log.

1.3.6 Gamma Ray Log

The gamma ray log is a record of a formation's radioactivity. The log responds to the natural gamma radiation from uranium, thorium and potassium in the formations. These gamma rays are high energy electromagnetic waves which are emitted by atomic nuclei as a form of radiation. The gamma ray log can either be simple or spectral. The simple gamma ray log gives the combined

radioactivity of the three elements while the spectral gamma ray log shows the amount of each individual element contributing to this radioactivity (Rider, 2000). However, emphasis will be laid on the simple gamma ray log.

Due to its principal use in determining shale volume, the gamma ray log is sometimes referred to as the "shale log". The degree of radioactivity varies from rock to rock, with shale having the strongest radiation and relatively low counts recorded in clean quartz sandstones and limestones. The gamma ray tool (GR Sonde) contains a detector (scintillation counter) to measure the gamma radiation originating in the volume of formation near the sonde and a photomultiplier which collects the flashes produced when gamma rays pass through the scintillation counter. The tool is small and can be combined with other tools, be it a resistivity or porosity device. The gamma sonde is run, either centred in the borehole or against the borehole's wall, which is eccentred. The distance that a gamma ray can travel through rocks is strongly dependent on the electron density of the medium because it is through scattering interactions with electrons that the gamma ray photons lose their energy. The distance travelled also depends on the initial energy level of the gamma rays and the rock density, so that distances are greater in low density rocks and much less in dense crystalline rocks. The accepted unit for gamma ray logging is the API (American Petroleum Institute) unit. The gamma ray log is normally recorded in track 1 along with the caliper, and sometimes the SP log.

The simple gamma ray log (see Figure 1.6) is used for estimating the shale volume, (shaliness) of a formation, lithology identification, mineral analysis, and determination of bed boundaries. Other uses of the log include determination of facies and grain size, correlation between wells, igneous and volcanic rock radioactivity. Normally, the values of gamma are plotted on the horizontal axis with the depth on the vertical axis. More details on the significance of the gamma log will be discussed in chapter four when we discuss the data which was provided for this study.

Using the gamma ray log, the volume of shale V_{sh} can be estimated from the simple formula in equation 1.2 (Zahid, 2008)

$$V_{sh} = \frac{Gr - Gr_{min}}{Gr_{max} - Gr_{min}} \tag{1.2}$$

where Gr is the recorded value of gamma as read from the log while Gr_{min} and Gr_{max} are the minimum and maximum values possible.

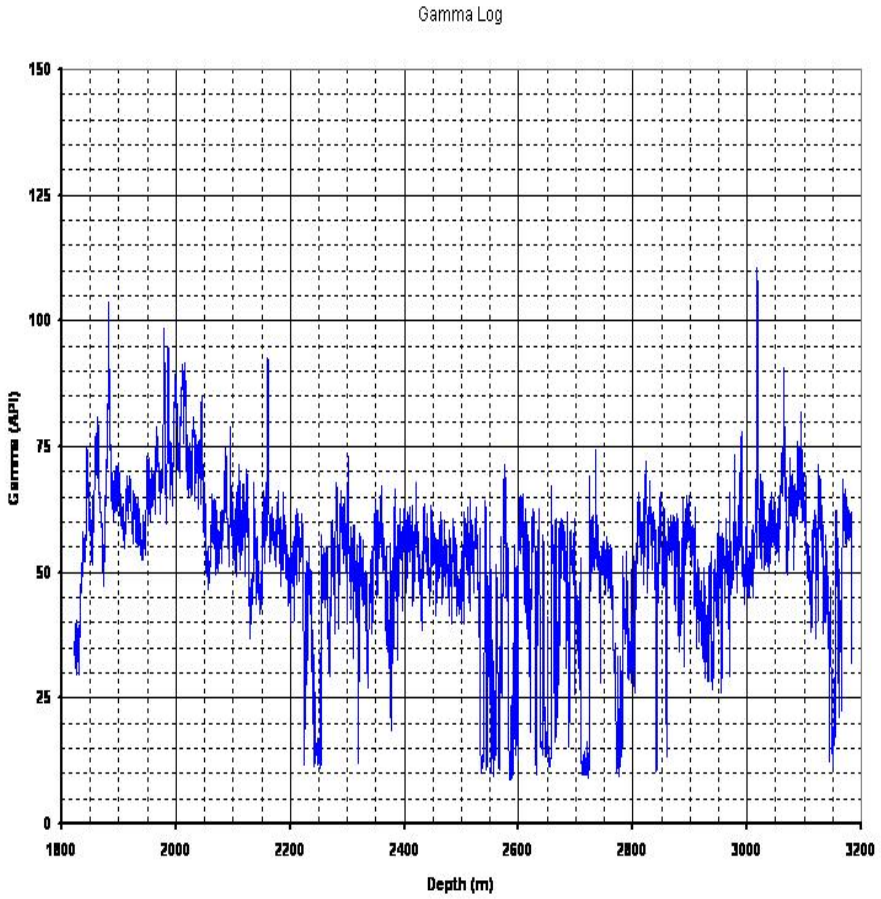

Figure 1.6: Gamma Ray Log

1.3.7 Density Logging

The total density of a rock including the solid matrix and the fluid present in the pores is known as a formation's bulk density. It is the continuous record of this bulk density that the density log shows (see Figure 1.7). The density of the formation is measured in gm/cc. The density log used in this study is introduced in chapter four and reveals more information. The logging technique entails subjecting the formation to a bombardment of medium-high energy gamma rays and measuring their scattering between the source of the density tool and the detectors. The log is recorded in the form of a plot of scattered gamma-ray intensity against depth. The deflections obtained on the plot are then translated to density of the formation. Dense formations absorb many gamma rays, while low-density formations absorb fewer. Thus, high-count rates at

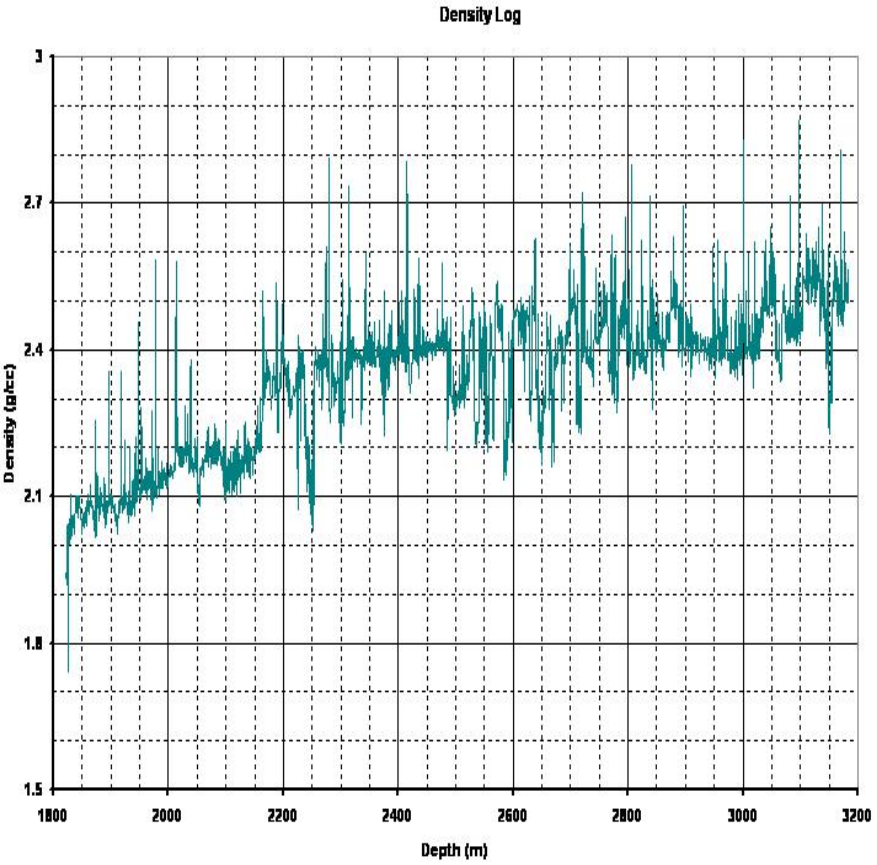

Figure 1.7: Density

the detectors indicate low-density formations, whereas low count rates at the detectors indicate high-density formations.

The density log is normally plotted on a linear scale of bulk density and is run across tracks 2 and 3 of most standard well log sheets. The density log is often run in combination with the neutron log along with the gamma ray and caliper log. The density and neutron log are often used in a complementary way.

Quantitatively, the density log is used to calculate the porosity of a formation, and they are related by equation 1.3 below:

$$\text{bulk density } (\rho_b) = \text{porosity } (\phi) \times \text{fluid density } (\rho_f) + (1 - \phi) \times \text{matrix density } (\rho_m) \quad (1.3)$$

so that porosity is defined in equation 1.4 as :

$$\phi = \frac{\rho_m - \rho_b}{\rho_m - \rho_f} \tag{1.4}$$

where ρ_b = formation bulk density measured by the tool, ρ_f = fluid density, and ρ_m = matrix density which should be known before ϕ can be estimated.

Apart from being able to estimate porosity, the density log is also used qualitatively to indicate lithology (a plot of travel time in μs/ft against density), estimate the total density of hydrocarbons present, and also help in identification of certain minerals and assess source rock organic matter content.

Also, as stated previously, being a good complement of the neutron log, the density log is suited for estimating porosities that are greater than 10%, while the neutron log which is discussed next, is suited to measure porosities between 1 to 10%.

1.3.8 Neutron Logging

Neutron logging is the continuous record of the induced radiation produced by the bombardment of a formation with a neutron source contained in the logging tool, which emits fast neutrons that are eventually slowed by collisions with hydrogen atoms until they are captured. The capture results in the emission of a secondary gamma ray. The neutron source has a very high energy and this energy is gradually lost as the neutrons collide with the hydrogen atoms in the formation.

If, in the formation, the number of hydrogen atoms is higher (a porous rock with water or oil), then it slows down the speed of the neutrons, and as a result, few neutrons will be received at the detectors (one or two). The opposite will result in the case of a low porosity rock or one with gas in the pores: a formation with low hydrogen content leads to a large deflection on the neutron log.

The tool results are given by the ratio of the near/far counts, thereby eliminating borehole effects as much as possible. This is because the far detector readings, which contain both hole and formation effects, are 'corrected' by the near detector readings which have mainly hole effects,

leaving only the effects of the formation. The ratio results are presented on the log as neutron porosity units after empirical calibration.

The neutron log is recorded in units of neutron porosity units which represent real porosity only in clean limestones. However, an API standard unit also exists for other neutron tools, so the calibration of a neutron tool is company dependent. Since the neutron log is run combined with the density log in one tool, it is also plotted across tracks 2 and 3 of a standard well log sheet.

The primary use of the neutron log is in the measurement of porosity (equation 1.5). Since the tool is a hydrogen detector, it exploits the hydrogen density, or hydrogen index. It responds to the volume of water-filled pore space which gives its porosity (assuming water in the pores) as (Rider, 2000)

$$\log_{10} \phi = aN + B \tag{1.5}$$

where ϕ is the true porosity, N is the neutron-tool reading, a and B are constants which depend on the calibration of the tool.

Other uses of the neutron log are in identification of gas, identification of gross lithology, hydrated minerals and volcanic rocks. When combined with the density log, it is one of the best subsurface lithology indicators available.

Other important logs which would not be discussed further because they were not run in my study area and as such not used in the evaluation of the well being studied, include the Dipmeter logs, Imaging logs, Induction logs, Magnetic Susceptibility logs and Induced Polarisation logs.

2. Literature Review, Objective and Overview

Geology of study area

The well, from which the logs used in this study come, has a very interesting geology, as it is from the offshore part of the Gulf of Guinea province which has been known, over the years, to produce large amounts of oil and gas. Most of the discoveries have been found to be concentrated in Cretaceous reservoirs on the continental shelf and adjacent onshore extensions in two basin areas, namely, the Ivory Coast to Tano basins of Cote d'Ivoire and Ghana, and the Keta basin to the Benin basin of westernmost Nigeria. Oil seeps and tar sand accumulation characterise these basins. The well site being studied comes from the Tano basin area.

The main source rocks in the area are the Devonian shales in the Saltpond basin and field. Most of the oil has been produced from Devonian to Carboniferous Takoradi Formation sandstones filled from these source rocks. Other source rocks in the area include the Neocomian lacustrine strata, lower to middle Albian gas-prone source rocks, Albian and Cenomanian black shale source rocks, and the Coniacian to Palaeocene source rocks (Brownfield and Charpentier (2006)).

Hydrocarbon generation in the study area is mainly from the upper Albian and Cenomanian black shale source rocks and these are mainly distributed around the offshore part of the Gulf of Guinea province. However, there may be a contribution from the Devonian shales and the lower Cretaceous lacustrine rocks.

2.1 Literature Review

Much research has been carried out on shear wave velocity and compressional wave velocity with results published in different journals. This research ranges from their estimation, measurement, and applications as far as location of hydrocarbons, detection of lithology etc. are concerned. In

much of this research, it is the rock physics relationships that are being used.

Rock physics relationships have been used extensively in the oil and gas industry to describe the nature of reservoir rocks. In fact, "Rock physics describes a reservoir rock by physical properties such as porosity, rigidity, compressibility - properties that will affect how seismic waves physically travel through the rocks" (Tönsing, 2006). The rock physics relationships concerned with wave propagation in saturated, porous media, when combined with more accurate geophysical exploration techniques, help in better determination of geological parameters and in general, proper evaluation of well logs.

Although there are many rock physics relationships, only a few of the empirical and theoretical relations, will be briefly discussed in this section. The section concludes with the results obtained by researchers using some of these relations.

2.1.1 Empirical relations

In log interpretation, empirical relations abound to help obtain an unknown parameter given one or more known parameters. Resistivity and sonic logs are among those logs to which this applies. It should be noted that although these relations can be used in log interpretation, most of them are strictly valid only for the data set from which they were derived. They may need to be recalibrated to specific locations or rock types.

Electric currents in fluid-saturated rocks caused by an applied dc voltage arise primarily from the flow of ions within the pore fluids. Archie, in 1942, defined a new term , the *formation factor*, F as the ratio of the conductivity of the pore fluid to the bulk conductivity of the fully saturated rock.

$$F = \frac{\sigma_w}{\sigma} = \frac{R}{R_w} \tag{2.1}$$

where $\sigma_w, R_w =$ conductivity and resistivity of pore fluid while $\sigma, R =$ conductivity and resistivity of fully saturated rock.

Archie (1942) also suggested an empirical relation relating formation factor to porosity ϕ in

brine-saturated clean (no shale) reservoir rocks:

$$F = \phi^{-m} \tag{2.2}$$

where the exponent m (sometimes referrred to as the cementation exponent) varies approximately between 1.3 and 2.5 for most sedimentary rocks and is close to 2 for sandstones (Mavko et al., 2003). This law forms the basis for resistivity log interpretation.

In shaly sands, Archie's law has been modified and several models have been formulated to account for the fractional volume of shale V_{sh}, as determined from logs. Almost all of the models account for the excess conductivity by introducing a shale conductivity term X:

$$\sigma = \frac{1}{F}\sigma_w + X \tag{2.3}$$

For Simandoux (1963), $X = V_{sh}\sigma_{sh}$ and Poupon and Leveaux (1971) modified the entire equation to be

$$\sqrt{\sigma} = \sqrt{\frac{1}{F}\sigma_w} + V_{sh}^{\alpha}\sqrt{\sigma_{sh}}, \qquad \alpha = 1 - \frac{V_{sh}}{2} \tag{2.4}$$

where σ_{sh} is the conductivity of fully brine-saturated shale. These equations are only empirical. They do not allow a complete representation of conductivity behaviour for all ranges of σ_w (see Mavko et al., 2003).

Next, we take a look at some of the empirical relations between P-wave and S-wave velocity and porosity in shales, sands and shaly sandstones. A relation between P-wave velocity and porosity in sedimentary rocks was found by Wyllie et al. (1956, 1958, 1963) and is often called the time average equation.

$$\frac{1}{V_p} = \frac{\phi}{V_{p-f}} + \frac{1-\phi}{V_{p-m}} \tag{2.5}$$

where V_p, V_{p-m} and V_{p-f} are the P-wave velocities of the saturated rock, of the mineral material making up the rock, and of the pore fluid respectively (Mavko et al., 2003). The equation implies that the total transit time is the sum of the transit time in the mineral plus the transit time in the pore fluid.

An improvement to the relation was made by Raymer et al. (1980) as follows:

$$V_p = (1-\phi)^2 V_{p-m} + \phi V_{p-f}, \qquad \phi < 37\% \tag{2.6}$$

$$\frac{1}{\rho V_p^2} = \frac{\phi}{\rho_f V_{p-f}^2} + \frac{1-\phi}{\rho_o V_{p-o}^2}, \qquad \phi > 47\% \tag{2.7}$$

where ρ, ρ_f and ρ_m are the densities of the rock, the pore fluid, and the minerals respectively.

For water saturated clean sandstones, and shaly sandstones, Han et al. (1986), Tosaya and Nur (1982), and Castagna et al. (1985) all had different relations between velocity and porosity, having introduced a clay content C by volume in the equations for shaly sands. In general, the relation can be written as

$$V_p(\text{km/s}) = a + b\phi + dC \tag{2.8}$$

$$V_s(\text{km/s}) = e + f\phi + gC \tag{2.9}$$

The values of the constants are shown in Table 2.1. (An assumption is that, the effective pressure was about 40Mpa).

	Han et al.	Tosaya and Nur	Castagna et al.
a	5.59	5.8	5.81
b	-6.93	-8.6	-9.42
d	-2.18	-2.4	-2.21
e	3.52	3.7	3.89
f	-4.91	-6.3	-7.07
g	-1.89	-2.1	-2.04

Table 2.1: Water-saturated shaly-sandstones (Mavko et al., 2003)

For water-saturated clean sandstones, Han et al. (1986) found the constants to be $a = 6.08, b = -8.06, d = 0, e = 4.06, f = -6.28, g = 0$. By eliminating porosity and clay content, other empirical relations were found for different rock formations between V_p and V_s and are also briefly discussed. If the general form of the equation is

$$V_s(\text{km/s}) = \alpha V_p + \beta \tag{2.10}$$

For water saturated shaly sandstones, Castagna et al. (1985) found $\alpha = 0.8042, \beta = -0.8559$ while Han et al. (1986) obtained $\alpha = 0.7936, \beta = -0.7868$.

Han (1986) considered the effect of clay content and porosity on his models which led to a change in the constants. (The velocities are in km/s).

$$V_s = 0.842V_p - 1.099 \qquad \text{for clay} > 25\% \tag{2.11}$$

$$V_s = 0.754V_p - 0.657 \qquad \text{for clay} < 25\% \tag{2.12}$$

$$V_s = 0.756V_p - 0.662 \qquad \text{porosity} > 15\% \tag{2.13}$$

$$V_s = 0.853V_p - 1.137 \qquad \text{porosity} < 15\% \tag{2.14}$$

Greenberg and Castagna (1992) also gave their empirical relations for estimating V_s from V_p in multimineralic, brine saturated rocks. The shear wave velocity in brine saturated composite lithologies is approximated by a simple average of the arithmetic and harmonic means of the constituent pure lithology shear velocities. It is this technique that is used to estimate the shear velocity used for interpretation in this project. More on the application of the relation is described in chapter four.

Finally, we take a look at a few of the velocity-density relations (Castagna et al., 1993). If the velocity V_p(km/s) is known, the bulk density ρ_b may be estimated using

$$\rho_b(g/cc) = aV_p^2 + bV_p + c \qquad \text{(Polynomial law)} \tag{2.15}$$

or

$$\rho_b = dV_p^f \qquad \text{(Power law)} \tag{2.16}$$

Gardner et al. (1974) made the following recommendations:

For shales: $a = -0.0261, b = 0.373, c = 1.458, d = 1.75, f = 0.265$ in a V_p range of 1.5 to 5.0 km/s .

For sandstones: $a = -0.0115, b = 0.261, c = 1.515, d = 1.66, f = 0.261$ in a V_p range of 1.5 to 6.0 km/s

A major limitation of the V_p-density relations is that because velocity is often not well related to porosity, it is also not well related to density.

2.1.2 Gassmann's relations

The prediction of saturated rock velocities from dry rock velocities, and vice versa is referred to as the fluid substitution problem. Gassmann (1951) formulated equations which would help estimate these rock velocities. He made the following assumptions for his equations to hold:

1. The wavelength of the seismic wave is much larger than the pore dimensions
2. The mineral material and the pore filling material is homogeneous
3. The pores of the frame are connected, and thus in pressure equilibrium

The equations hold for both isotropic and anisotropic frames. Gassmann's theory predicts the effective bulk modulus, K_{sat}, of the saturated rock through the following equation:

$$\frac{K_{sat}}{K_m - K_{sat}} = \frac{K_{dry}}{K_m - K_{dry}} + \frac{K_f}{\phi(K_m - K_f)}, \qquad \mu_{sat} = \mu_{dry} \tag{2.17}$$

where K = bulk modulus, μ = shear modulus ($_{dry}$ = dry rock, $_f$ = pore fluid, $_{sat}$ = rock with pore fluid, $_m$ = mineral making up the rock) and ϕ = porosity.

The process of fluid substitution is to transform the moduli from the initial fluid saturation to the dry state and then transform the dry state to the new fluid saturated state. Equivalently, we can eliminate the dry rock moduli from the equation and relate the saturated rock moduli K_{sat1} and K_{sat2} in terms of the two fluid bulk moduli K_{f1} and K_{f2} as follows: (Mavko et al., 2003)

$$\frac{K_{sat1}}{K_m - K_{sat1}} - \frac{K_{f1}}{\phi(K_m - K_{f1})} = \frac{K_{sat2}}{K_m - K_{sat2}} - \frac{K_{f2}}{\phi(K_m - K_{f2})} \tag{2.18}$$

A step by step application of this transformation is described in chapter four.

In order to apply Gassmann's equations for fluid substitution, one must have a knowledge of lithology, a measured value of the initial compressional velocity V_{p-sat} and a measured shear velocity V_{s-sat}, as well as a density ρ_{sat}. This will enable us to calculate the saturated bulk modulus, K_{sat1} and proceed with the transformation (e.g. brine-dry-oil, or brine-dry-gas). However the shear velocity is often not measured. This means that K cannot be obtained from V_{p-sat} alone and so Gassmann's relations cannot be applied. In this case, a V_s can be estimated from

an empirical V_s-V_p relation (as was done in one of the models considered in this project) or a dry rock Poisson's ratio can be assumed (Castagna et al., 1985; Greenberg and Castagna, 1992)

Also, where the measured V_{p-sat} is that of oil or gas saturated rock, we cannot use the empirical relations to estimate V_s. Mavko et al. (1995) therefore suggested an approximate method that operates directly on the P-wave modulus, $M = \rho V_p^2 = K + \frac{4}{3}\mu$. The Gassmann's relation then takes the form

$$\frac{M_{sat}}{M_m - M_{sat}} \approx \frac{M_{dry}}{M_m - M_{dry}} + \frac{M_f}{\phi(M_m - M_f)} \tag{2.19}$$

where $M_{sat}, M_{dry}, M_m,$ and M_f are the P-wave moduli of the saturated rock, the dry rock, the mineral, and the pore fluid respectively. It is this approach that was used in the estimated shear wave model of this project and has been explained further in chapter four.

2.1.3 Case studies

The case studies presented below ranges from the numerous research which has been carried out on sonic log acquisition, processing, and interpretation. Emphasis is on shear wave velocity estimation and application of fluid substitution using Gassmann's relations.

Han et al. (1986) in the paper titled "Effects of porosity and clay content on wave velocities in sandstones" concluded that both V_p and V_s correlate linearly with porosity ϕ and clay content C in shaly sandstones. The best least squares fit to their velocity data are

$$V_p(\text{km/s}) = 5.59 - 6.93\phi - 2.18C \tag{2.20}$$

$$V_s(\text{km/s}) = 3.52 - 4.91\phi - 1.89C \tag{2.21}$$

They showed that a very small amount of clay significantly reduces the elastic moduli of sandstones. They also showed that an increase in porosity reduces the velocities. In general, they concluded that "For shaly sandstones, to first order, clay content is the next most important parameter to porosity in reducing velocities, with an effect which is about 0.31 for V_p to 0.38 for V_s that of the effect of porosity".

Xia et al. (1999) estimated near-surface shear wave velocity by inversion of high frequency Rayleigh waves. Previously, Turner (1990) had obtained poor results by inversion of Rayleigh

waves to determine P-wave velocities.

Avadhani et al. (2006) in their paper "Acoustic Impedance as a lithological and hydrocarbon indicator - a case study from Cauvery Basin" showed that acoustic impedance can be used to characterise the lithology of Kamalapuran pay sand. They found values of 18000-20500 KPa.s/m for shale layers and 21000-26000 KPa.s/m for sand layers depending on the saturating fluid. They also showed that acoustic impedance log analysis carried out with the help of cross plots led to good understanding of formation lithology and saturating fluids, guiding the interpretation of seismic inversion.

Ensley (1989) in his paper "Analysis of Compressional- and Shear wave seismic data from the Prudhoe bay field" indicated that, by cross plotting the ratio of travel times of shear wave (Ts) and Compressional wave (Tp) against interval velocities, one can correctly predict gross lithology. However, the technique could not determine the percentages of the different rock types within an interval with a mixed lithology.

Adam et al. (2006) investigated the applicability of Gassmann's theory to a set of carbonate data. They observed, inter alia, that the rock shear modulus is sensitive to brine saturation, especially at seismic frequencies. They did not find any positive correlation between the rock shear modulus weakening and the failure of Gassmann's theory to predict the saturated bulk modulus at seismic frequencies. Therefore, they concluded that knowledge of the reservoir pore-space geometry can aid one in the understanding and applicability of Gassmann's theory.

Oden et al. (2002) in the paper "Sonic logging case histories using advanced equipment and data processing techniques", were able to show that compressional velocity can be easily determined in all rock types with a full waveform sonic tool, as also can shear velocities in hard rocks. It was not easy to obtain the shear velocity in soft rocks, so they used an inversion of the Stoneley velocity. They made several checks with the measured shear velocities, and noticed that the values matched with the ranges of shear velocities for the given rock types. Therefore, they concluded that the combination of flexural mode survey, semblance, and inverse Stoneley modeling, makes it easier to obtain a good shear velocity and increases confidence in the results.

Todorov et al. (1997) were able to predict sonic log parameters using seismic attributes. In their research, they used linear multi-regression analysis and neural networks successfully to derive log properties from seismic attributes. They used cross-validation tests to evaluate the predicting process and it showed good correlation between the predicted model and the measured log property - sonic velocity.

Carr et al. (2004) used fluid substitution for correction of oil based mud filtrate invasion in sandstone reservoirs. The correction process yielded results that produced significantly better synthetic ties. Earlier, Walls and Carr (2001), and later Vasquez et al. (2004) had presented methodologies to correct for water based mud filtrate invasion. The problem of invasion had been detected using multiple depth resistivity logs and the correction was done by careful application of Biot-Gassmann fluid substitution.

The use of synthetic seismic data is another important concept which must be reviewed as it formed the concluding part of this project. It is discussed briefly in the next subsection.

2.1.4 Use of synthetic seismic data

One of the analyses done with logs is the generation of a synthetic seismic profile or seismogram for comparison with the real seismic data. An example of a synthetic is shown in Figure 2.1. Because the seismic data is time-based while the log data is depth-based, one would require a time-depth log or chart to make the comparison. There are times when the synthetics would not tie with the seismic data and other times, it may tie very well. When the synthetic does not tie, this becomes a problem, and this may be solved through the use of other data and preparation of a suite of synthetics (Figure 2.2) from a range of parameters.

Creating synthetics often, goes with Amplitude Versus offset (AVO) modeling. When full-offset synthetics are formed, one of the problems which might occur is post critical reflection being observed in the synthetics and there has been research to study this effect.

Simmons and Backus (1994) showed that primaries-only Zoeppritz modeling of thin layers can be very misleading and that synthetic seismograms obtained by use of a linearised approxima-

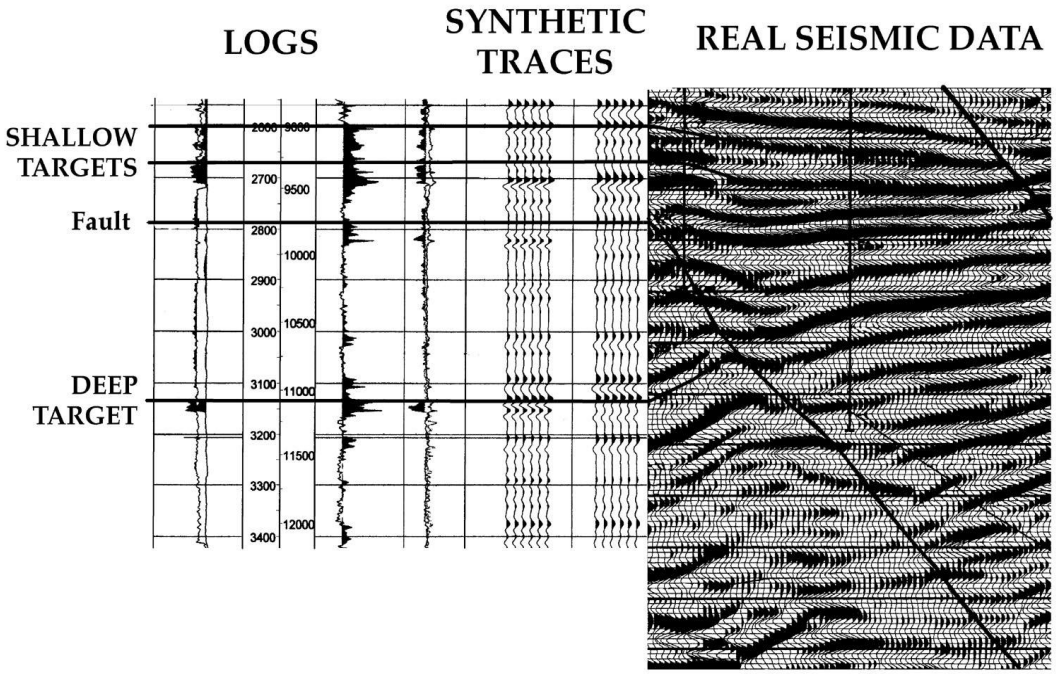

Figure 2.1: Synthetic seismogram and real seismic data (taken from Ewing, 2001)

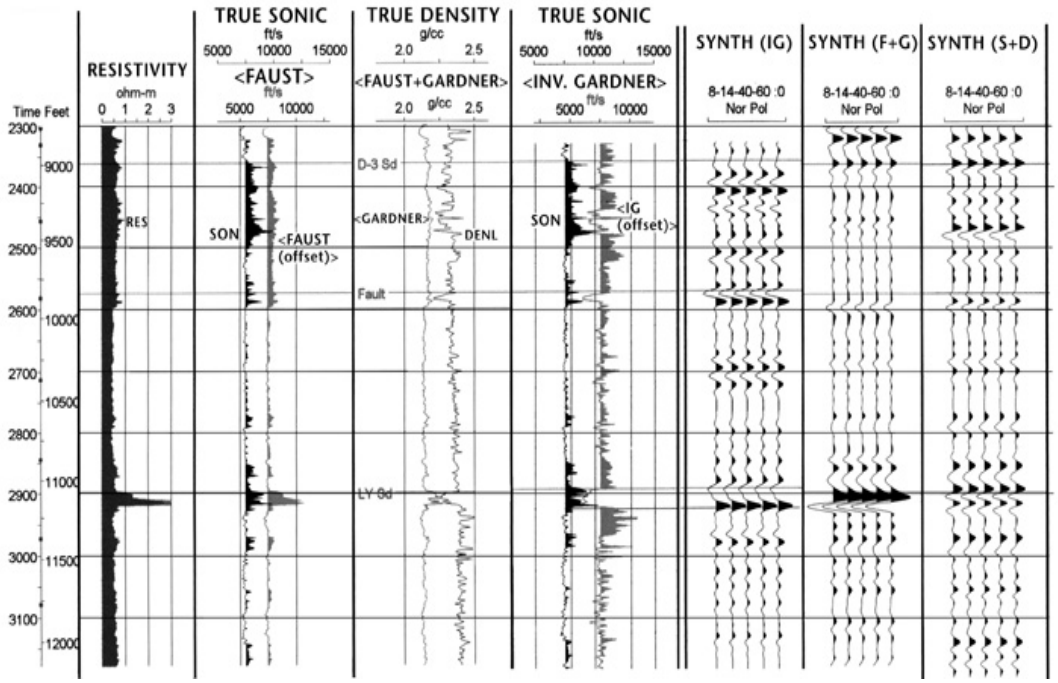

Figure 2.2: Suite of synthetics (taken from Ewing, 2001)

tion to the Zoeppritz equations to describe the reflection coefficients are more accurate than those obtained by use of the exact Zoeppritz reflection coefficients. They used the linearized

approximation to the Zoeppritz equations which was presented by Aki and Richards (1980).

Reilly (1994) also postulated that "Zoeppritz modeling of wireline data, particularly when shear velocity information is available, can be critical in the accurate calibration and quantification of surface seismic information and subsequent AVO analysis".

2.2 Objective of the study

The objective of this study is to compare the result of using an estimated shear wave log for interpretation with the result of using a measured shear wave log for the same interpretation. We aim to, after several analyses of the measured and estimated shear waves, make a conclusion as to which should be used for interpretation. We also hope to develop a model which most closely fits with available 3D-seismic data. In summary, the objective of this study is to develop a workflow for quantitative interpretation of well log data, especially sonic logs, which may be useful for a quantitative interpretation of the seismic data. The workflow is developed using wireline logging data from a well in the study area. The study helps in the formation evaluation of the well.

The aim and objective of this study was achieved in several steps. Firstly, with rock physics relationships, an estimated shear wave log was created and was compared with the measured shear wave log which had been obtained after a reprocessing of the full sonic waveform since the original shear wave log was observed to have cycle skips and missing data. Secondly, cross plots of shear wave velocity and compressional velocity were made. This allowed for observation of the characteristics of the respective shear wave velocities and the effect of fluid substitution.

Analysis done with the logs include calculation of mineral volumes using best available data (e.g Gamma ray), and calculation of fluid (water, oil and gas) saturation and total porosity using resistivity logs and density logs. Also, crossplot analysis was also carried out of elastic properties such as bulk density, and density porosity versus compressional velocity, compressional velocity versus shear velocity, Poisson's ratio versus acoustic impedance.

Fluid substitution was another tool which aided analysis of the estimated shear wave model and the measured shear wave model.

2.3 Overview of the study

Having discussed the concept of well logging and the various types of well logs available in the previous chapter, the development of the workflow is reported in three chapters, and a brief overview is provided of each below.

Chapter three starts by looking at the propagation of sound waves and seismic waves in rocks and formations. The acquisition of the sonic log is explained. It then discusses the tool used for acquiring the shear sonic log - the Dipole Shear Sonic Imager (DSSI). The processing leads to interpretation which is also discussed in detail. The chapter concludes by discussing some of the seismic applications of the sonic log which is one of the principal aims of acquiring the log in the first instance.

Chapter four describes the available input wireline log data. Each of the wireline logs is carefully examined for interesting features and the observations briefly stated. The process of obtaining an estimated shear velocity is also explained leading to a full detailed discussion on the possible models. The models being considered are separately analysed with emphasis on the variation or similarity in their cross plots and synthetic gathers. The fluid substitution process performed for each of the models is also explained in this chapter. A detailed interpretation is described here to support the conclusion which will come later.

In chapter five, the results of the analyses done in chapter four are compared in order to identify the best possible model. Based on the analysis done, a model which would nearly match the available seismic data is suggested.

3. Sonic Log : Introduction, Acquisition, Processing and Interpretation

3.1 Acquisition of Sonic Logs (Measurement and Principles)

3.1.1 Wave Propagation in Rocks

There are two kinds of waves that propagate through rocks: - compressional waves and shear waves. These waves are produced when there is a source of excitation in the formation. Compressional waves are created when a rock is sharply compressed and their passage is effected by small particle vibrations in the same direction as the wave is travelling. Shear waves are waves of shearing action whose passage is effected by rock particle vibrations perpendicular to the direction of wave propagation. Compressional waves are also known as longitudinal, primary, pressure or P-waves while shear waves are known as transverse, secondary or S-waves. Compressional and shear waves are called body waves because they travel through the body of the rock, as opposed to surface waves.

When a formation is excited by a sound source (transmitter) from a tool, the elasticity of the medium enables wave propagation to take place. This transmitted sonic pulse (wave) travels through the rock in two modes while undergoing dispersion and attenuation. Being a wave, it is reflected, and refracted as it passes from one medium to another until it finally reaches a receiver (which may be present in the tool). However, because of the many possible paths the waves could have taken, there will be different arrival times at the receiver. It is the compressional waves that are usually the first to arrive because they are fast and have small amplitude. After the arrival of the compressional waves, come the shear waves which have higher amplitude. Shear waves do not propagate in fluids as fluids cannot resist a shear deformation. In most cases, the arrival of the compressional and shear waves is followed by arrival of surface waves such as Rayleigh waves

and Stoneley waves, and mud waves.

The waveform observed at the receivers, which consists of several different modes of acoustic energy, depends on such factors as the mechanical properties of the rock around the borehole, the compressional velocity in the borehole fluid, the source frequency and the borehole size. For example, in a formation in which the S-wave velocity in the rock is less than the P-wave velocity in the fluid, the shear head wave and shear normal modes will be absent in the waveform. Such a formation is referred to as a "slow formation" or "soft formation". In "fast formations", the speed of propagation of the compressional wave in the fluid is less than the speed of propagation of the shear waves in the rock, an inverse of the case of slow formations.

Since the mechanical properties of a rock greatly influence the nature of the waveforms observed at the array of receivers, two very important properties (elastic parameters) worthy of note are the bulk modulus (K) and the shear modulus (μ). According to Mavko et al. (2003), while bulk modulus (K) is defined as "the ratio of hydrostatic stress to volumetric strain", shear modulus (μ) is defined as "the ratio of shear stress to shear strain". Mathematically,

$$K = -\frac{\Delta P}{\Delta V/V} \tag{3.1}$$

and

$$\mu = \frac{P_s}{\mathrm{e}} \tag{3.2}$$

where ΔP is the change in pressure of the rock from when the hydrostatic stress is applied to it; ΔV is the corresponding change in volume from initial volume V; P_s is the applied shear stress; e is the shear strain or angular distortion developed by the shear stress.

Figure 3.1 diagrammatically illustrates the bulk (a) and shear modulus (b). Comparing the figure with equation (3.1) and (3.2), ΔP = P2-P1, ΔV = V2-V1 and V = V1.

If the magnitude of the bulk modulus and shear modulus are known, and the density of the rock can also be obtained, then both the compressional velocity and the shear velocity can be computed using the equations below

$$V_p = \sqrt{\frac{K + \frac{4}{3}\mu}{\rho}} = \sqrt{\frac{\lambda + 2\mu}{\rho}} \tag{3.3}$$

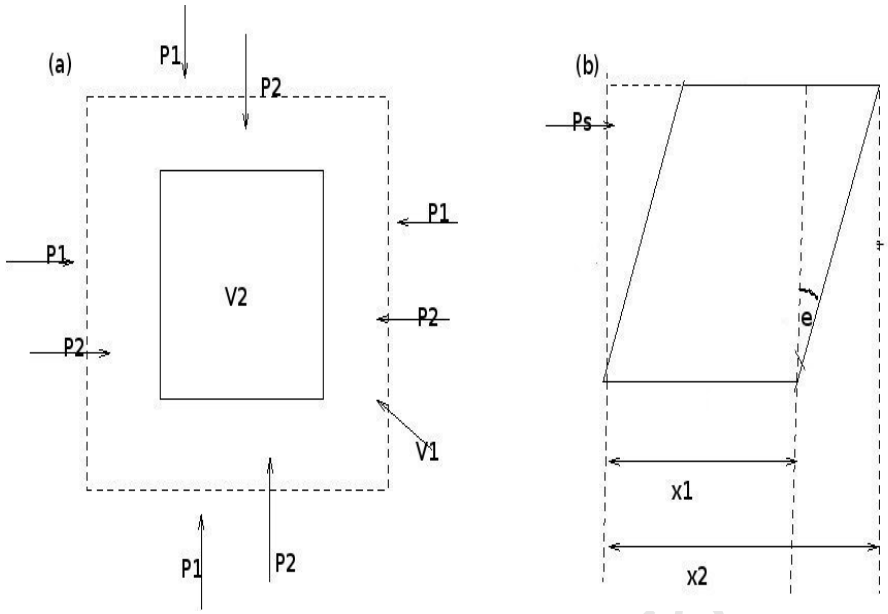

Figure 3.1: The definition of bulk and shear moduli (Glover, 2008)

$$V_s = \sqrt{\frac{\mu}{\rho}} \tag{3.4}$$

where λ = Lamé's coefficient ; ρ = density of the rock

Another very important parameter of particular interest is the Poisson's ratio which describes the amount by which a material increases in width along one axis when compressed a certain amount along the other. It is a very useful indicator of a formation's consolidation, and it is related to both the compressional and shear velocity by the equation below

$$\sigma = \frac{(V_p^2 - 2V_s^2)}{2(V_p^2 - V_s^2)} \tag{3.5}$$

where σ is the Poisson's ratio.

It should be noted that these equations are only valid for an isotropic, linear and elastic medium. Figure 3.2 gives a pictorial definition of Poisson's ratio in terms of the transverse and longitudinal strain. We can then define Poisson's ratio as

$$\sigma = -\frac{\varepsilon_x}{\varepsilon_y} \tag{3.6}$$

where ε_x is the transverse strain (dx/x), and ε_y is the longitudinal or axial strain (dy/y) .

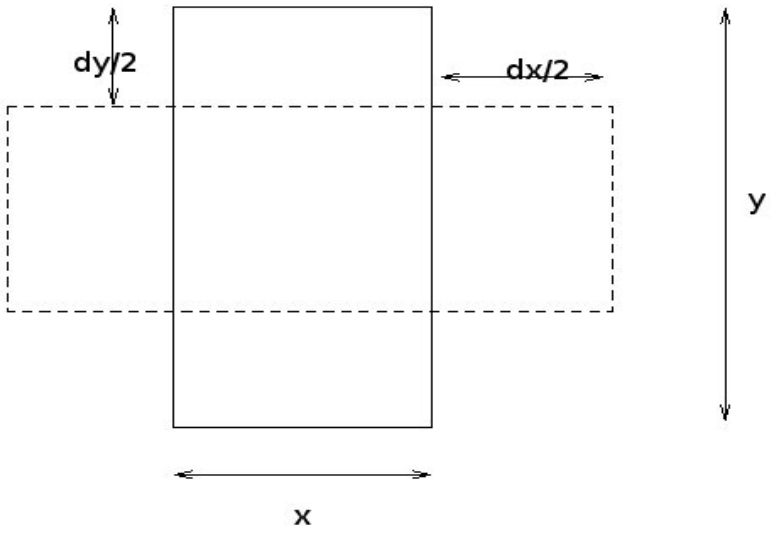

Figure 3.2: The definition of poisson ratio

3.1.2 Principles of measurement of sonic logs

The sonic log measures the travel time of an elastic wave through the formation. This travel time, designated Δt, is referred to as the slowness. It is the inverse of Δt that gives the velocity of the P-wave or S-wave in the formation, hence

$$V = \frac{10^6}{\Delta t} \tag{3.7}$$

where V is velocity in m or ft per second and Δt is slowness in μs per m or ft.

As briefly described earlier, a sonic tool is made up of at least one source (transmitter) and one or more receivers and what it does is to measure the time it takes a sound pulse to travel between a transmitter and a receiver or between two receivers placed at a fixed distance on the tool. The transmitter generates a compressional wave signal (by using a transducer to translate electrical signal into an ultrasonic vibration) which travels through the formation undergoing reflection and refraction at interfaces. This is converted into several modes in the formation, and because the compressional waves are the fastest, they are first to arrive at the receivers. This is followed by the arrival of the shear and Stoneley waves which, in conventional tools, are ignored, but in the

modern array acoustic tools, can be fully measured as will be discussed in the next section.

Sonic logs are presented as interval transit time $\Delta t(\mu s/\text{ft})$ with depth. The reciprocal of these transit times, then yield the velocity as given in equation (3.7) above. If the sonic log is run alone, it is presented in track 2 and 3, but if it is combined with other logs, it is usually put in track 3 (Rider, 2000). When the sonic log is recorded, an integrated travel time (or TTI) is recorded simultaneously. This represents the derived time from the average velocity of the formations logged and is plotted over the vertical depth of the interval in milliseconds.

As with any logging process, there are always some problems or characteristics attached. One of the characteristics of the sonic log is its low depth of investigation. Although it varies from tool to tool, in general the depth of investigation is small and the detected wave is from the immediate borehole wall or the invaded zone in permeable intervals. For any given tool frequency, the higher the velocity in the formation, the higher the wavelength. Another characteristic of a sonic log is the vertical resolution which depends on the receiver spacing (e.g. 2ft), so that beds less than a certain thickness will be registered on the log but a true velocity will not be recorded.

Common problems associated with sonic logging include cycle skipping, and noise triggering; cycle skipping occurs when the first cycle of the wave's first arrival is too weak to activate the receiver so that it is the second or third cycle that is recorded. This generally leads to a "too large" interval transit time. Noise triggering of the receivers causes noise spikes on the log and this makes the receiver measure something different from the time it should have recorded. This phenomenon is found in hard formations such as limestone.

The sonic log finds applications and uses in a variety of disciplines. The primary or principal use of the sonic log is for the evaluation of porosity in liquid- filled holes. It is also used as an aid to seismic interpretation to estimate interval velocities and produce velocity profiles, and can be used for seismic calibration given information from check shots. Also when the density is known, the sonic log is used to produce the acoustic impedance log which is necessary in order to produce a synthetic seismogram. Other uses of the sonic log include lithology identification, stratigraphic correlation, source rock evaluation, and compaction and overpressure identification (Rider, 2000).

3.1.3 The Sonic tool

Tools used for sonic log acquisition have developed over the years. The early tools had one transmitter and one receiver. The body of the tool was made from a low velocity and high attenuation material to stop waves from travelling preferentially down the tool to the receiver. However, two main problems were common with this tool. The tools measured a longer travel time because it was including the time taken for the elastic waves to pass through the mud instead of just measuring the time it takes to pass through the formation. The other problem was that the length of the formation through which the elastic wave travelled was not constant because changes in the velocity of the wave, depending upon the formation, altered the critical refraction angle.

These problems in the early tools were resolved after the invention of the dual receiver tool which still makes use of one transmitter, but has two receivers a few feet apart. The tool was designed to measure the difference in the arrival times of the elastic waves at each receiver from a given pulse from the transmitter. This measured time is called the sonic interval transmit time. However, the tool was also not completely void of limitations. This is because a problem arises when the tool is tilted in the hole, causing a distortion of the geometry or arrangement of the receivers.

In both the early tools and the dual receiver tools, the transmitters were placed at the top of the sondes while the receivers were at the bottom of the sondes. In order to compensate for the problems with tool misalignment and the varying size of holes encountered with the dual receiver tools, the Borehole Compensated Sonic (BHC) tool was developed. The tool had two transmitters and several receivers. The receivers were arranged in two dual receiver sets, but with one set inverted (i.e. in the opposite direction). Each of the transmitters is pulsed alternately, and the interval transit times are measured from alternate pairs of receivers. The average of the interval transit times is then computed to compensate for tool misalignment and to some extent for changes in the borehole size. There are several versions of the BHC tool which depends on the separation between the transmitters and receivers. Normally the distance between pairs of receivers is approximately 2ft for each of the versions.

After the BHC tool, came the Long-spaced sonic (LSS) tool. According to ldeo.columbia.edu (2010), this tool consist of two transmitters (2 feet apart) and two receivers (also 2 feet apart). the receivers and transmitters are 8 to 10 feet apart, depending on the receiver-transmitter position along the tool. The tool makes a measurement by noting the first DT reading and averaging it with the second reading, after the tool has been pulled up along the borehole. due to the long spacing between the receivers and transmitters, the depth of investigation is high, which leads to an improved measurement of the sonic travel time.

An example of a tool which makes use of the principle of borehole compensation, and which was used for the collection of the sonic log examined in this report, is the Dipole Shear Sonic Imager (a tool developed and used by Schlumberger). A brief discussion on its mode of operation follows: The Dipole Shear Sonic Imager (DSSI) acquires travel times of waves using monopole and dipole transmitters. It has one monopole and two electrodynamic dipole transmitters. While the monopole transmitter generates compressional and shear waves in the formation, the dipole transmitter generates flexural wave around the borehole. Depending on which transmitter is fired, four basic operating modes are usually fired in sequence, giving four sets of eight waveforms. (slb.com (2010)). As an example, four basic operating modes of this tool used by Schlumberger are :

- Lower Dipole Mode - which acquires and processes received dipole waveform data from the firings of the lower dipole transmitter for the purpose of making a shear slowness measurement.
- Upper Dipole Mode - which acquires and processes received dipole waveform data from the firings of the upper dipole transmitter for the purpose of making a shear slowness measurement.
- Stoneley Mode - which acquires and processes received monopole waveform data from the firings of the monopole transmitter driven with a low frequency pulse for the purpose of making a low frequency Stoneley wave slowness measurement.
- P and S Mode - which acquires and processes received monopole waveform data from the firings of the monopole transmitter driven with a high frequency pulse for the purpose of

making a monopole compressional and shear wave slowness measurement.

3.2 Processing of Sonic Logs

As discussed earlier, what is actually obtained during a sonic log run is the full waveform which includes the compressional (P), shear (S) and Stoneley (St) waves. The processing of this full waveform entails the identification of each of these waves using special techniques. The separation of these waves, and their inter-relationships such as Poisson's ratio, can provide information on the fractures present in the formation, (from the Stoneley wave amplitude), permeability in porous rocks (from the Stoneley wave amplitude and velocity), determination of porosity in porous rocks (from the compressional wave velocity), lithological correlation (compressional and shear wave velocity), and fluid content (from the compressional and shear wave velocity).

The mechanism or mode of operation of the full wave form sonic tools, especially the dipole shear sonic imager of Schlumberger, has already been discussed and will not be repeated here. However, it must be noted that all tools using an array of receivers acquire a number of receiver measurements from one or more transmitters at each depth station; this number depends on the number of receivers and/or transmitters used. The common data points from a selected interval are then gathered either by using one transmitter position and a full receiver array or by using a sub-array as done by Schlumberger, when several consecutive transmitter and receiver points are used.

When full, digital waveforms are acquired from the receivers depending on the operating mode, in an array at each sampling depth, they must be processed to extract the various waves' arrival times and slowness. At a particular depth, each of the receiver arrays will produce a waveform with different offsets, and one needs to derive the separate P, S and St wave velocities using a specific technique. The derivation of the respective velocities starts by passing the waveforms through a receiver and transmitter array. This produces the final slowness values which are Δt-shear, Δt-Stoneley and Δt-compressional. It is from these values that we obtain the respective P and S wave velocities.

As an illustration of what is being described above, Figure 3.3 shows an acoustic well logging tool and the waveform that was obtained from it .

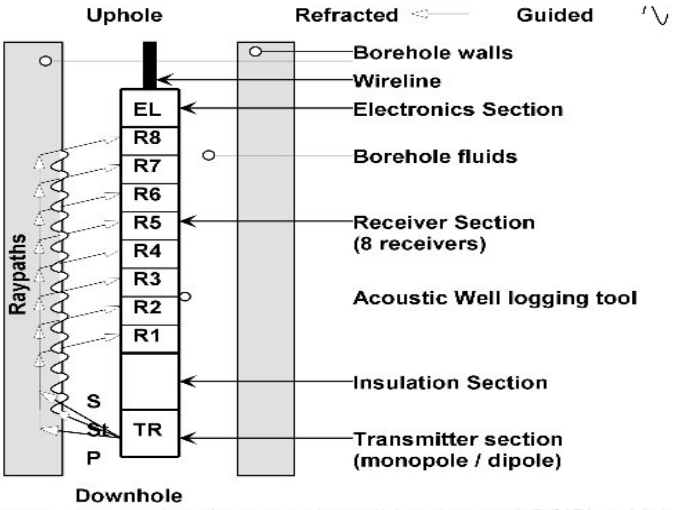

Figure 3. Diagram representing the acoustic well-logging tool DSI™, which was used to acquire the PanCanadian full-waveform data sets (modified after Schlumberger, 1997).

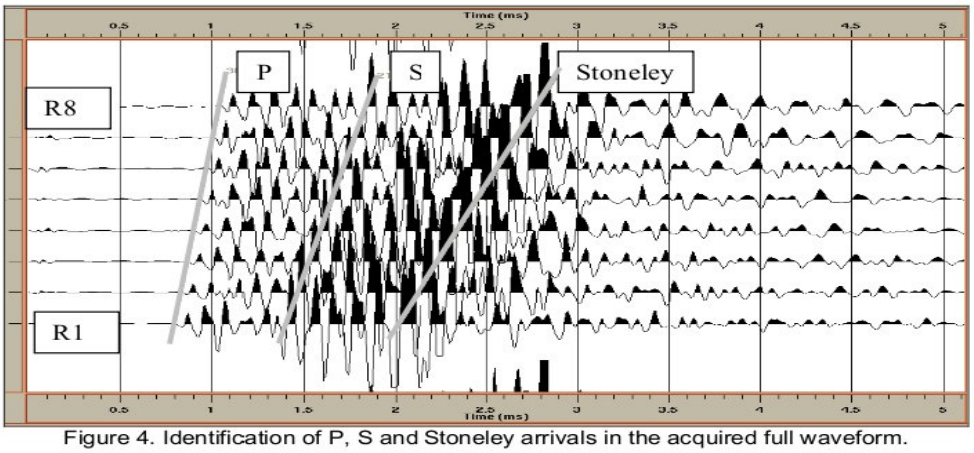

Figure 4. Identification of P, S and Stoneley arrivals in the acquired full waveform.

Figure 3.3: Top: Acoustic well logging tool; Bottom: Acquired full waveform showing the velocities (picture copied from Chabot et al. (2000))

A common error in processing occurs when using a tool with only monopole transmitters present, in slow formations for which it is difficult to extract the shear wave slowness. Often times, the shear velocity is modelled from the available Stoneley information which may be fraught with errors. However, with a dipole transmitter, it is possible (with care) to detect the shear arrival in any kind of formation.

3.3 Interpretation of Sonic Logs

One of the major or primary aims of the sonic log is to calculate the porosity of the rock. The principle is quite simply that there is an increase in travel time (lower velocity) with increase in porosity, and a decrease in travel time (higher velocity) in less porous rock. A complete interpretation of a sonic log includes an understanding of the effects of porosity and perhaps shale content on compressional and shear wave velocities in various rock samples and formations and porosity determination from suitable equations.

Most of the interpretation of a sonic log stems from the information present in the compressional transit time log, and hence from the use of the compressional velocity log. However, applications of the shear wave data have developed over time and it is now very useful in calculating rock elastic and inelastic properties, and as an adjunct to shear seismic data, amongst other uses which will be highlighted later.

In order to be able to calculate the porosity in a formation, apart from having information on the velocity of sound as measured by the sonic logging tool, an important parameter which must be known is the type of rock matrix or grain mineral (sandstone, limestone, dolomite, anhydrite, carbonate, etc.) present in the formation. Also the type of saturating fluid (water, oil, gas) must be known as well. Finally, the shape and distribution of the various pore sizes is another factor which must be known to aid interpretation.

In 1956, Wyllie proposed, for clean and consolidated formations (compacted formations) with uniformly distributed small pores, a time-average equation relating porosity and compressional transit time:

$$\Delta t = \phi \Delta t_f + (1 - \phi)\Delta t_m \tag{3.8}$$

$$\frac{1}{V} = \frac{\phi}{V_f} + \frac{(1 - \phi)}{V_m} \tag{3.9}$$

where Δt and V are the measured compressional transit time and velocity respectively; Δt_f and V_f are the transit time and velocity of the saturating fluid respectively; Δt_m and V_m are the transit time and velocity of the matrix material respectively.

ϕ is the porosity to be determined as

$$\phi = \frac{\Delta t - \Delta t_m}{\Delta t_f - \Delta t_m} \tag{3.10}$$

Ranges of values of sonic velocities and transit time for common rock matrix materials and casing which may be used as inputs to the above equations are listed in tables 3.1 and 3.2.

	$\Delta t_m(\mu s/ft)$	$V_m(m/s)$
Sandstone matrix	55.5-51	5490-5980
Quartz	55.1	5530
Limestones	53-47.6	5750-6400
Calcite	46.5	6555
Dolomites	43-38.5	7090-7920
Dolomite	40	7620
Shale	167-62.5	1830-4880

Table 3.1: Some typical sonic matrix velocities, taken from Rider (2000)

	$\Delta t(\mu s/ft)$	Average Velocity(m/s)
Water (saline)	200-189	1610-1525
Halite	67-66.7	4550-4570
Anhydrite	50	6100
Gypsum	52-53	5860-5750
Anthracite	90-120	3390-2540
Lignite	180-140	1690-2180
casing (steel)	57.8	5270

Table 3.2: Some diagnostic (mineral) velocities , taken from Rider (2000)

Wyllie's equation implies that the measured transit time by the logging tool detectors is a sum of the time the sound pulse spends in the solid matrix and the time spent in the fluid. The equation also applies to carbonates. However, in carbonates, there is often some secondary porosity consisting of vugs or fractures with much larger dimensions than the pores of the primary

porosity. Generally, primary porosity refers to "the porosity remaining after the sediments have been compacted but without considering changes resulting from subsequent chemical action or flow of waters through the sediments" and secondary porosity is "created by chemical changes, dissolution, dolomitization, fissures, and fractures" (spwla.org, 2010).

Suppose the total porosity (ϕ_t) is known, say from the neutron and/or density log, and the primary porosity (ϕ_p) is obtained using Wyllie's equation, the secondary porosity (ϕ_s) can be estimated as

$$\phi_s = \phi_t - \phi_p \tag{3.11}$$

In an uncompacted and unconsolidated formation, Wyllie's equation is not 100% applicable, as it leads to an over-estimation of porosities. Uncompacted formations can be inferred when adjacent shale beds have Δt values greater than 100μs/ft. In such formations, Wyllie's equation can be modified and will take the form

$$\phi = \frac{\Delta t - \Delta t_m}{\Delta t_f - \Delta t_m} \times \frac{1}{B_{cp}} \tag{3.12}$$

where an empirical correction factor, B_{cp} has been added. This factor is best determined by comparing porosities obtained from the original equation with the true porosity obtained from the neutron, density or resistivity log.

For the density log, a cross-plot of density and sonic velocity yields a line which can be scaled in porosity units so that the correction factor can be obtained. In the case of the neutron log, the factor is simply the ratio of the porosity from the Wyllie's equation to that obtained from the neutron log. From the resistivity log, porosity is calculated using Archie's law and the correction factor is obtained as the ratio of the porosity from Wyllie's equation to that obtained using Archie's law.

Shortly after Wyllie's proposed equation for finding porosity, Raymer et al. (1980) proposed another method for calculating the porosity from the sonic log, in what is now referred to as the Raymer-Hunt equation:

$$\frac{1}{\Delta t} = \frac{\phi}{\Delta t_f} + \frac{(1-\phi)^2}{\Delta t_m} \tag{3.13}$$

or

$$V_p = \phi V_f + (1-\phi)^2 V_m \tag{3.14}$$

In this case, the relationship is no longer linear but a quadratic function.

Also, in deriving porosity from sonic logs , it is important to know how the calculated porosity is affected by the volume of shales and the amount of gas present in formations. The effect of shale with high density is to give smaller transit times and hence lower porosities, whereas low density shale in the formation increases the transit time and hence gives too high sonic-derived porosities. For gases, which have low density and therefore decrease the density of a formation, an increase in the transit time results. The decrease in the compressional velocity leads to an overestimation of the porosity. The effect of shale on porosity derived from the sonic log is generally not as great as the effect of gas (Han et al., 1986).

Finally, as stated earlier, while most of the interpretation of a sonic log is in the domain of the compressional velocity, the shear-wave transit time data is also very useful. For example, it is useful in identifying matrix materials and pore fluids when it is cross-plotted with the compressional transit time. This technique is similar to other porosity log cross-plotting techniques such as sonic-neutron. Also, its ability to identify fluids (hydrocarbons) as evident from laboratory observations is another quality of the shear wave velocity, as it increases slightly when measured in a formation that has some hydrocarbon saturation whereas the compressional wave velocity decreases. It should also be noted that the time-average equation which relates compressional transit times to porosity also apply to shear transit time as well, of course with different parameters. This is evident from the relationship between both velocities.

3.4 Seismic Applications of the Sonic Log

The presence of a sonic log in a well that occurs on a seismic line or in a 3-D survey, enables the log data to be used to calibrate and check the seismic data. One of the best ways to tie seismic data back to a "ground truth" is through comparison with a sonic log. This comparison is the

link between seismic travel time and depth from the well log.

While sonic velocities are measured directly from the interval transit time through each formation during a sonic log run, seismic velocities are averages from the surface, deduced statistically to provide the best stack or migration of reflectors in the seismic data. The statistics are quite robust due to the large amount of data required to produce a single seismic trace. Interval velocities may be inferred from the stacking or migration velocities. The fact that both measurement techniques sample very different volumes of rock in order to determine velocity and reflectivity at the same location implies that one should not necessarily expect a one-to-one correspondence between all reflectors seen in the two data sets.

Other differences in the sonic velocities and seismic velocities can be found in their mode of acquisition and tool resolution. While the frequency of the sound pulse used in sonic logging is in the range of 10-40KHz, the pulse in seismic acquisition ranges from 10-50Hz. Also while a sonic logging tool can detect beds down to about 60cm or even thinner, that of the seismic technique is from 10m to 50m, dependency on the velocity and wavelength. However, the higher resolution of the sonic log may enable the log information to resolve indications of beds that are just beyond the resolution of the seismic technique (Rider, 2000).

In order to be able to make an effective comparison of the sonic log data to seismic data, both must be brought to the same scale. It should also be noted that while the sonic log gives a one-way travel time, the seismic technique gives a two-way travel time i.e. time for a seismic signal to reach the reflector and then to return to the receiver geophone.

For sonic log data to be used in seismic interpretation, the results may be presented either as a time-depth curve or interval velocity plot. The interval velocity is found by counting the integrated travel-time marks over an indicated depth interval on the seismic section, and then dividing the depth covered by the time. The result is usually presented in histogram from against depth.

The time-depth curve (Figure 3.4) is obtained by accumulating the travel-times with depth, which will give the total time to a given depth, and plotting this against depth. A time-depth curve obtained in this fashion can be referred to as a sonic-derived time-depth curve. Since the shallow part of the borehole generally does not have a sonic log, the accumulated times are only relative,

whereas the depths are absolute.

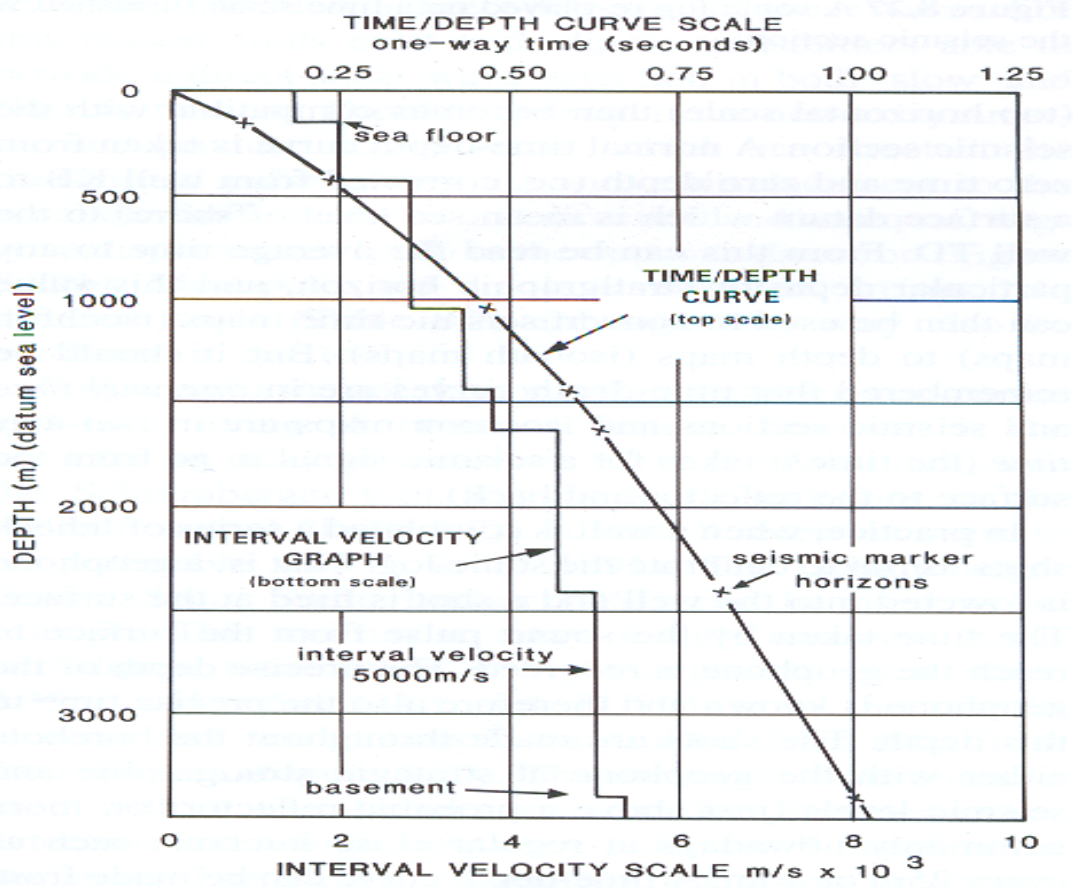

Figure 3.4: The presentation of sonic velocity data to match the scale of seismic data: the time-depth curve and the interval velocity graph. The two horizontal scales are independent: the depth scale is common to both curves. (Rider, 2000)

To solve this problem, a seismic-derived time-depth curve is often obtained to calibrate the sonic log. In this case, a geophone is lowered to a known depth in the well, and "check shots" are fired at the surface in order to measure the time taken for the sound pulse to reach the geophone. The position of the geophone is varied and the shots are fired over again, so that a time-depth curve is made independent of the sonic log.

A synthetic seismogram is a presentation derived from the sonic log data, in the form of a seismic trace. A seismic section, which consists of many seismic traces, is the result of acoustic reflections from subsurface interfaces. These reflections depend on the variation of the acoustic impedances

of the adjacent layers. The synthetic seismogram represents the seismic trace that should be observed with the seismic method at the well location. It is useful to compare such a synthetic seismogram with the seismic trace actually measured at the well to improve the picking of seismic horizons, and to improve the accuracy and resolution of formations of interest. The variation of the acoustic impedances, AI, (velocity $\times$ density) of the adjacent layers is best described by the reflection coefficient (R): where

$$R = \frac{AI_2 - AI_1}{AI_2 - AI_1} = \frac{\rho_2 V_2 - \rho_1 V_1}{\rho_2 V_2 + \rho_1 V_1} \tag{3.15}$$

where the subscript 2 and 1 represents a lower and upper layer of an interface respectively, while ρ, and V are the densities and seismic velocity respectively.

In order to obtain a synthetic seismic response (seismogram), a synthetic wavelet is computed, and convolved with the reflectivity log (on a time scale) derived from the acoustic impedance log. This produces a filtered form of the reflectivity log, which is the synthetic seismogram (Rider, 2000).

There are several items which need to be addressed with the sonic log velocity profile before one can expect it to tie very well with check shot velocity profile because the sonic log is integrated to obtain the sonic, time-depth curve. Any errors are liable to accumulate during the integration. The check shot provides a time-depth curve measured from the surface, whereas the integrated sonic-time is not tied to the surface because the sonic log is not recorded all the way to the surface. The sonic time-depth curve is fitted to the check-shot time depth curve in order to give the absolute times relative to the surface, and also to correct the sonic log integrated times for any remaining errors. Some of the systematic errors or problems which may be present in a sonic log include cycle skips and noise spikes (caused by washed out zones), gaps in sonic log coverage, relative pressure differences between the drilling fluid and the confining stress of the rocks around the well bore, and shale alteration (caused by desiccation of the in-situ shales). The presence of some or all of the above problems reduces the likelihood of achieving a quality tie of the sonic log to the check shot data.

When a better tie is achieved, it can be used for seismic inversions, effective stress calculations,

phase determination, relative wavelet extractions, etc. A major step towards correcting the problems associated with a sonic log described above is to generate a pseudosonic data from other wireline log data, for which the best is often the deep resistivity log because it is not affected by the near borehole environment and it also has adequate vertical resolution to tie to seismic data.

4. Dataset, Geophysical Models and Geophysical Well Log Analysis

4.1 Input Log Data

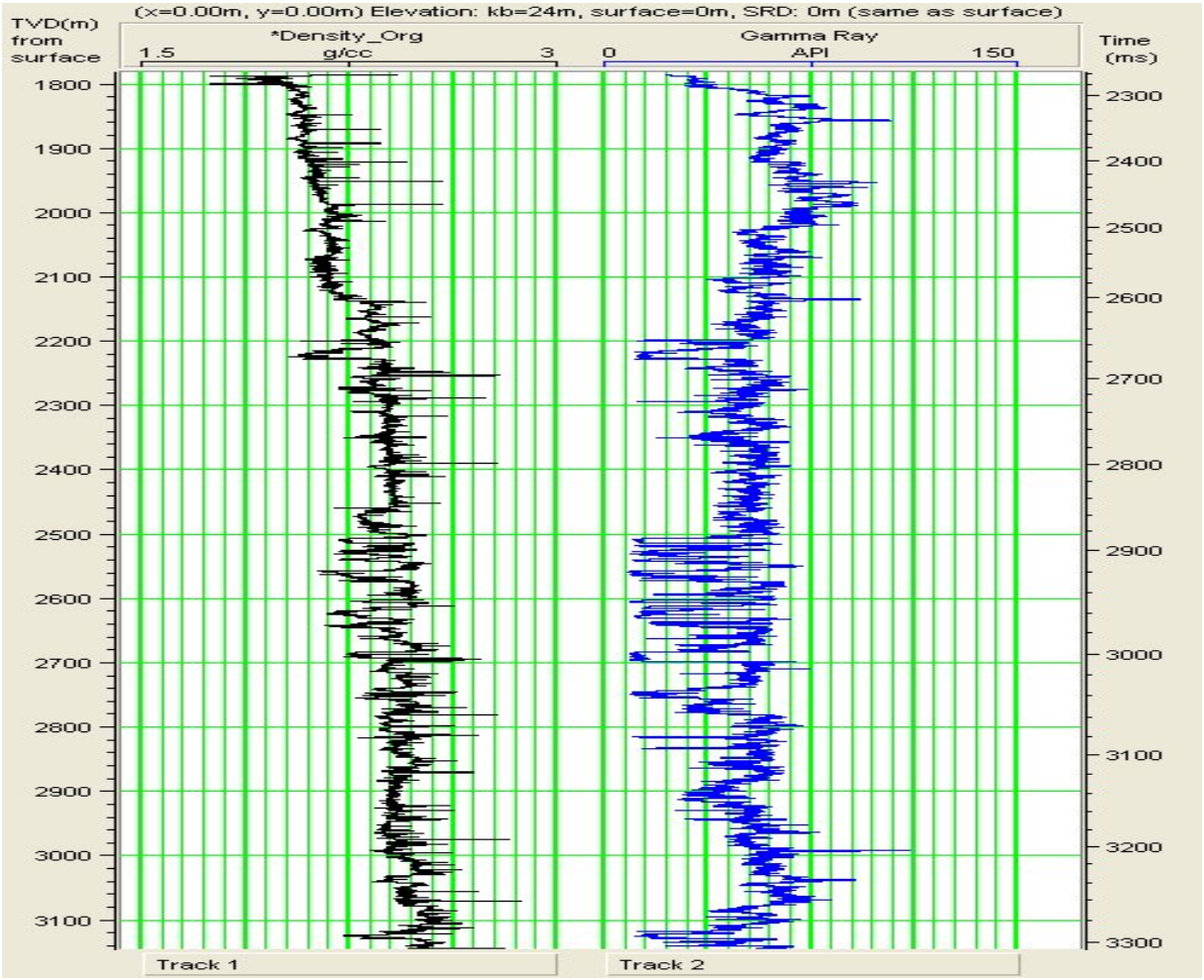

Figure 4.1: Density and Gamma Log

The density log shown in track 1 of Figure 4.1 is used to compute the porosity log and indirectly hydrocarbon density (low density implies high porosity), to correlate lithology and to calculate acoustic impedance. In the shallow part of the borehole ($<$ 2200m), we observe that the density is below 2.2g/cc, and it suddenly increases as we go deep down into the well. This shallow part

comprises of mostly shales.

The gamma ray log shown in track 2 of Figure 4.1 is used to determine the lithology, and estimate shale volume (low gamma implies low Volume of shale). The presence of low density shales between 1800 and 2000m accounts for the high value of gamma shown on the curve; the low gamma value shown around depth 2250m and between 2500 and 2800m is strong evidence of high quality sandstones. The gamma tool was also able to detect more sandstones around a depth of 3150m. Between 2400 and 2500m, is a zone of interbedded sands and shales.

Track 1 of Figure 4.2 shows the combined density and gamma log from which we see that above ≈2160m, the interval is high gamma, low density (shale). Track 2 shows the resistivity log, which will be discussed later.

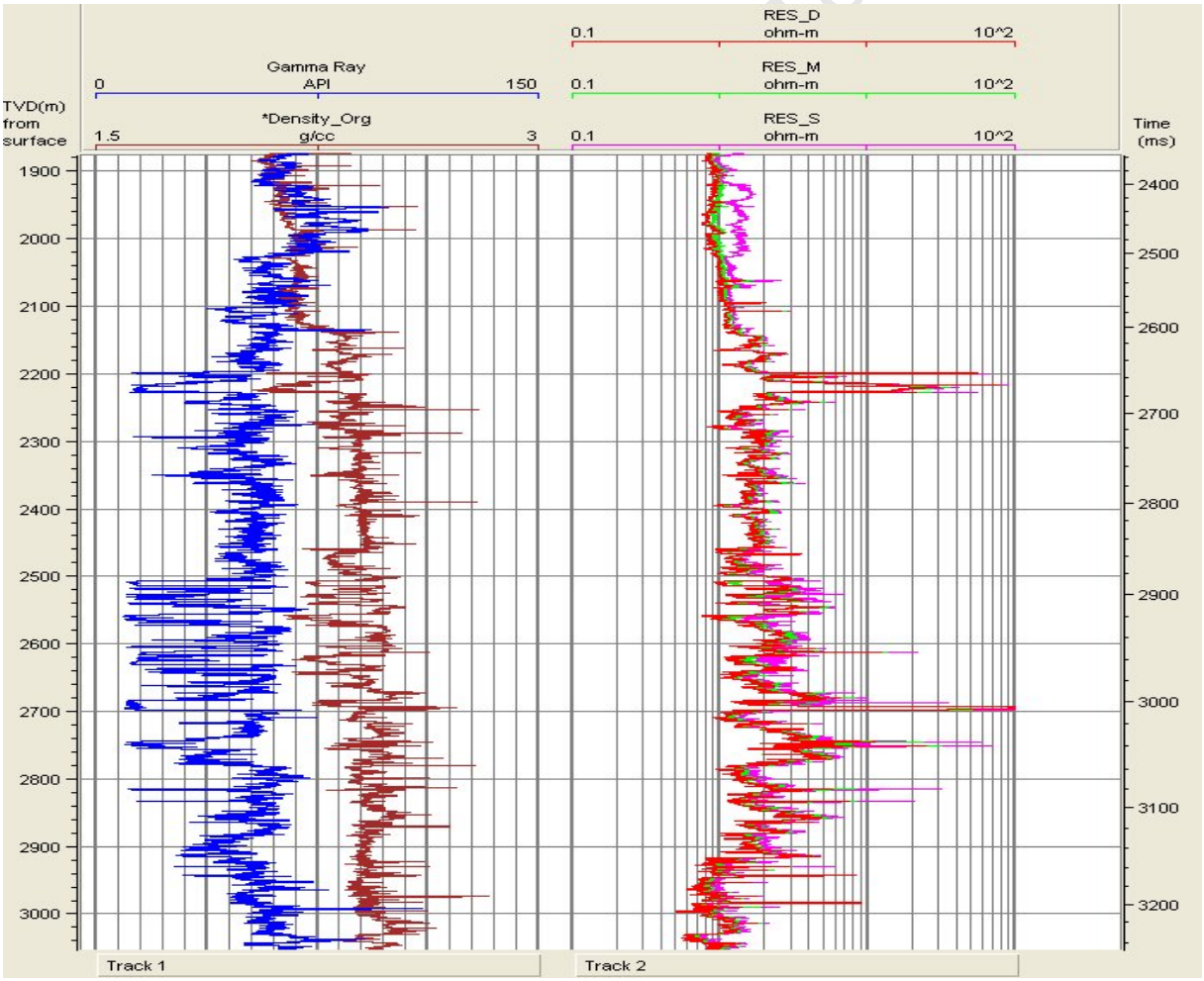

Figure 4.2: Display of density, gamma, and resistivity log

From a compressional transit time log (Δt_{co}) and a shear transit time log (Δt_s) which were collected, the respective velocities (Vp and Vs) are calculated as

$$V_p = \frac{1}{\Delta t_{co}}, \qquad V_s = \frac{1}{\Delta t_{sh}} \tag{4.1}$$

The results are plotted against the borehole depth in track 2 and 3 of Figure 4.3. The plot also shows the gamma log in track 1.

The first set of sonic logs generated which shows the poor quality of the shear wave log is shown in Figure 4.3 as S-wave-org. A look at the P-wave log (between 2600 and 2800m) shows a very high velocity, which was found to be due to carbonates (calcite) found in the zone. We also notice the P-wave velocity ranging from 2500 to 3000m/s in the reservoir zone (identified from the resistivity log as 2200 to 2300m (see Figure 4.2)). Other zones showing high P-wave velocity, will be referred to as the wet sandstone zone ($\approx$ 2600-2800m) and the deep sands ($\approx$ 3200m). The zones between these sand zones are either shale zones or interbedded sand and shale zones.

A look at the shear log in track 3 of Figure 4.3 shows quite a lot of missing values and cycle skips. This was found to be due to the settings made by the drilling company on the tool. The company apparently set a cut-off on the tool so that certain measurements would not be recorded by the dipole shear tool. They had not noticed this during the whole process of the log run. However, there was also a full waveform sonic recording. This was later reprocessed to get a reprocessed P-wave and reprocessed S-wave which was used in this study as the measured shear wave. In Figure 4.3, the missing shear values occur in zones which could be termed as "interesting". Another "interesting" zone is the reservoir or pay zone. A very important observation is that the missing data occured in the wet sands and deep sands; the measured shear wave log is good over the pay zone. However, if there are missing data in some zones, we cannot trust the quality of the remaining data in the other zones. It is as a result of this reason, that the contractor (Well log analysis company) discarded the shear wave log and decided to estimate a shear log from the compressional wave log.

It is in a bid to understand why the company had not requested for a reprocessed shear wave log instead of using an estimated one, that led to this study. I requested for the reprocessed

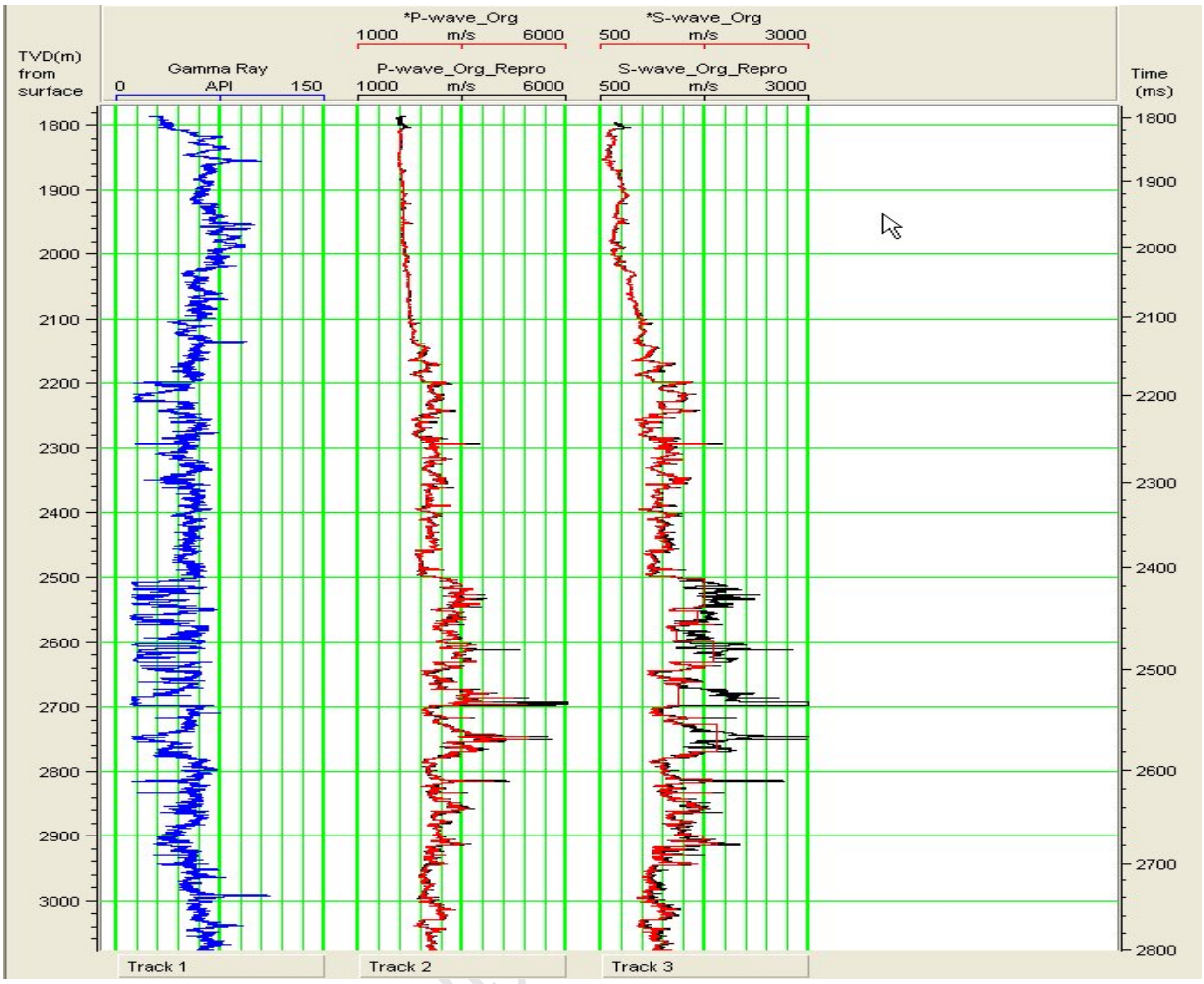

Figure 4.3: Display of gamma and sonic log

shear log and also generated an estimated shear wave log and decided to do the interpretation on both, leading to the two models: measured and estimated, with the aim of suggesting which is better for interpretation. Here we assume safely that the reprocessed shear and compressional log is our measured log, and then we use the reprocessed P-wave log to get an estimated wave. After a reprocessing of the log to remove the cycle skips and missing values, the new sonic log is as shown in Figure 4.3 represented as P-wave-Org-Repro and S-wave-Org-Repro. It also appears to be a little spikier but that has to do with the display parameters. The superposition of the original log and the reprocessed log enables one to see how much of the P-wave changes after reprocessing.

Compressional and Shear velocity log can also be used to estimate porosity (high Vp implies low

porosity) and Impedance. It can also be used for correlating lithology.

4.1.1 Effect of invasion by oil-based mud on sonic and density logs

The density, gamma and sonic logs can not indicate if there was invasion of the sandstones or not, by the oil based mud (versaclean) which was used for drilling. Hence, the resistivity log was also run to determine the possible invaded zones (see track 2 of Figure 4.2). Although, the resistivity log is very useful for estimation of water and hydrocarbon saturation, it is the main key to detecting the zones of invasion. It is very important that the effect of invasion is considered when correcting sonic and density logs, hence a brief discussion of the effect of oil based mud invasion on sonic and density logs, and how it is deduced from the resistivity log, follows:

Figure 4.4 shows how the invading fluid sweeps away the oil sands during drilling. This also occurs in the wet sands depending on the porosity and permeability of the formation. This invasion is caused due to relative pressure difference between the borehole pressure and formation pressure. The effect is that it changes resistivities, densities, electric potentials and affects the quality of sonic, density and other logs which may be reading the invaded zone.

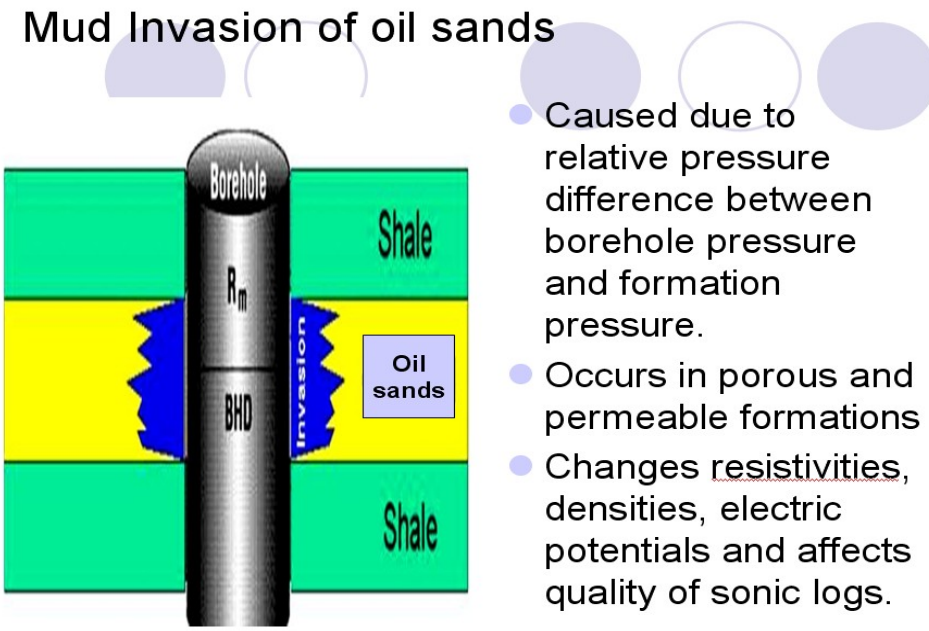

Figure 4.4: Diagram showing mud invasion of oil sands. Walls and Carr (2001)

Mud filtrate invasion affects mostly the density and sonic log because the tools used for measuring and collecting their measurements have lower depths of investigation, depending on the source-detector spacing and on the petrophysical properties of the rock such as porosity, permeability. The smaller the source-detector spacing, the smaller the range of the depth of investigation of the sonic or density tool (ldeo.columbia.edu, 2010). Mud filtrate invasion can cause significant problems when using well log data for correlation to seismic data, as the correct in situ fluid is necessary to create accurate synthetic seismograms. So, in order to get a very good correlation between sonic and seismic, one must first correct the sonic log for invasion.

The first step in correcting logs for invasion is to identify the possible invaded zones and to what extent the invasion occurs, using the multiple array resistivity tool, which gives the resistivity log. As we can see from the Figure 4.2, the AT10 (RES-S) resistivity tool could be measuring the formation being measured by the sonic and density tool, so that we can conveneiently assume that the AT60 (RES-M) or AT90 (RES-D) is measuring the virgin formation, which is what a passing seismic wave would measure. We also safely assume that invasion does not penetrate more than 60 inches.

As stated earlier, the fluid saturation in both the invaded zone and virgin zone is computed from the shallow (AT10 tool) and deep (AT60 or AT90) resistivity log respectively, using Archie's law (see equation 1.1). The water saturation in the invaded zone is labelled Sxo, while the water saturation in the deep zone or virgin formation is labelled Sw.

Oil based mud (OBM) filtrate invasion correction is more difficult than water based mud (WBM) filtrate invasion correction due to the fact that one cannot easily determine the type of invasion profile. Also one needs to consider the type of saturation in the water sands because we have a case of OBM filtrate with brine, unlike brine filtrate with brine in WBM.

The oil based mud filtrate does not completely mix with the formation brine, so one may assume a kind of "'patchy saturation"' for which its treatment is different from the "effective fluid behaviour" (Mavko et al., 2003).

In a recent study by Carr et al. (2004) on oil based mud invasion, they showed the possible kinds of invasion profiles (see Figure 4.5) which may be present in both hydrocarbon saturated

sandstones and water or brine saturated sandstones. Notice that R_{xo} and R_t are the resistivities measured in the shallow and deep zones respectively. Sw is computed from R_t, and Sxo is computed from R_{xo}; S_{wirr} is the irreducible water saturation, which is always present in the pores of the sandstones. From the resistivity log which was provided and the processed log showing the computed Sxo and Sw, we notice that Sxo is lower than Sw in the water saturated sandstones because OBM and brine have different resistivities whereas in the oil sandstones, Sxo is about the same as Sw because OBM and natural oil have very high resistivities.

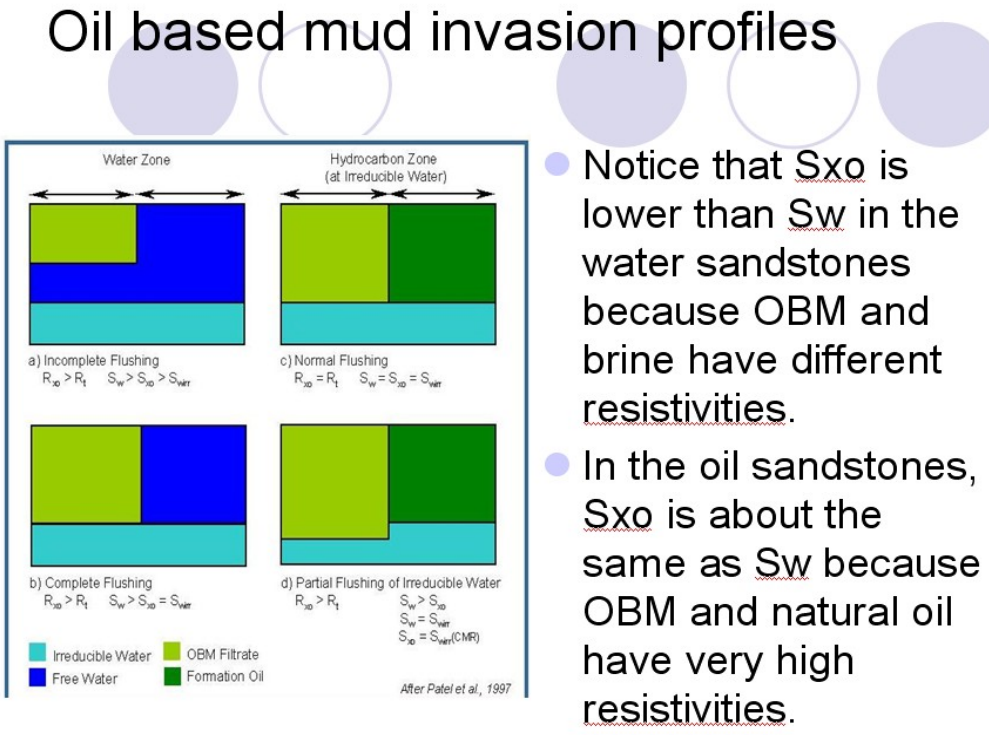

Figure 4.5: Oil based mud invasion profiles. Carr et al. (2004)

4.2 Computation and Methodology

In this section, we attempt to present a simple workflow of the processes involved in the models studied in this project. Two main models were considered namely the Measured shear sonic model and the Estimated shear sonic model. For both models, the extent of invasion of the density and sonic log was not known initially. Also from the resistivity log (as described previously), we

can affirm that there was indeed invasion in the oil and wet sandstones. However, the density log has more probability of reading invaded values than the sonic log. This is beacuse the depth of investigation of the density tool is less than that of the sonic. This could cause a variation in the extent of invasion on the sonic and density logs. It is these assumptions that has led to considering the following possible cases:

- Density log reading invaded zone partially, sonic log not reading invaded zone (likely)
- Density log reading invaded zone partially, sonic log also reading invaded zone partially (most probably)
- Density log reading invaded zone fully, sonic log not reading invaded zone (rarely)
- Density log reading invaded zone fully, sonic reading invaded zone partially (probably)
- Density log reading invaded zone fully, sonic also reading invaded zone fully (not likely)

We have made the above assumptions because the resistivity log implies that at least one of the logs is reading the invaded formation. Oil based mud was used in the drilling, so the extent of mixing of the oil based mud filtrate with the brine in the wet sandstones during invasion needs to be investigated. Naturally, the filtrate will mix well with the oil in the reservoir or oil sands, but this will not be the case in the wet sandstones. This has led to assuming a kind of "patchy saturation" for which the treatment is completely different from the effective fluid behaviour or what is sometimes referred to as "homogeneous" where we assume a proper mixing of the fluid phases. A major difference between the effective fluid behaviour and patchy saturation behaviour is largely a matter of the scales at which the various phases are mixed. There exists a critical relaxation scale L_c, which separates the two domains, and is related to the seismic frequency Mavko et al. (2003). The effective fluid behaviour is achieved when the fluid phases are mixed at the finest scales while the patchy saturation behaviour is achieved when there is the greatest separation of phases.

In order to correct the sonic log assuming a patchy saturation, we make use of the Voigt Average approximation (according to Mavko et al. (2003)) to obtain an effective bulk modulus of the

brine-filtrate mixture.

$$K_f = \sum S_i K_i \tag{4.2}$$

where K_f is the effective bulk modulus of the fluid mixture, K_i denotes the bulk moduli of the individual fluid phases, and S_i represents their saturations. Next, K_f is put into Gassmann's equations to predict the overall rock moduli.

If we do not assume patchy saturation, then we use the effective fluid model which makes use of the Reuss Average Approximation to obtain the effective bulk modulus of the brine-filtrate mixture.

$$\frac{1}{K_f} = \sum \frac{S_i}{K_i} \tag{4.3}$$

where K_f is the effective bulk modulus of the fluid mixture, K_i denotes the bulk moduli of the individual fluid phases, and S_i represents their saturations.

The models being considered will assume a patchy saturation while the "non-patchy" case may be considered in future. Hence, this study does not attempt to discuss the effect of differences in assuming patchy and homogeneous model. The above relations are vital in the application of Gassmann's relations during fluid substitution. However, it must be noted that Gassmann's theory only works in static or very low frequency range. For sonic logging, the velocity of fluid-filled rock could be much different from that of seismic wave. On the other hand, the effective bulk modulus of the patchy saturation model could vary drastically with the frequency (Johnson, 2001). In the paper, he affirmed that his theory of frequency dependent acoustics, in conjunction with relevant experiments, would allow one to deduce information about the sizes and shapes of the patches, or conversely, to make accurate sonic-to-seismic conversion if the size and saturation values are approximately known.

The processing which will go into the models is described in the algorithm below.

1. Use the gamma ray log to ascertain the sandstones (oil and brine) as these are the likely zones of invasion

2. Use the resistivity log to calculate the fluid saturations in the invaded and virgin zone

3. Use the resistivity log and fluid saturations to correct the density log for invasion

4. Correct the reprocessed P-wave and reprocessed S-wave for invasion - this becomes the Measured Shear Wave Model

5. Use the corrected P-wave to compute an estimated S-wave, using the Greenberg-Castagna technique - This becomes the Estimated Shear Wave Model

6. Generate crossplots and 2D synthetics each for the Measured Shear wave model and Estimated Shear wave model

4.3 Density Log Correction

The input resistivity log was used to obtain the degree of water saturation (S_w) and oil saturation (S_o) in virgin formation from Archie's equation, and the log was provided. The gamma ray log (Gr) was used to estimate the shale content (V_{sh}) and therefore the sand content $(1-V_{sh})$ which was also provided. The following parameters were now available to proceed with the computation: measured V_p, measured density (ρ), shale content (V_{sh}), sand content $(1-V_{sh})$, water saturation (S_w) in virgin formation and (S_{xo}) which is water saturation in invaded zone also derived from the resistivity log, oil saturation $(S_o = 1 - S_w)$.

Below is a step by step process of the computations carried out on the sandstones, which were defined by a cut-off on the gamma ray log (i.e. where Gr < 30). I also modeled what the density of the sandstones (oil and water) would be if they had been completely saturated with water, oil or gas. i.e. I did fluid substitution by replacing the oil sands with water or/and gas. I also performed fluid substitution on the wet sands.

1. Calculation of porosity ϕ from the density where

$$\phi = \frac{\rho - \rho_m}{S_{xo}\rho_{brine} - \rho_m + (1 - S_{xo})\rho_{fil}} \tag{4.4}$$

   where ρ_m is the matrix density of quartz sandstone taken as 2.65g/cc, ρ is the measured density from the log, which varies, ρ_{fil} is the density of the mud filtrate if it were to be the water sandstones and ρ_{fil} would be the combined density of the natural oil and filtrate

if it were to be the oil sandstones. ρ_{brine}= 1.09g/cc; ρ_{oil} is the assumed density of oil = 0.75g/cc; ρ_{fil} is the density of mud filtrate (versaclean) $\approx$ 0.77g/cc.

We had assumed that the density log could have been reading a zone that has been fully invaded by the oil based mud but this would mean that S_{xo} is equal to zero which is not the case as deduced from the calculations from the resistivity log. Hence, our assumption of full invasion of the density log is probably invalid and would not be considered further. This therefore reduces our suggested models to two which are

(a) MODEL 1 - Density PARTIALLY invaded, Sonic PARTIALLY invaded

(b) MODEL 2 - Density PARTIALLY invaded, Sonic NOT invaded

2. Perform fluid substitution. i.e model the density of the oil sandstones were they filled with brine or gas. Also model the density of the wet sandstones were they filled with oil or gas i.e. wet case,(ρ_w), oil case,(ρ_o), and gas case(ρ_g) from fluid substitution. In the oil zone, we know what S_o actually is, but by fluid substitution, we would assume 80% oil saturation and 20% brine saturation. The same applies when we do a fluid substitution for the gas case.

$$\rho_w = (1-\phi)\rho_m + \phi\rho_{brine}, \qquad \text{in situ} \tag{4.5}$$

$$\rho_o = (1-\phi)\rho_m + \phi S_o\rho_{oil} + \phi S_w\rho_{brine}, \qquad \text{in situ} \tag{4.6}$$

$$\rho_g = (1-\phi)\rho_m + \phi S_g\rho_{gas} + \phi S_w\rho_{brine} \tag{4.7}$$

where S_g is the gas saturation. For the fluid substitution above, we use $S_g = S_o = 0.8$ and $S_w = 0.2$.

Finally, the corrected density log is obtained from the equations above, where in the oil zones, equation 4.6 holds and in the wet sandstones, the density is given by equation 4.5. A plot of the original and corrected density log is shown in Figure 4.6.

4.4 Sonic Log Correction

Since we have two types of shear wave logs we are dealing with, i.e. the measured and the estimated shear waves, the correction procedure will differ. However, the porosity

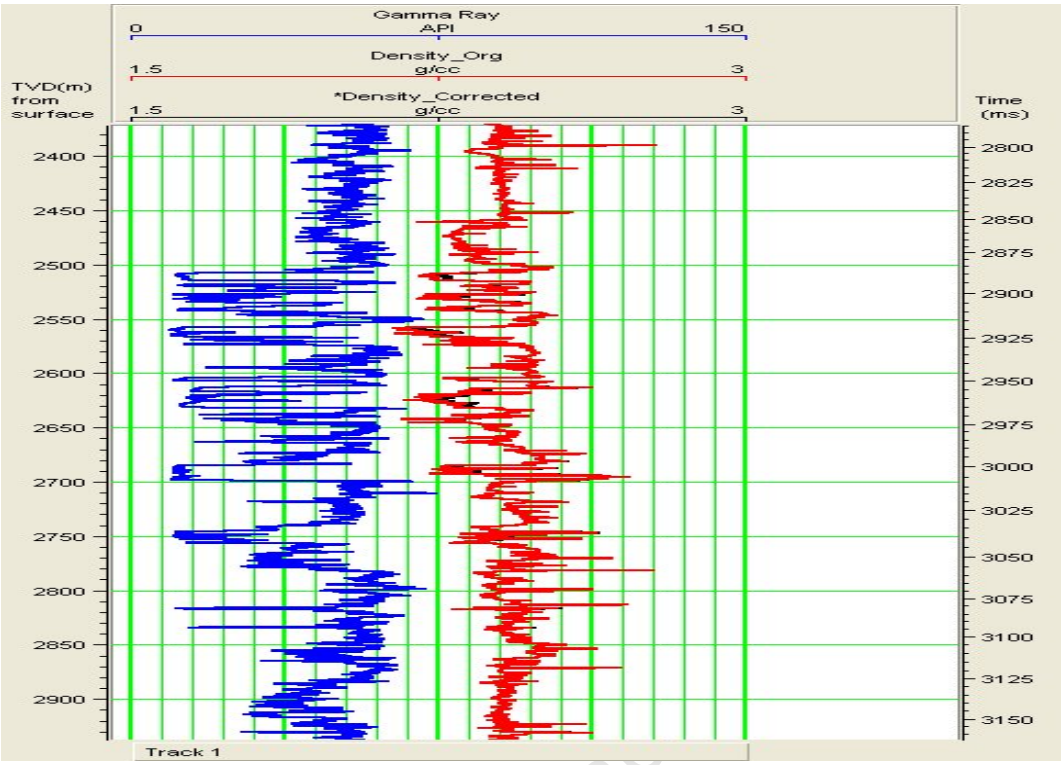

Figure 4.6: Original and corrected density log after invasion

calculated during the density log correction will be used in both cases. First we evaluate the measured Vp and Vs and then we consider how the estimated Vs was obtained, as well as the correction procedure.

4.4.1 Obtaining the Measured Shear wave Log

The correction process on the measured sonic log is as stated below. It is for the case where we assume the sonic log is reading a partially invaded formation. For the assumed case of the sonic not reading the invaded formation, we would use the corrected density calculated in equations 4.5 and 4.6.

(a) Calculate the shear μ and bulk K modulus from the measured density ρ, measured

V_p and V_s (which have been assumed to be partially invaded)

$$\mu = \rho V_s^2 \tag{4.8}$$

$$K = \rho V_p^2 - \frac{4}{3}\mu \tag{4.9}$$

(b) We now proceed with computations using Gassmann's relations for fluid substitution. First we obtain the dry rock bulk modulus K_{dry}

$$K_{dry} = \frac{K_{sat}(\frac{\phi K_m}{K_f} + 1 - \phi) - K_m}{\frac{\phi K_m}{K_f} + \frac{K_{sat}}{K_m} - 1 - \phi} \tag{4.10}$$

where $K_{sat} = K$ has been estimated in the previous step and is in fact the bulk modulus of rock saturated with brine and filtrate or brine, oil and filtrate mixture depending on the zone being considered. K_m is the mineral bulk modulus, for sandstone $\approx$ 40Gpa. ϕ is porosity calculated during correction of the density log in equation 4.4. K_f is the effective bulk modulus of pore fluid, obtained from the Voigt Average approximation, since we have assumed a "patchy" saturation in the wet sandstones. In the oil sandstones we calculate K_f using the Reuss average approximation because the filtrate will mix better with the oil. Therefore, assuming patchy saturation in wet sandstones

$$K_f = S_{xo}K_{brine} + (1 - S_{xo})K_{fil} \tag{4.11}$$

where K_{fil} and K_{brine} are the bulk moduli of the oil mud filtrate and brine respectively. S_{xo} is water saturation in invaded zone. ($K_{fil} \approx$ 1.60Gpa, $K_{brine} =$ 2.38Gpa). K_f is then plugged into equation 4.10 to calculate K_{dry}.

Again, if we assumed the sonic log was not reading the invaded formation, then we would have to further assume that,

In wet sandstones, $S_{xo} = 1$ and K_{fil} is insignificant; In oil sandstones, $S_{xo} = 0$, K_{fil} becomes $K_{oil+brine}$ mixture.

However, as we have seen previously, S_{xo} can neither be zero nor one. Hence, our assumption of the sonic log not reading invaded formation is also probably invalid and would be dropped here. Therefore, the only model we have to work with is that for which we assume that the density log and sonic log are reading a partially invaded formation.

(c) Having obtained K_{dry}, we now model what the bulk modulus of the rock would be if it were saturated with in situ fluids (only brine in wet sands, and oil in oil sands); the bulk modulus of a gas saturated sandstone was also modeled by fluid substitution i.e. we estimate the saturated bulk modulus K_{sat} of the wet case (K_w) , oil case(K_o) , and gas case (K_g) by doing fluid substitution in originally wet sandstones and originally oil sandstones.

$$K_w = K_{dry} + \frac{(1 - \frac{K_{dry}}{K_m})^2}{\frac{\phi}{K_{f_w}} + \frac{1-\phi}{K_m} - \frac{K_{dry}}{K_m^2}}, \qquad K_{f_w} = K_{brine} \tag{4.12}$$

$$K_o = K_{dry} + \frac{(1 - \frac{K_{dry}}{K_m})^2}{\frac{\phi}{K_{f_{ow}}} + \frac{1-\phi}{K_m} - \frac{K_{dry}}{K_m^2}}, \qquad K_{f_{ow}} = \left(\frac{S_w}{K_{brine}} + \frac{1 - S_w}{K_{oil}}\right)^{-1} \tag{4.13}$$

$$K_g = K_{dry} + \frac{(1 - \frac{K_{dry}}{K_m})^2}{\frac{\phi}{K_{f_{gw}}} + \frac{1-\phi}{K_m} - \frac{K_{dry}}{K_m^2}}, \qquad K_{f_{gw}} = \left(\frac{S_w}{K_{brine}} + \frac{1 - S_w}{K_{gas}}\right)^{-1} \tag{4.14}$$

The assumed bulk modulus of the fluids are K_{brine} = 2.38Gpa, K_{oil} = 1.5Gpa , K_{gas} = 0.021Gpa.

(d) With the respective densities calculated in the previous section, shear modulus μ estimated in the first step(which is independent of the saturating fluid), and the K_{sat} obtained in the previous step, we can now obtain the corrected V_p and V_s for the rocks saturated with the respective in situ fluids.

$$V_{P_w} = \sqrt{\frac{K_w + \frac{4}{3}\mu}{\rho_w}}, \qquad V_{S_w} = \sqrt{\frac{\mu}{\rho_w}} \tag{4.15}$$

And

$$V_{P_o} = \sqrt{\frac{K_o + \frac{4}{3}\mu}{\rho_o}}, \qquad V_{S_o} = \sqrt{\frac{\mu}{\rho_o}} \tag{4.16}$$

And

$$V_{P_g} = \sqrt{\frac{K_g + \frac{4}{3}\mu}{\rho_g}}, \qquad V_{S_g} = \sqrt{\frac{\mu}{\rho_g}} \tag{4.17}$$

Finally, the corrected sonic log is obtained from the equations above, where equation 4.15 and 4.16 gives the corrected sonic log in the wet sandstones and oil sandstones respectively.

A plot of the original (measured and reprocessed) sonic log and the corrected log is shown in tracks 2 and 3 of Figure 4.7. Figure 4.8 and 4.9 has been added to show how much the Vp and Vs changed respectively, after correction for mud invasion.

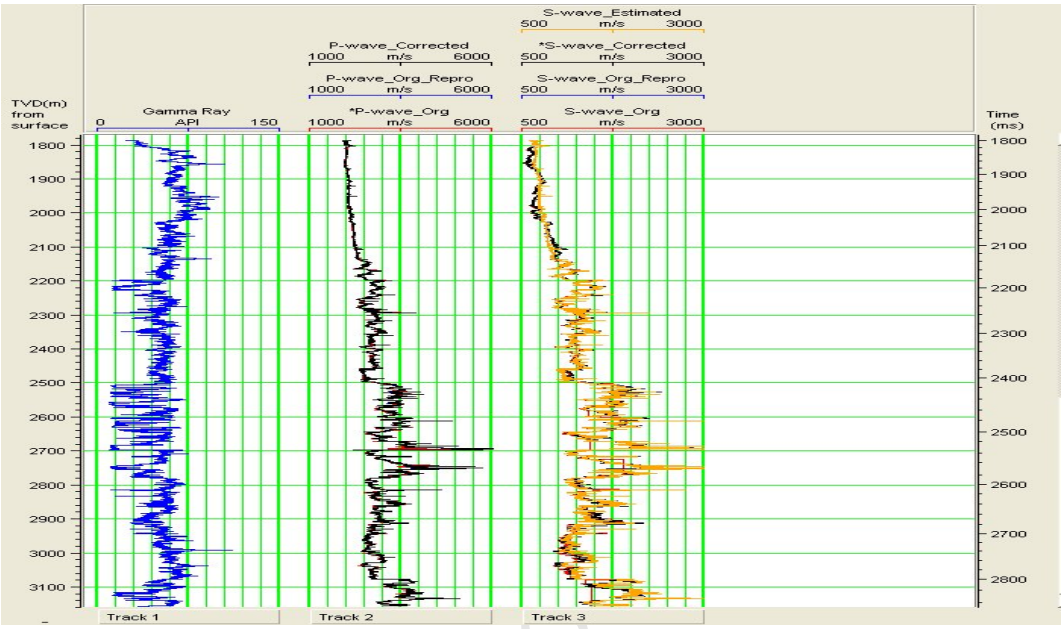

Figure 4.7: Original and corrected sonic log after invasion

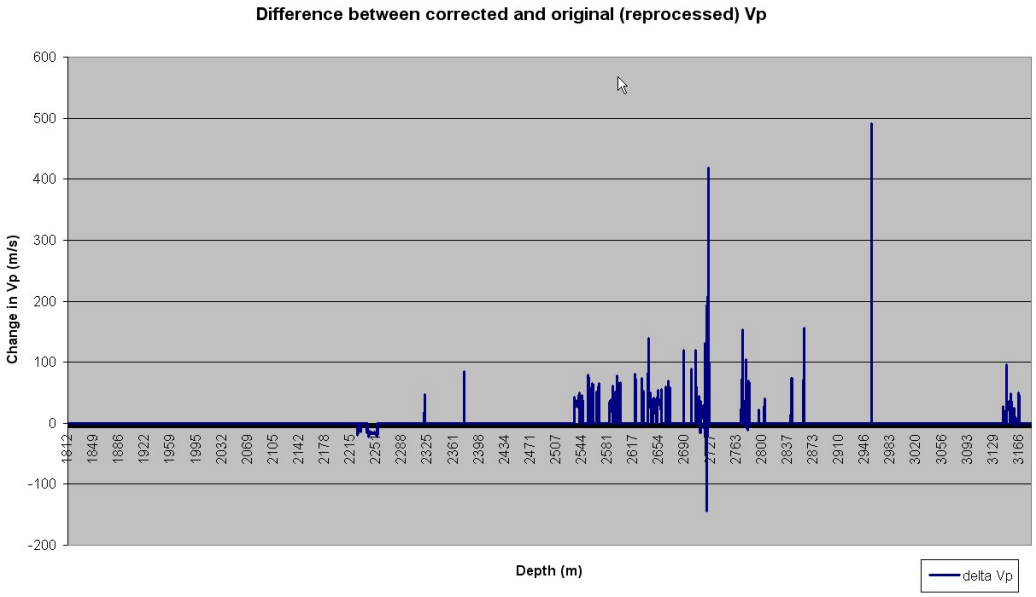

Figure 4.8: Difference plot of original and corrected Vp

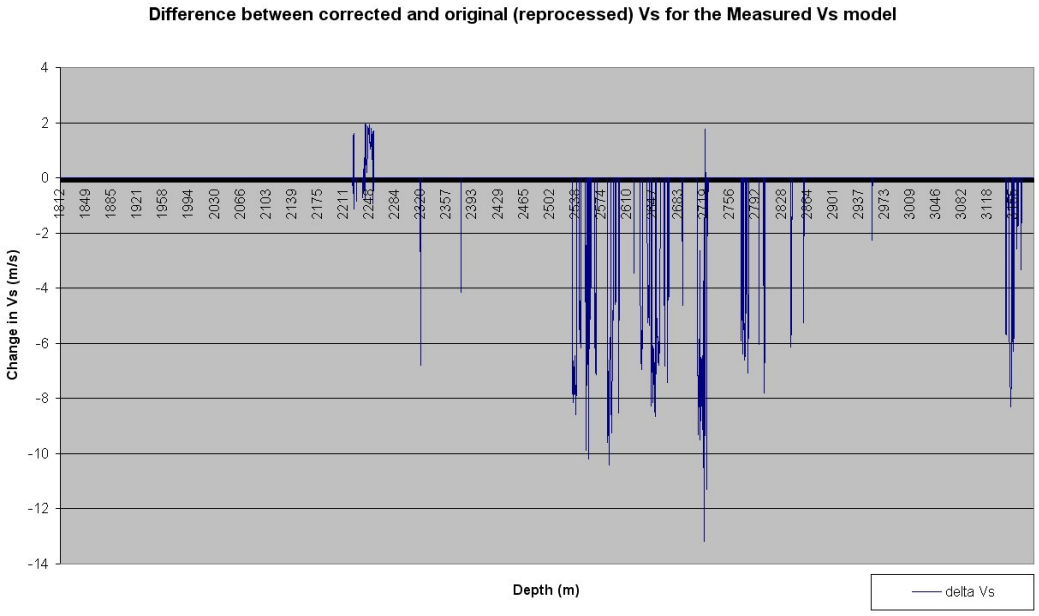

Figure 4.9: Difference plot of original and corrected Vs (measured)

4.4.2 Estimating a Shear wave velocity from the corrected P-wave velocity

Most empirical relations for estimating a Vs from a Vp assume that the sandstones must be water saturated. An example of such estimation procedure is that of Greenberg-Castagna which is briefly described below

(a) Calculation of an estimated shear wave velocity (sandstones must be water saturated), Vs from the measured Vp(in km/s), using Greenberg-Castagna relation, which accounts for the shale and sand content. The regression for pure lithologic constituents gives us

$$V_{s-sand} = 0.80416V_p - 0.85588 \tag{4.18}$$

$$V_{s-shale} = 0.76969V_p - 0.86735 \tag{4.19}$$

(b) Computation of the weighted arithmetic and harmonic means being

$$V_{s-arith} = (1 - V_{sh})V_{s-sand} + (V_{sh} \times V_{s-shale}) \tag{4.20}$$

$$V_{s-harm} = (\frac{1 - V_{sh}}{V_{s-sand}} + \frac{V_{sh}}{V_{s-shale}})^{-1} \tag{4.21}$$

so that the estimated Vs is given by

$$V_s = \frac{1}{2}(V_{s-arith} + V_{s-harm}) \tag{4.22}$$

which is finally converted to metres per second (m/s).

A problem arises when we have an oil saturated sand, and we need to estimate a Vs from the measured Vp. In our case, all the sands (oil and wet) have been invaded by oil based mud. In order to get around this problem, we begin with the fluid substitution technique. However, since there is no Vs, we cannot use the Gassmann's equation directly, as the calculation requires the shear modulus which is derived from the shear velocity.

To solve this problem, we consider the suggestion of Mavko et al. (1995). They suggested an approximate form of Gassmann's equations, which operates directly on the P-wave modulus, $M = \rho V_p^2$. It replaces the bulk moduli of the rock and mineral in Gassmann's relation with the corresponding P-wave moduli, i.e. Equation 4.10 becomes

$$M_{dry} = \frac{M_{sat}\left(\frac{\phi\, M_m}{M_f} + 1 - \phi\right) - M_m}{\frac{\phi\, M_m}{M_f} + \frac{M_{sat}}{M_m} - 1 - \phi} \tag{4.23}$$

where $M_{sat},\ M_{dry},\ M_m,$ and M_f are the P-wave moduli of the saturated rock, the dry rock, the mineral, and the pore fluid, respectively. In this case, $M_{sat} = M_{sat}$ oil and filtrate $= \rho_b\, V_p^2$.

Since $M = \rho V_p^2 = K + \frac{4}{3}\mu$, (where ρ and V_p are the measured density and P-wave velocity respectively),

$$M_m = K_m + \frac{4}{3}\,\mu_m$$

So that for sandstone with assumed values of $K_m = 40\,GPa$ and $\mu_m = 33\,GPa$, $M_m = 84\,GPa$. Since we know the values of M_{sat}, M_m, and ϕ, which was used in the previous

section during the density correction, the next step is to estimate the P-wave moduli of the pore fluid and it is the same assumption and process that was followed in the previous section for the measured shear wave log that would be used.

Assuming patchy saturation in wet sandstones,

$$M_f = S_{xo}M_{brine} + (1 - S_{xo})M_{fil}$$

where M_{brine} and M_{fil} are the P-wave moduli of the brine and the mud filtrate respectively. S_{xo} is still the water saturation in the invaded zone. ($M_{fil} \approx$ 1.60Gpa, $M_{brine} =$ 2.38Gpa) Plugging M_f into equation 4.23 allows us to be able to estimate M_{dry}. In the above calculations, we have used the fact that μ_f (shear moduls in a fluid) is zero.

Having obtained M_{dry}, we do a fluid substitution of brine in the sandstones, by calculating M_w (the P-wave moduli of the sandstones assuming they were saturated with brine) using the modified Gassmann's relation

$$M_w = M_{dry} + \frac{\left(1 - \frac{M_{dry}}{M_m}\right)^2}{\frac{\phi}{M_{f_w}} + \frac{1-\phi}{M_m} - \frac{M_{dry}}{M_m^2}} \tag{4.24}$$

where $M_{f_w} = 2.38GPa$ for brine. The above then gives us the P-wave moduli of the rock saturated with 100% brine.

The next step in the process is to find the V_{p_w} (the P-wave velocity of the rock saturated with brine) from M_w i.e.

$$V_{p_w} = \sqrt{\frac{M_w}{\rho_w}} \tag{4.25}$$

where ρ_w is the density of the rocks saturated with brine calculated in equation 4.5.

M_o (the P-wave moduli of the sandstones assuming they were saturated with oil which is the real situation in the sandstones) is calculated as

$$M_o = M_{dry} + \frac{\left(1 - \frac{M_{dry}}{M_m}\right)^2}{\frac{\phi}{M_{f_{ow}}} + \frac{1-\phi}{M_m} - \frac{M_{dry}}{M_m^2}}, \qquad M_{f_{ow}} = \left(\frac{S_w}{M_{brine}} + \frac{1 - S_w}{M_{oil}}\right)^{-1} \tag{4.26}$$

($M_{brine} = K_{brine} = 2.38Gpa, M_{oil} = K_{oil} = 1.5Gpa, S_w = 0.2$) From the P-wave moduli, the P-wave velocity of the rock saturated with oil is

$$V_{p_o} = \sqrt{\frac{M_o}{\rho_o}}.$$

where ρ_o is the density of the rocks saturated with oil calculated in equation 4.6.

M_g (the P-wave moduli of the sandstones assuming they were saturated with gas by fluid substitution) is calculated as

$$M_g = M_{dry} + \frac{\left(1 - \frac{M_{dry}}{M_m}\right)^2}{\frac{\phi}{M_{f_{gw}}} + \frac{1-\phi}{M_m} - \frac{M_{dry}}{M_m^2}}, \qquad M_{f_{gw}} = \left(\frac{S_w}{M_{brine}} + \frac{1-S_w}{M_{gas}}\right)^{-1} \tag{4.27}$$

($M_{brine} = K_{brine} = 2.38Gpa, M_{gas} = K_{gas} = 0.021Gpa, S_w = 0.2$).

From the P-wave moduli, the P-wave velocity of the rock saturated with gas is

$$V_{p_g} = \sqrt{\frac{M_g}{\rho_g}}.$$

where ρ_o is the density of the rocks saturated with gas calculated in equation 4.7.

In our estimation process, we did not use the constants of Greenberg-Castagna, as the crossplot of the reprocessed Vp and Vs for sands and shales was calibrated to obtain my constants. The plots are shown in Figures 4.10 and 4.11. The resultant equations obtained are

$$V_{s-sand} = 0.7831V_p - 0.8358 \tag{4.28}$$

$$V_{s-shale} = 0.7703V_p - 0.8473 \tag{4.29}$$

Having found V_{p_w} in equation 4.25, my constants are then used to obtain the arithmetic and harmonic shear velocities as described earlier by the Greenberg-Castagna procedure for finding Vs, which finally leads to the estimation of the V_{s_w} (S-wave velocity of rock saturated with brine), as explained above. With V_{s_w}, and ρ_w, μ (which is independent of the fluid saturating the rock) is estimated as

$$\mu = \rho_w V_{s_w}^2 \tag{4.30}$$

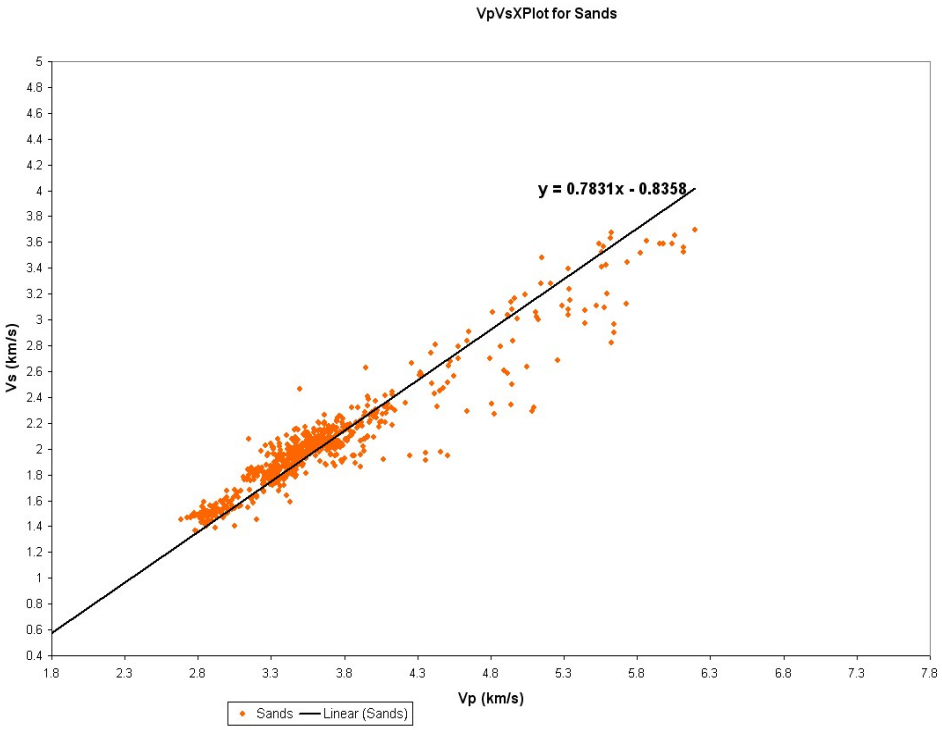

Figure 4.10: Vp and Vs crossplot for sands

From the μ calculated, we can estimate the shear wave velocity for the rocks assuming they were saturated with oil (which is the real situation in the oil sandstones) or gas.

$$V_{s_o} = \sqrt{\frac{\mu}{\rho_o}}, \qquad V_{s_g} = \sqrt{\frac{\mu}{\rho_g}} \tag{4.31}$$

After obtaining the velocities and densities, the next step is the computation of the respective impedances (P-wave and S-wave Impedances). If P-wave impedance is I, and S-wave impedance is J,

$$I_w = \rho_w \times V_{p_w}, \qquad J_w = \rho_w \times V_{s_w} \tag{4.32}$$

$$I_o = \rho_o \times V_{p_o}, \qquad J_o = \rho_o \times V_{s_o} \tag{4.33}$$

$$I_g = \rho_g \times V_{p_g}, \qquad J_g = \rho_g \times V_{s_g} \tag{4.34}$$

where the subscripts w,o,g, represents wet case, oil and gas case respectively.

After estimating the shear wave velocity, a plot of the difference between its value and the

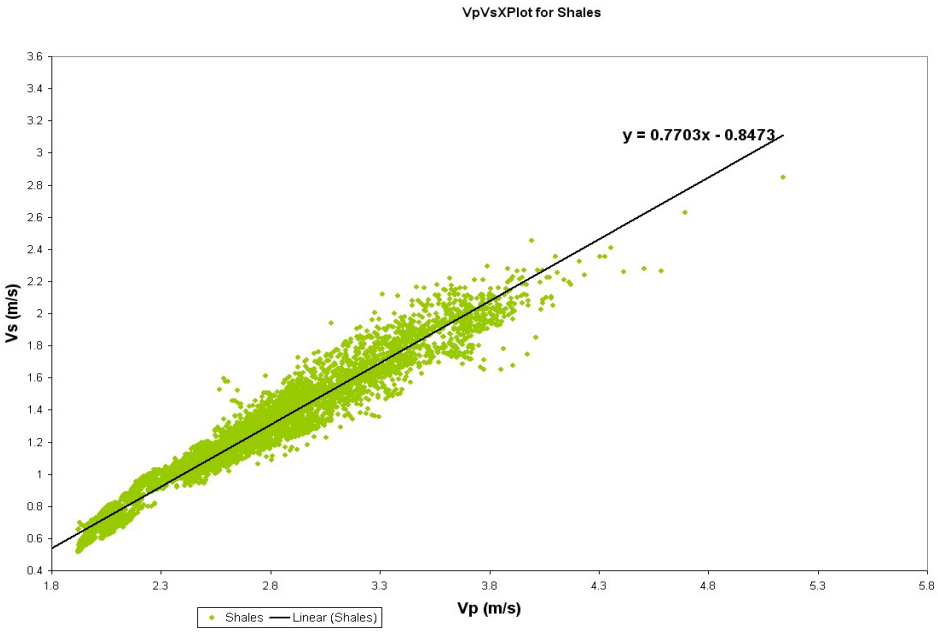

Figure 4.11: Vp and Vs crossplot for shales

corrected measured value, is shown in Figure 4.12. This is the difference between the shear wave logs used in the seismic modelling which is described in Chapter 5.

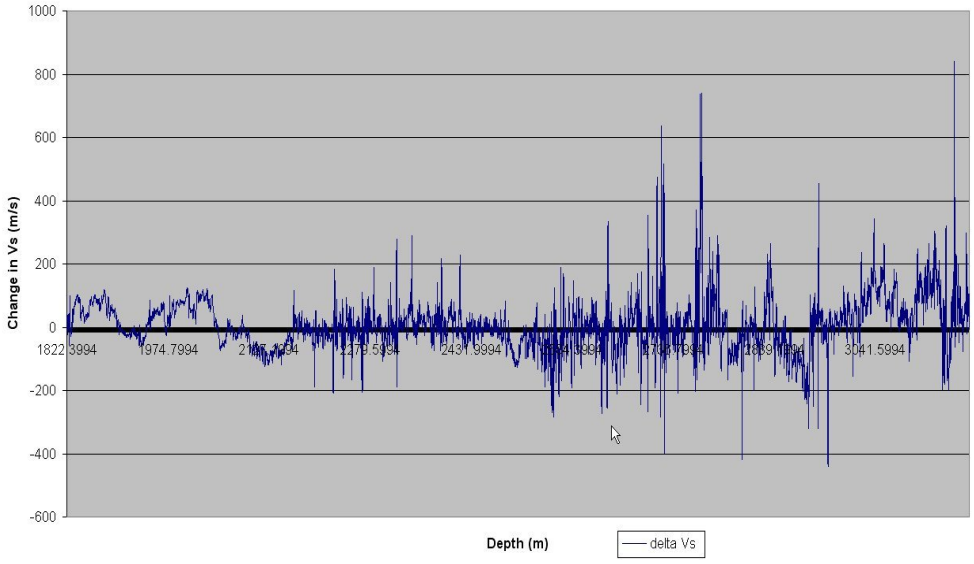

Figure 4.12: Difference plot of corrected Vs (measured) and corrected Vs (estimated)

Cross plots of velocities (V_p and V_s) for the wet case and oil case in both the reservoir zone and the water bearing sand zones, are made and are discussed in section 4.5.1 and 4.5.2 below.

4.5 Comparing models based on crossplots

Having completed the correction based on the assumption that the sonic and density logs were reading a partially invaded formation, both for the Measured shear log and the Estimated shear log, one quick way of analysing the results is by making crossplots of the compressional velocity and shear velocity. The alignment of the sand and shale lines and points might aid one in understanding which could be a better model. Also the extent of invasion may be observed in these cross plots. The separation of the respective fluid phases is also another feature to watch out for. In order to observe the effect of correction of the logs especially the sonic log, it is important to plot the original data points (oil and wet sandstones) and the points which are generated after the correction has been made. Figure 4.13 shows what the crossplot of Vp and Vs look like before the correction. The shale points have been plotted in lime; the oil sandstones plotted in bright green, while the wet sandstones have been plotted in orange.

4.5.1 Vp and Vs Crossplots for the Measured Sonic Model

Track 4 of figure 4.14 shows the combined plot of the reprocessed shear wave log and the corrected (measured) shear wave log. The display is actually over a smaller depth interval, where the pay zone is.

After correction of the measured logs, having assumed partial invasion by patchy saturation, the crossplot shown in Figure 4.15 is what results. It shows how the measured oil sands initially in bright green changes to the corrected oil sands (green), and how the measured wet sands initially in orange changes to the corrected wet sands (blue). From this crossplot, we can clearly see that the invasion affects mostly the wet sands and the change is very significant. This is not the case in the oil sandstones since the oil mud filtrate and the natural oil have almost the same resistivity and density. It is almost as if invasion did not occur in the oil sandstones. The shale points

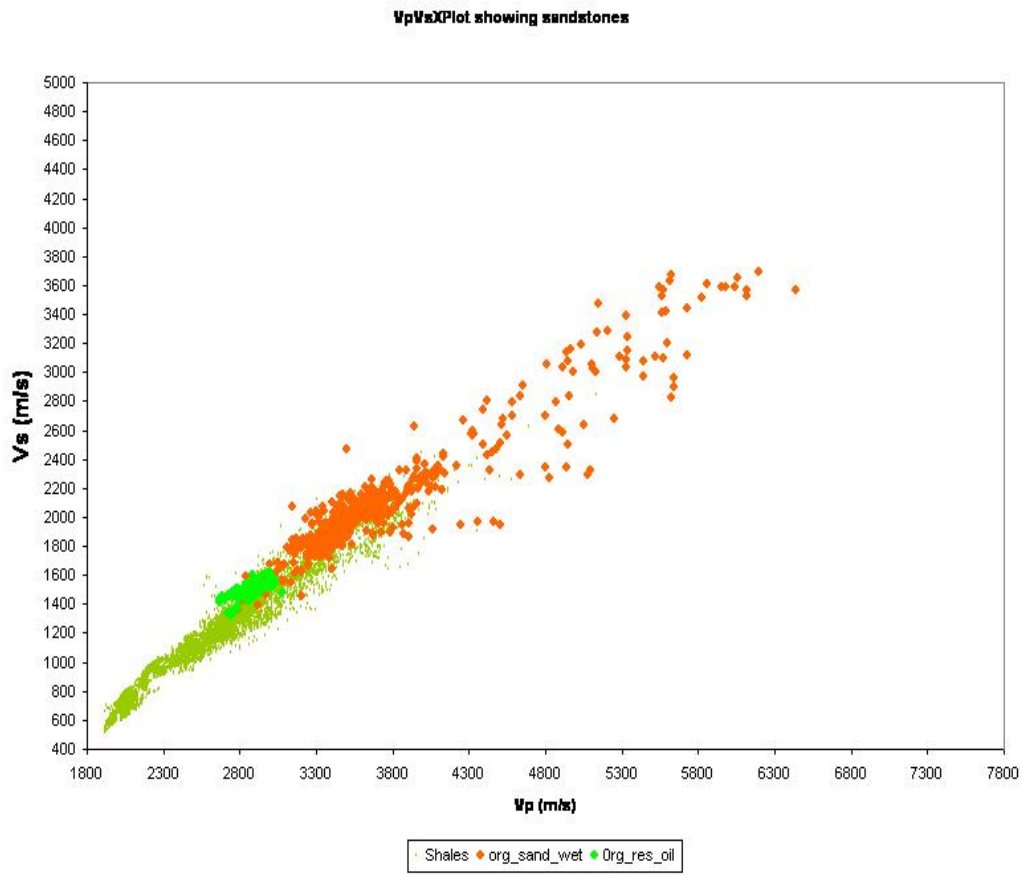

Figure 4.13: Original crossplot of Vp and Vs before correction - green(oil sands),orange(wet sands), lime(shales)

remain the same as no correction was done on them because invasion does not affect shales due to their low permeability.

After performing fluid substitution, i.e. placing brine in the oil sandstones and placing oil in the water sandstones, the Vp-Vs crossplot which we obtained is shown in Figure 4.16. From the plot, we see that, in the oil sands, the new water points move towards the right, which is an indication that the compressional velocity of sound in water sandstones is higher than that in oil sandstones. It appears that the wet sands decrease velocity when corrected for invasion for values around Vp $=$ 4500m/s but increase velocity for Vp around 5800m/s. this appearance is caused by the presence of carbonates in that zone i.e. it seems we have corrected carbonates and not sandstones. Also a look at the wet sandstones shows that the measured log in the wet

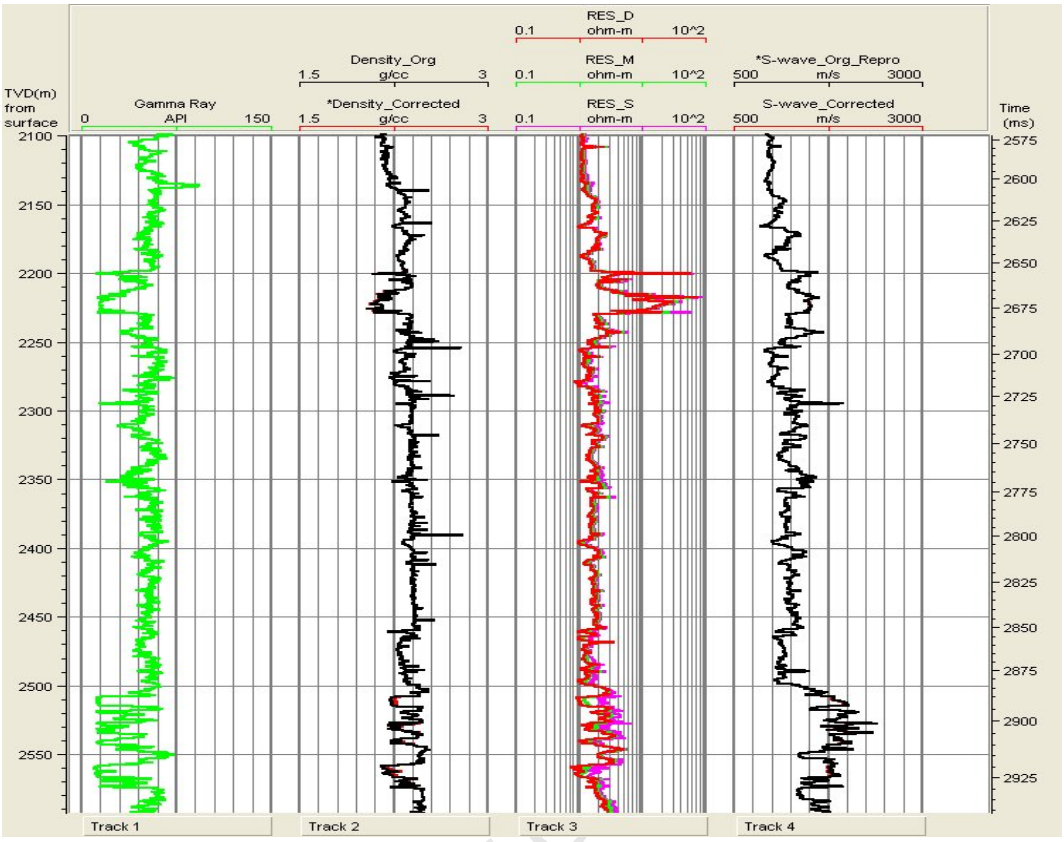

Figure 4.14: Suite of logs showing effect of correction on the shear wave log after reprocessing

sandstones was actually reading the invaded zone as the new oil points just seem to lie on the measured wet sandstone points.

4.5.2 Vp and Vs Crossplots for the Estimated Sonic Model

For the case of the estimated shear log, in order to observe the effect of correction of the logs, we must plot the original data points (oil and wet sandstones) and the points which are generated after the correction and estimation has been done. Track 4 of figure 4.17 shows the combined plot of the reprocessed shear wave log and the corrected (estimated) shear wave log. It is also plotted over a smaller depth range showing the pay zone.

Figure 4.18 shows what the crossplot of Vp and Vs (which was discarded) look like before the correction and estimation process started. The shale points have been plotted in lime; the oil sandstones plotted in bright green, while the wet sandstones have been plotted in blue, just as

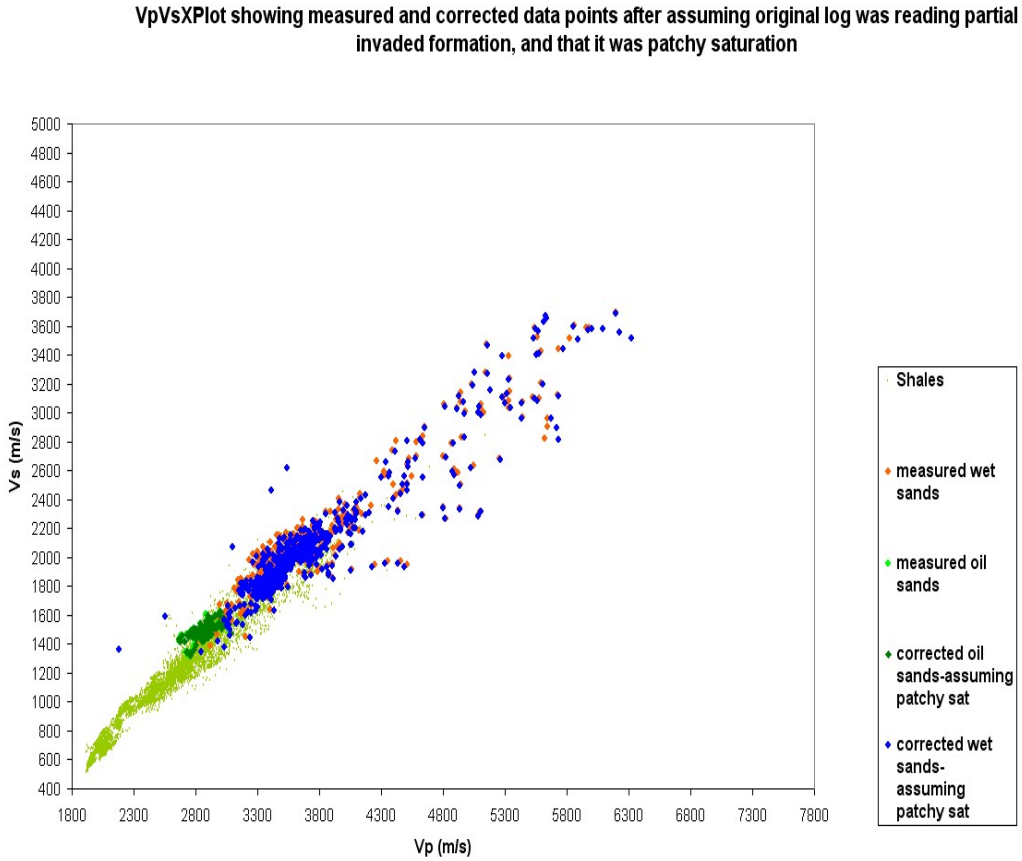

Figure 4.15: Crossplot of Vp and Vs after correction assuming original log was partially invaded by patchy saturation

was done for the measured shear wave model in the previous section.

After correction and estimation of the shear velocity has been done, having assumed partial invasion by patchy saturation, the crossplot shown in Figure 4.19 is what results. It shows how the measured oil sands initially in green and dispersed, changes to the corrected oil sands (green) in a straight line, and how the measured wet sands initially in blue and dispersed, also changes to the corrected wet sands (blue) also in a straight line. From this crossplot, it is difficult to tell the extent of invasion. The crossplot shows a good separation between the oil and wet sandstones. It also shows a good and fine line between the sands and shales, a feature which is not easily noticed in the crossplot of the measured shear wave model.

After performing fluid substitution, i.e. placing water in the oil sandstones and placing oil in the

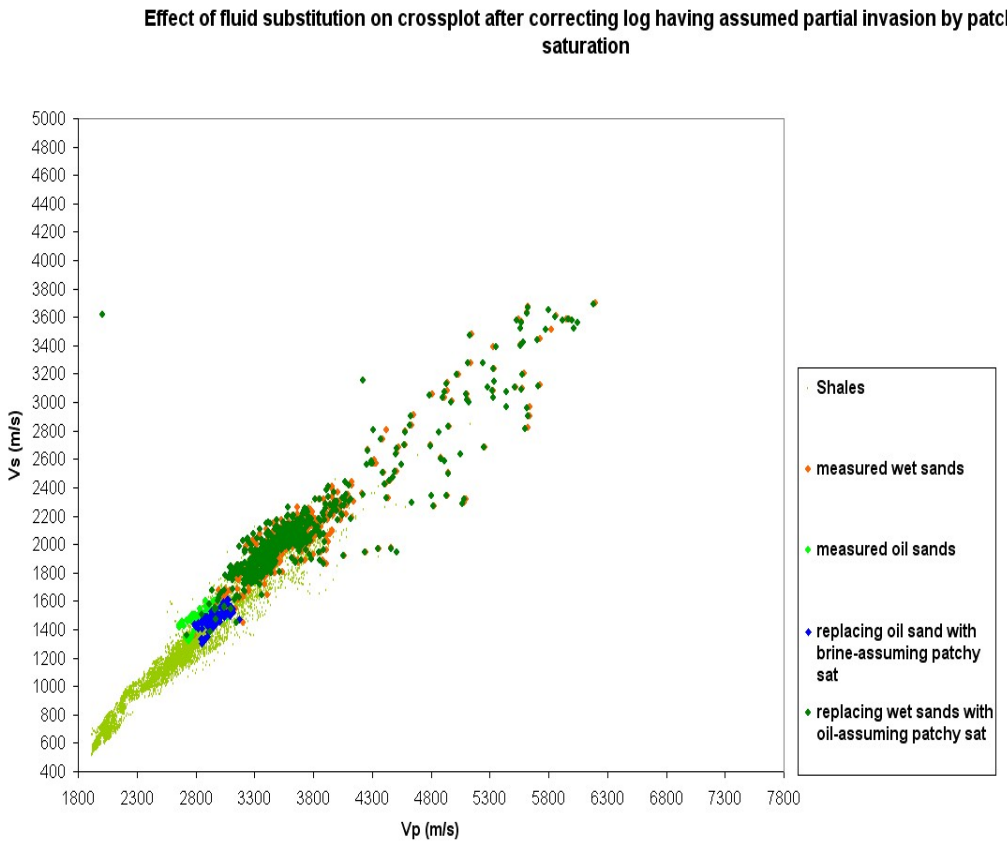

Figure 4.16: Crossplot of Vp and Vs, showing the result of fluid substitution, after correction assuming original log was partially invaded by patchy saturation

water sandstones, the Vp-Vs crossplot which we obtained is shown in Figure 4.20. From the plot, we see that, in the oil sands, the new water points move towards the shale line while the new oil points in the wet sands move away from the shale line. We also observe that there is still a bit of scatter in the data for the oil sandstones when we replace the wet sandstones with oil.

If we were to superpose Figures 4.19 and 4.20, we would notice that the original oil sandstones will align with the oil sand that have replaced the water sands from fluid substitution. Again, one cannot make a definite conclusion on the best possible shear wave model based on the crossplots.

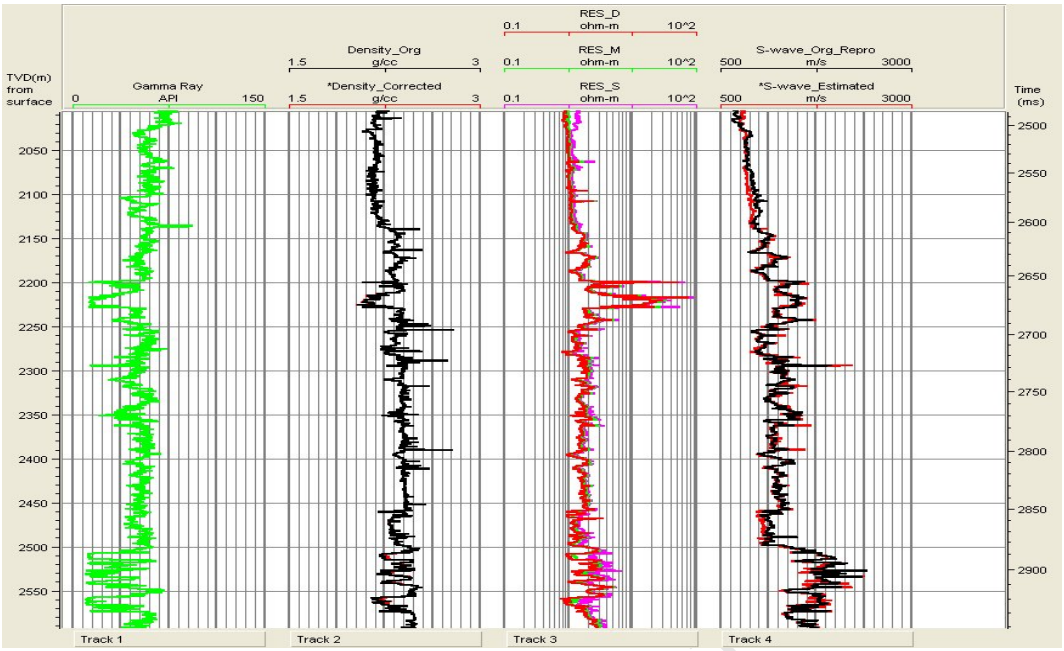

Figure 4.17: Suite of logs showing effect of correction on the shear wave log

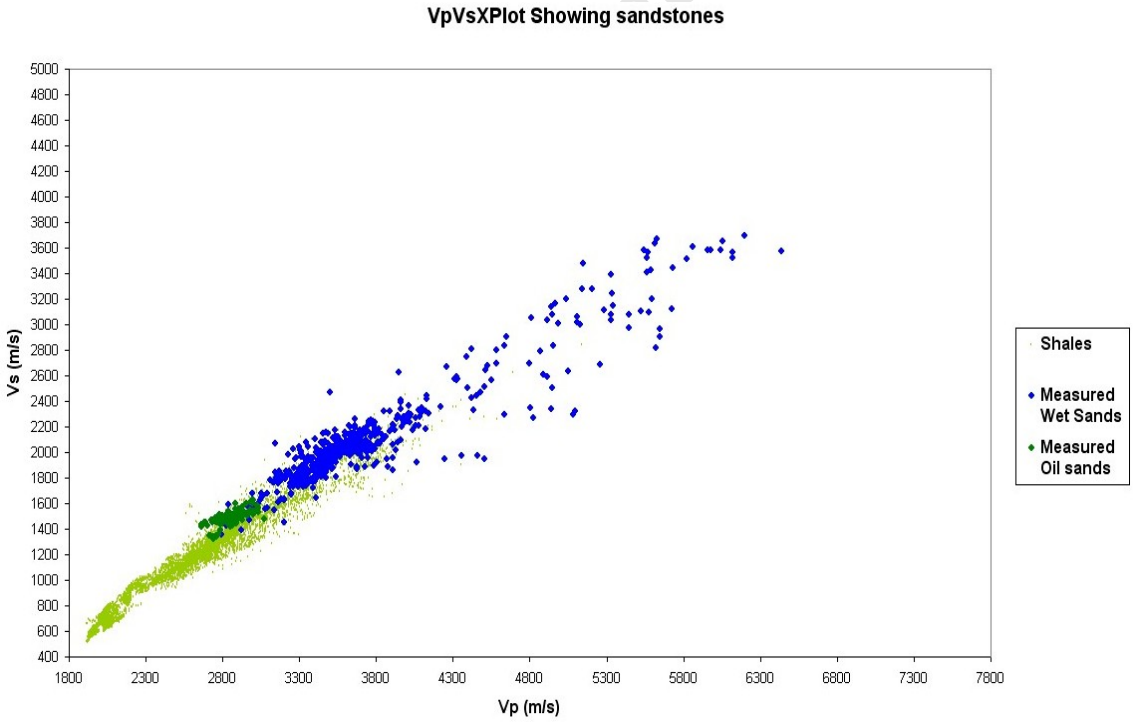

Figure 4.18: Original crossplot of Vp and Vs before correction - green(oil sands), blue(wet sands), lime(shales)

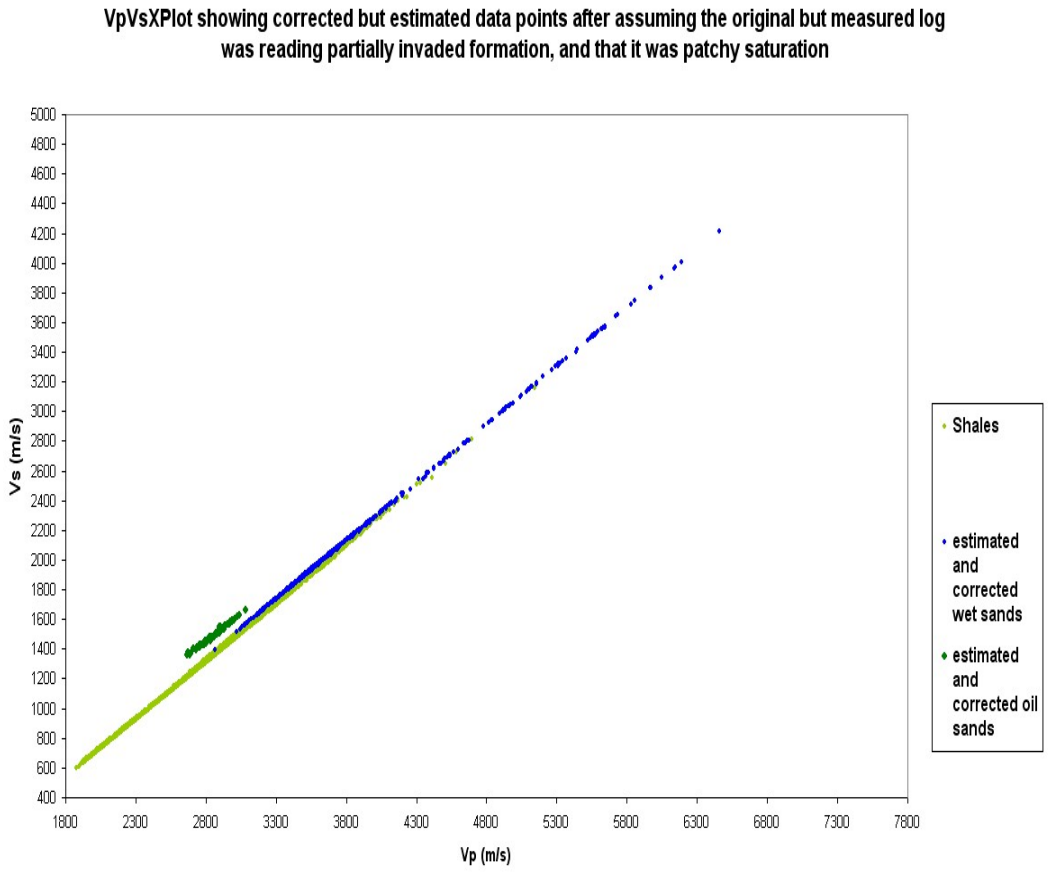

Figure 4.19: Crossplot of Vp and Vs after correction assuming original log was partially invaded by patchy saturation

4.6 Generating a synthetic seismic data for comparison with real data

The Vp and Vs of the subsurface layers determines the amplitude variation with offset (AVO) recorded in the pre-stack seismic data. It is for this reason that a shear log is required for a pre-stack seismic tie. The Vp log and Vs log, together with the density log and a time-depth log can be used to generate the synthetic seismic stacks and gathers with which the true data can be compared. Here we have assumed that the field data (processed seismic data) is the true representation of the subsurface.

In order to generate a synthetic seismogram, we need a software that can load in the P-wave

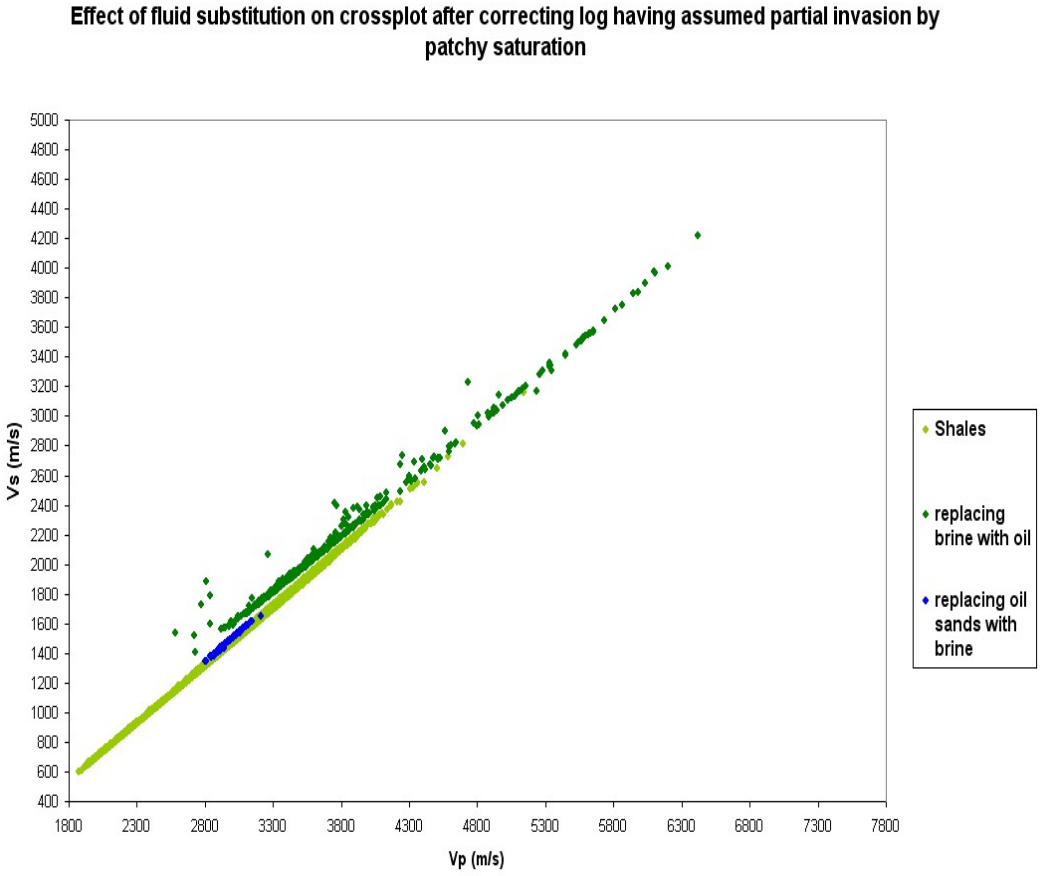

Figure 4.20: Crossplot of Vp and Vs, showing the result of fluid substitution, after correction assuming original log was partially invaded by patchy saturation

velocity, S-wave velocity and density. The software used for this, is the Hampson Russel Software (HRS). It incorporates the AVO modeling technique in describing the variations of the P-wave amplitude with offsets. Examples of two equations used by the software are the Zoeppritz equations and the Aki and Richards equation. A brief discussion of both method follows:

Zoeppritz equations relates the reflection and transmission coefficients for plane waves and elastic properties of a medium through which the waves propagate. The equations describe how the respective coefficients vary with the angle of incidence, offset and other rock parameters. Figure 4.21 shows how the incident wave is converted at the point of incidence, for non-normal incidence. The angles of incidence (α) and transmission (β) are related by Snell's law as follows

$$\eta = \frac{\sin\ \theta}{\sin\ \beta} = \frac{V_{P_1}}{V_{P_2}} \tag{4.35}$$

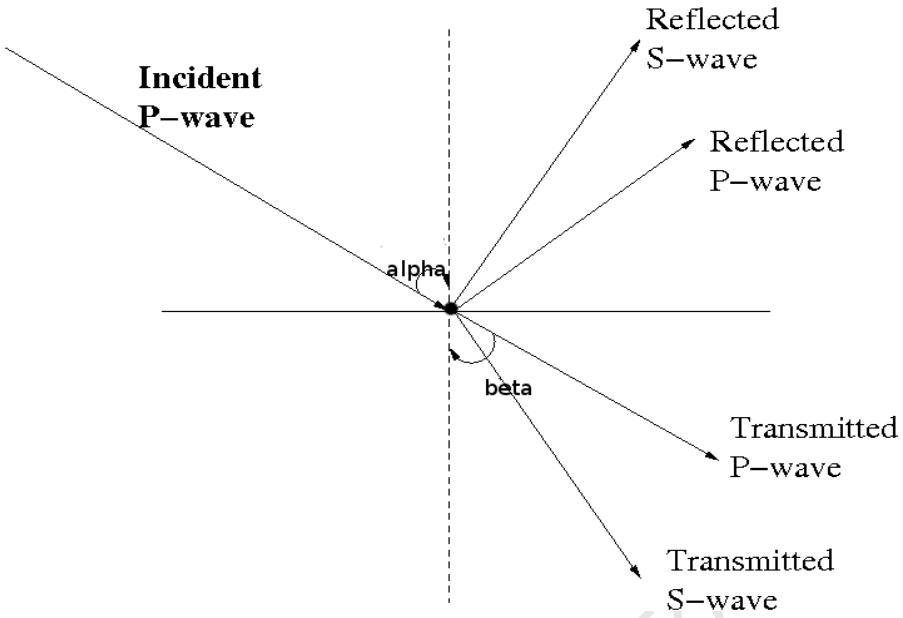

Figure 4.21: Conversion of Incident P-wave to Reflected and Transmitted waves at non-normal incidence (alpha $\rightarrow \theta$, beta $\rightarrow \beta$)

where η is the refractive index or the ray parameter. V_{P_1} and V_{P_2} are the P-wave velocities in the mediums. As a result of the nonlinearity in Zoeppritz equations, it has being subject to different modifications by different scientists.

Firstly, Shuey (1985) modified the equation and it became

$$R(\theta) \approx A + B \sin^2\theta \tag{4.36}$$

where A is called the AVO intercept attribute; B is the AVO gradient attribute. By definition,

$$A = \frac{1}{2}\left(\frac{\Delta V_p}{V_p} + \frac{\Delta\rho}{\rho}\right) \tag{4.37}$$

$$B = \left(-2\frac{V_s^2}{V_p}\frac{\Delta\rho}{\rho} + \frac{\Delta V_p}{2V_p} - 4\frac{V_s^2}{V_p^2}\frac{\Delta V_s}{V_s}\right) \tag{4.38}$$

where $V_p = \frac{V_{P_1} + V_{P_2}}{2}$; $V_s = \frac{V_{S_1} + V_{S_2}}{2}$; $\rho = \frac{\rho_1 + \rho_2}{2}$; $\Delta V_p = V_{P_2} - V_{P_1}$; $\Delta V_s = V_{S_2} - V_{S_1}$; $\Delta\rho = \rho_2 - \rho_1$

Aki and Richards (1980) also proposed an approximation to the Zoeppritz equation, which is given by

$$R(\theta) = R_0 + A\sin^2\theta + B\sin^2\theta\tan^2\theta \tag{4.39}$$

with $R_0 = \frac{1}{2}\left(\frac{\Delta V_p}{V_p} + \frac{\Delta \rho}{\rho}\right)$; $A = \frac{1}{2}\left(\frac{\Delta V_p}{V_p} - \psi\frac{\Delta \rho}{\rho} - 2\psi\frac{\Delta V_s}{V_s}\right)$; $\psi = 4\left(\frac{V_p}{V_s}\right)^2$; $B = \frac{1}{2}\left(\frac{\Delta V_p}{V_p}\right)$

An algorithm of how the synthetic gathers was created using the HRS is summarized below

1. Firstly, the corrected density, P-wave and S-wave logs (both estimated and measured) are loaded into a well database. Others such as the gamma log, and resistivity log are also loaded.

2. Next, the check shot data (which was provided) is also loaded, and the logs are displayed

3. The next step is the loading of the pre-stack seismic data as a 3D volume, entering the appropriate coordinates, and displaying the SEGY volume in the AVO modeling window. A portion of the pre-stack seismic data (having the original P-wave inserted) is shown in Figure 4.22.

4. A wavelet with specific parameters is extracted from the seismic data, a CDP stack is formed and a super gather is also formed from the seismic data. The wavelet is shown in Figure 4.23 while the amplitude spectrum of the wavelet is shown in Figure 4.24. The specific parameters used in extracting the wavelet were chosen based on the quality of the prestack seismic data. A look at the data shows that above offset of about 4000m, there is a lot of post critical events. Also the seismic data had only one inline (at 2633) and crosslines ranging from 4056 to 4101. Therefore, the wavelet was extracted from offset 225 to 3500m and from a time window of 1000ms to 4000ms, which is the interval over which the well is located. The number of traces used for the wavelet extraction is 220, and the software showed that the wavelet had a zero degree phase rotation, a constant phase, a wavelength of 100ms, and peak frequency of 35Hz.

5. Check shot corrections are applied to the sonic log to create a sonic log on a time scale

6. Using the Zoeppritz model, synthetics are created for all models which includes all the fluid cases modeled from fluid substitution. The modeling was done from the top to the bottom of the well.

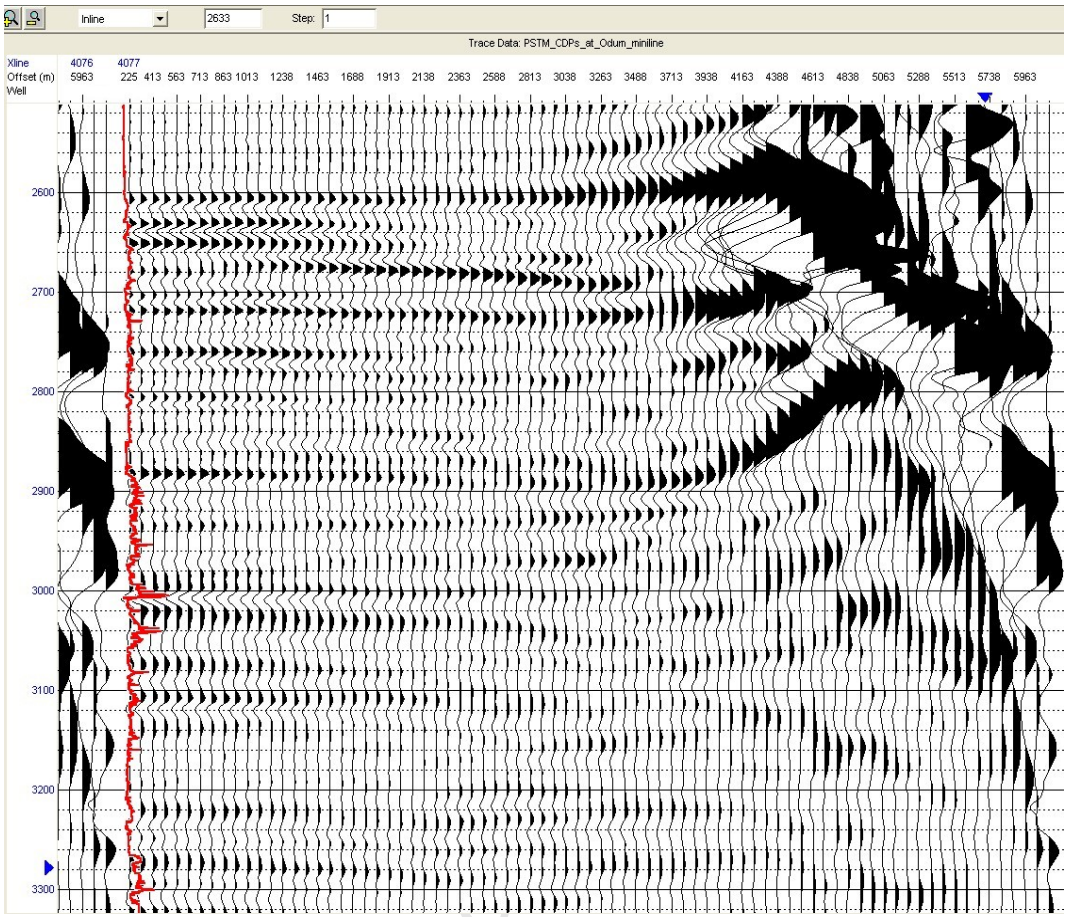

Figure 4.22: Pre-stack seismic data showing CDPs from 225 to about 6000

4.7 Model to model comparison using AVO modeling technique

The AVO modeling is done on both models, namely the estimated shear wave model and the measured shear wave model. The synthetic gathers of both models were compared. The synthetics created for the models are then compared with each other, and with the original seismic data.

For the estimated shear wave model, having assumed partial invasion by patchy saturation, synthetic gathers were created for different fluid saturation cases. Another synthetic gather was also created for the in situ case. i.e. the real case where oil is in oil sandstones and brine in wet sandstones. This was the final corrected log from the estimated model having assumed

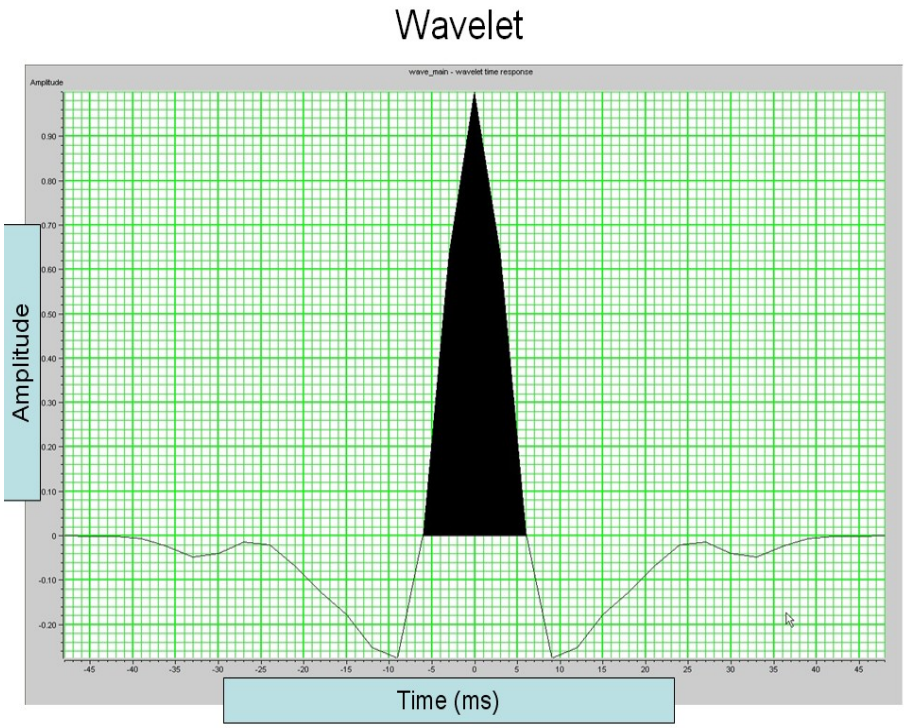

Figure 4.23: Wavelet extracted from seismic data

the measured density and sonic logs were reading a partially invaded formation, and that the saturation was patchy.

The AVO modelling (creating of synthetics) of the measured shear wave model was also done, and it followed the same process that was done with the estimated model. The only difference between them is that, instead of using the estimated shear wave velocity, the corrected reprocessed shear wave velocity was used.

The modeling was done on the Hampson Russel Software and the results are displayed in the next chapter.

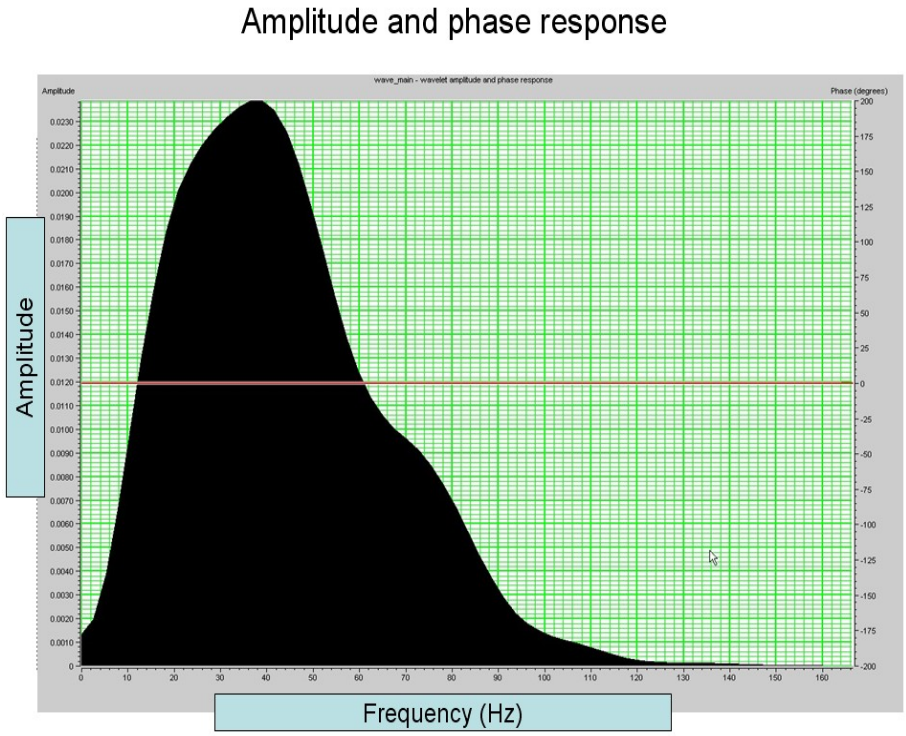

Figure 4.24: Amplitude spectrum of wavelet

5. Results and Conclusion

5.1 In Situ synthetics, Whole well - gather and stack

The first gather which is shown in Figure 5.1 is the super gather obtained from the real seismic data. The figure shows the gather and the stack from the real field data. The gamma ray log has been inserted and it shows the three different sand zones which have been labeled as the pay zone which is the target zone, wet zone and deep sands. From the gather and stack, we can see that the target zone is approximately between 2650 and 2700ms which corresponds to a borehole depth of between 2200 and 2280m. This is a zone of low gamma value and high quality sandstones. It is also a very shallow reservoir.

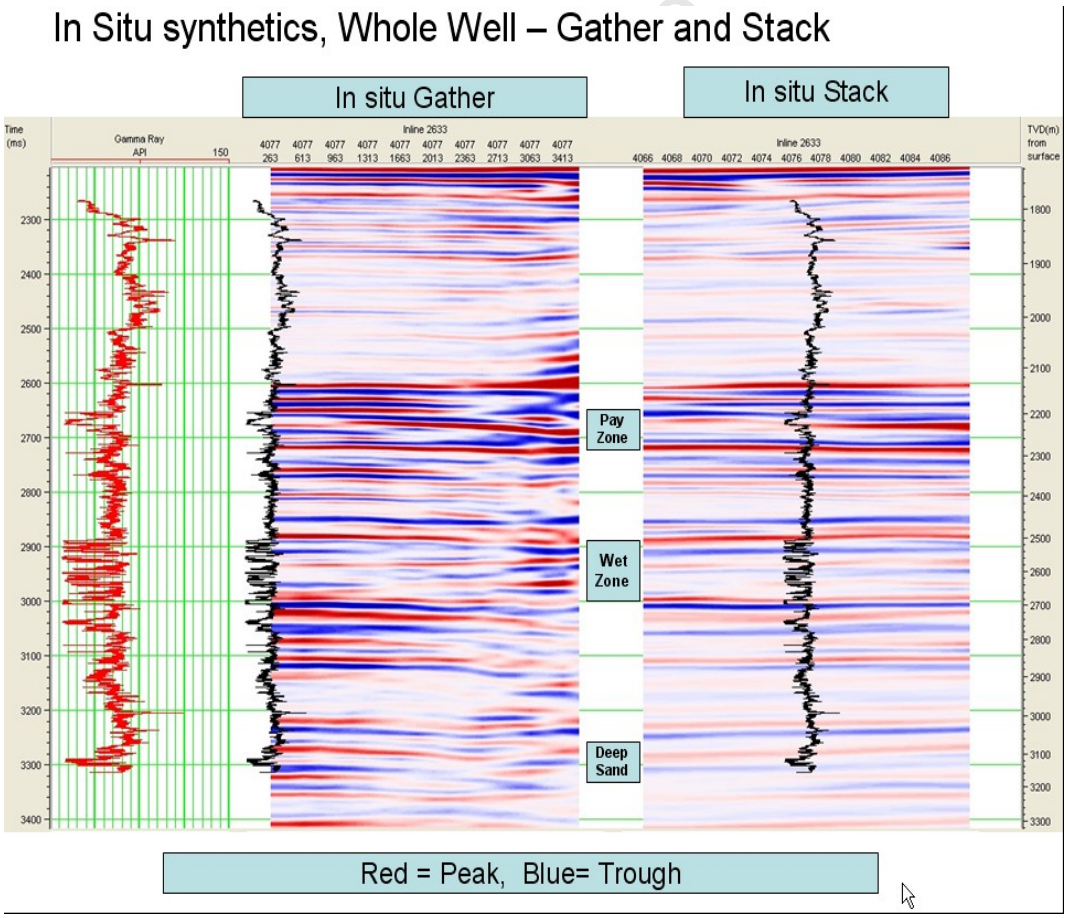

Figure 5.1: Real data as stack and gathers

5.2 Comparison of synthetics

After creating the respective synthetics as described in the latter part of the previous chapter, they were placed side by side with the real data for comparison. Here, we safely assume the real data is the true representation of the subsurface. The comparison was done between the measured and estimated models. The synthetics showing the modeled fluid substitution cases are also compared to understand the AVO behaviour of the effect of oil and gas in a water bearing sandstone as well as the AVO effect of having water or brine in an oil bearing sandstone. The synthetic gathers showing the corrected logs are then displayed for both the estimated and measured models , starting with the measured shear wave model. Thereafter, the measured model is compared with the estimated model, in order to find the best fit to the real data.

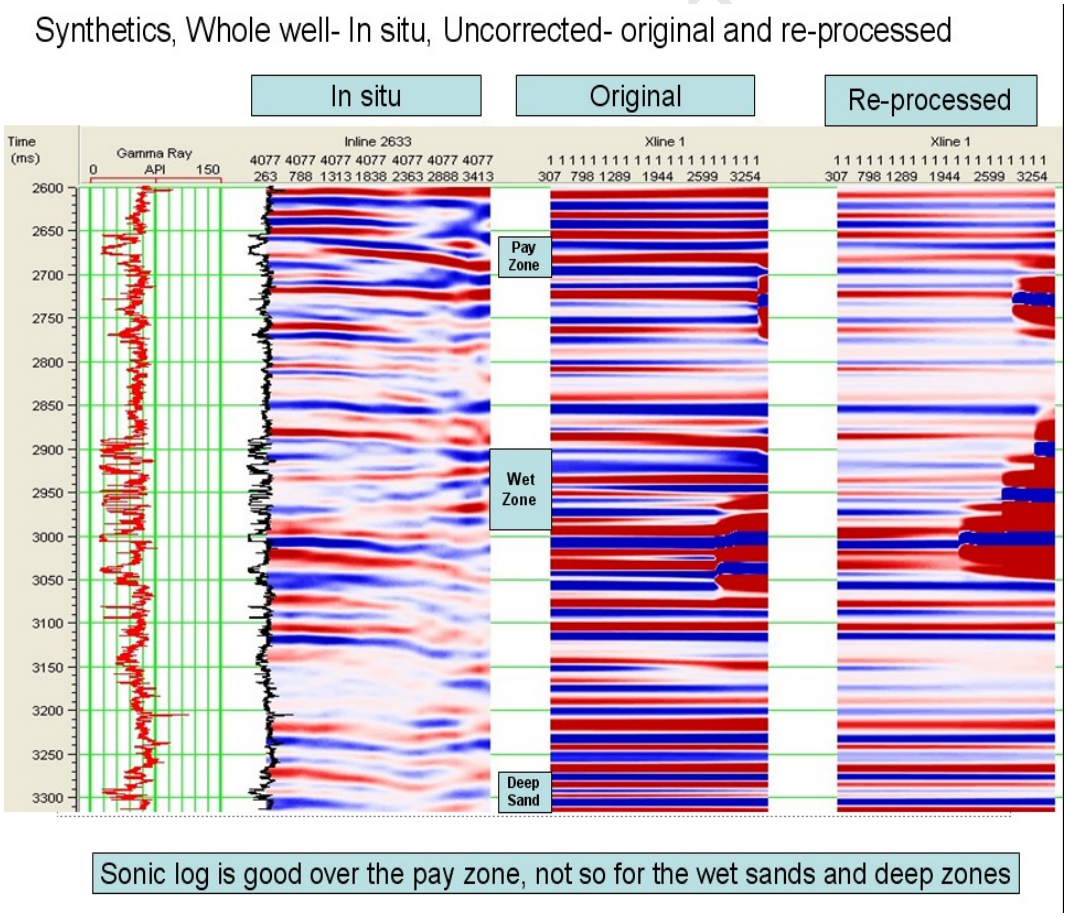

Figure 5.2: Synthetics, Whole well - In situ, uncorrected- original and re-processed logs

Figure 5.2 shows what the synthetic data look like when they are created using the Zoeppritz

equations, it actually shows the synthetics created from the original sonic logs which had missing data and cycle skips, and the reprocessed sonic log (not corrected for invasion) which accounts for the missing data. The gamma ray log has been inserted on the real data which is the In Situ gather.

From the display, we can see that the original sonic log was fairly good over the pay zone or reservoir zone, although there is no noticeable change in the amplitude variation with offset. The reprocessed log clearly shows this expected AVO anomaly in the pay zone and also in some parts of the wet zone. None of the synthetics seem to match with the in situ gather obviously because they have not been corrected for invasion. Also, we notice the post critical event taking place in the synthetics but not very obvious in the real data. This is due to the spikes noticed on the reprocessed logs which affected the P-wave log. This event or anomaly was observed in all the synthetics which were generated in both the estimated and measured models. Efforts were made during the synthetic data generation, to eliminate or reduce the post-critical reflections for the purpose of making useful comparisons with the real gather.

5.2.1 Comparing measured model based on fluid cases

Figure 5.3 shows a comparison of the AVO effect of having either brine or oil or gas in the sandstones, if we were working with the measured shear wave log. It shows the synthetics obtained from fluid substitution, having assumed that the measured sonic log was reading a partially invaded formation and that the saturation especially in the water sandstones was patchy. From the display, we can see that, in the pay zone, the wet case shows slight or no AVO anomaly and yields a weak peak, whereas the oil case gives slight AVO anomaly and shows a brightening trough with offset. The gas case gives the strongest AVO anomaly with a brightening trough with offset. This behaviour is expected as one moves from water to oil to gas. This same AVO behaviour is also noticed in some parts of the wet sandstones and deep sandstones.

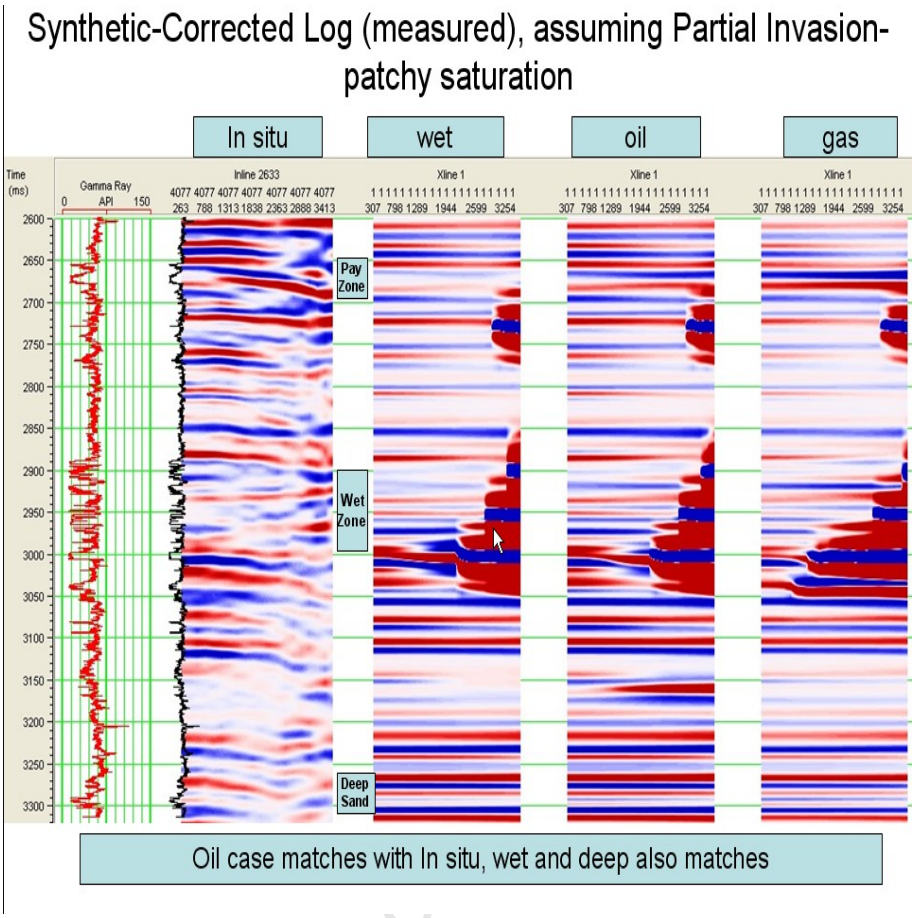

Figure 5.3: Synthetics from corrected logs from the measured sonic data - All fluid cases assuming Partial Invasion : patchy saturation

5.2.2 Comparing estimated model based on fluid cases

Figure 5.4 shows a comparison of the AVO effect of having either brine or oil or gas in the sandstones, assuming we were working with the estimated shear wave log. It shows the synthetics obtained from fluid substitution in the respective sandstones, having assumed that the original sonic log (P-wave) was reading a partially invaded formation and that the saturation especially in the water sandstones was patchy. From the display, we can see that, in the pay zone, the wet case shows little or no AVO anomaly and yields a weak peak, whereas the oil case gives slight AVO anomaly and shows a brightening trough with offset. The gas case gives the strongest AVO anomaly with a brightening trough with offset. This behaviour is expected as one moves from water to oil to gas. This same AVO behaviour is also noticed in some parts of the wet sandstones

and deep sandstones. Another thing we notice from the display is that the oil case appears to match more with the real data especially in the pay zone while the wet case matches more with the In situ gather in the wet sandstones.

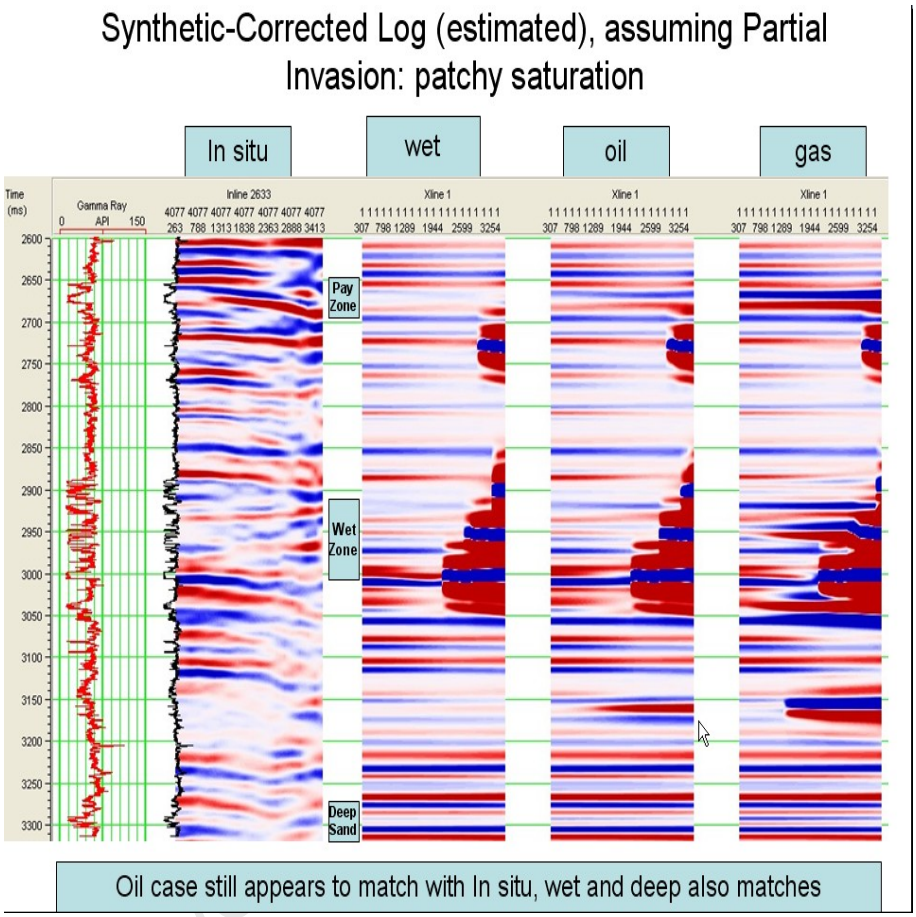

Figure 5.4: Synthetics from corrected logs from the estimated sonic data - All fluid cases assuming Partial Invasion : patchy saturation

5.2.3 Comparing measured and estimated model

Having modeled and analysed the estimated and measured models individually, we now bring them side by side and compare them with the real data. Figure 5.5 shows the comparison of both models. At this point, a final conclusion on the best type of model would be reached. Observing Figure 5.5 clearly, in the pay zone, it is very obvious that the AVO shown by the measured model is more than that of the estimated model, and it is safe to conclude that the measured model

fits well with the real data. Also, looking at the time 2850ms, we observe a slight decrease in the intensity of the trough in the estimated model. This does not seem to be the case in the real data. At this point, it is also safe to choose the measured model over the estimated model. Finally, around a time of 3000 to 3050ms, while the brightness of the peak decreases rapidly in the estimated model, it last for a while in the measured model which is almost exactly what we can see from the real data. Therefore, based on the aforementioned points, one can finally conclude that the measured shear wave model gives the best fit to the real seismic data.

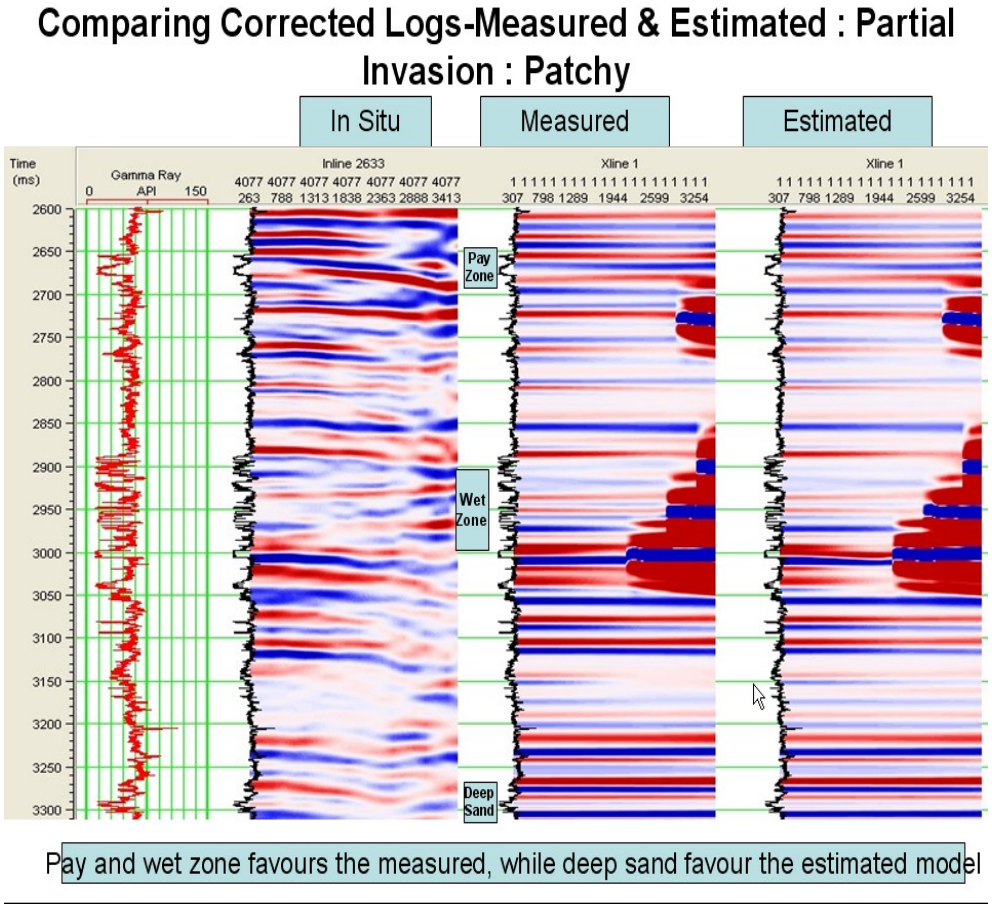

Figure 5.5: Comparison based on Partial Invasion : Patchy saturation

Having chosen and accepted the measured shear wave model as the best possible model, I decided to use the Aki and Richard's method to generate another synthetic in order to observe the difference between Zoeppritz method and that of Aki and Richards. The results are shown in Figures 5.6 and 5.7.

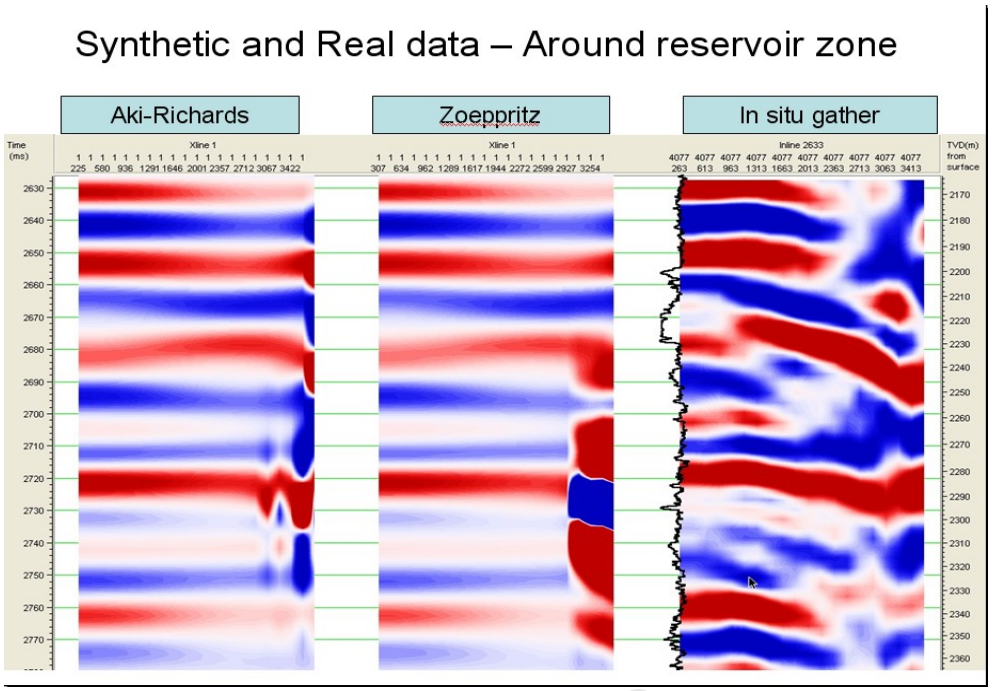

Figure 5.6: Synthetic model around the reservoir zone

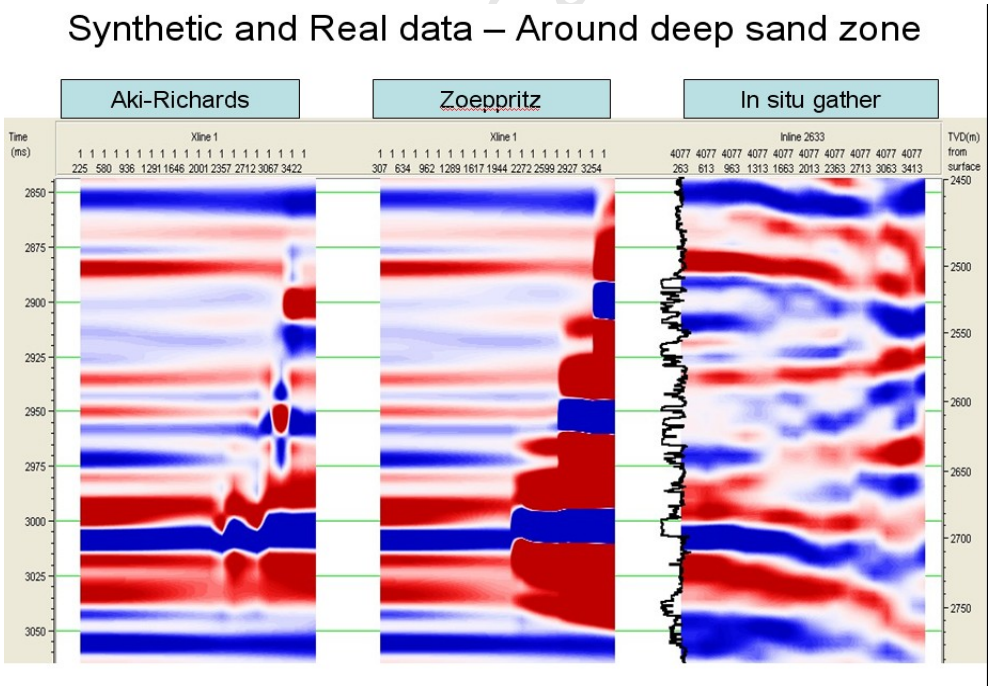

Figure 5.7: Synthetic model around the deep sand zone

5.3 Conclusions

By employing the Aki and Richard's model in the Hampson Russell Software, the effect of the post critical event noticed in the synthetic is reduced and hardly noticeable. The reason for this was given by Simmons and Backus in their paper titled "AVO modeling and the locally converted shear wave", which has been discussed in the literature review.

In conclusion, we have understood how a well is logged, the making of logs and the advantages of logging a well. We have also shown the factors that affect a log run and the logging environment; the possible types of logs that could be run have also been discussed with special emphasis on the sonic and density logs which form the core of this study.

We have also highlighted some significant research that has been carried out on logs in general and especially shear wave logs in particular. Empirical relations used for finding an unknown parameter given others, were also discussed in a bid to understand how for instance, shear wave velocities can be obtained from compressional wave velocities. Gassmann's relations and its application in fluid substitution was also introduced and we have seen that it is a very useful and important tool especially when one wants to perform AVO modeling of sands saturated with different fluids.

The principle of sonic log acquisition, and the tool used for it has also been discussed, coupled with the mode in which the log is processed. Interpretation of sonic logs as well as the seismic applications of the log rounded off the section under which this was explained.

On the shear wave velocity, we have also seen that, if regional shear wave information is not available, there are global relations e.g. Greenberg-Castagna that can possibly be used to generate a shear wave log. However, we have seen that the estimated shear wave velocity based on some of the global predictions may in most case, not show the expected AVO response during AVO modeling. This is why it is advisable to work with a locally calibrated or estimated shear wave velocity.

In this study, we have also seen that the resistivity log is a very important log that must be available when one wants to correct a log for invasion and it is very important that one knows

the type of drilling fluid that was used - water or oil. This is because the way one corrects a log for oil based mud invasion is different if the invasion was by water based mud. (Walls and Carr, 2001)

Based on the results of the synthetics produced as shown in the previous section, the following are some other general conclusions which may be deduced

- The measured P-wave velocity and density data used in this study are generally good
- The reprocessed S-wave is also good and may be used for modeling and interpretation
- The estimated S-wave may not be the best in any case of invasion (oil-based mud or water-based mud), although it could be used if the quality of the P-wave is very high especially in the case of water based mud invasion
- Fluid substitution shows good separation between fluid phases in the synthetic gathers

The work presented in this study has shown that a better model is the **Measured** model, and based on comparison and correction of the logs, we conclude that the logs were reading a *partially* invaded formation and the saturation in the wet sands is *patchy*. Therefore, the measured shear wave log should be used for interpretation and subsequent analysis that will be done on the study area for the purpose of improving the productivity of the field. The work flow which has been developed in this study can therefore be used for quantitative interpretation of a well log data especially sonic logs and also for a good interpretation of a seismic data.

Bibliography

L. Adam, M. Batzle, and I. Brevik. Gassmann fluid substitution and shear modulus variability in carbonates at laboratory seismic and ultrasonic frequencies. *Geophysics*, 71(6):1–11, November - December 2006.

K. Aki and P. Richards. *Quantitative seismology: Theory and Methods*. W.H Freeman and Co., San Francisco, 1980.

G. Archie. The electrical resistivity log as an aid in determining some reservoir characteristics. *Petroleum Transactions, AIME*, 146:54–62, 1942.

V. Avadhani, M. Anandan, B. Thattacherry, K. Murthy, B. Gariya, and A. Dwivedi. Acoustic impedance as a lithological and hydrocarbon indicator - a case study from the cauvery basin. *The Leading Edge*, 25(7):854–858, July 2006.

J. G. Berryman. Elastic wave propagation in fluid-saturated porous media. *Journal of the Acoustical Society of America*, 70(6):416–424, December 1981.

M. A. Biot. Theory of propagation of elastic waves in a fluid saturated porous solid. I. Low frequency range and ii. Higher-frequency range. *Journal of the Acoustical Society of America*, 28:168–191, 1956.

J. Blangy. *Integrated seismic lithologic interpretation : The petrophysical basis*. PhD thesis, Stanford University, 1992.

M. Brownfield and R. Charpentier. Geology and total petroleum systems of the Gulf of Guinea province of west Africa. Technical Report 32, U.S Geological Survey Bulletin 2207-C, 2006.

M. B. Carr, M. Ascanio, M. Smith, and J. Walls. The use of fluid substitution modelling for correction of oil based mud filtrate invasion in sandstone reservoirs. 2004.

J. Castagna, M. Batzle, and R. Eastwood. Relationships between compressional-wave and shear wave velocities in clastic silicate rocks. *Geophysics*, 50:571–581, 1985.

J. P. Castagna, M. Batzle, and T. K. Kan. Rock physics - The link between rock properties and AVO response. In J. P. Castagna and M. M. Backus, editors, *Offset-Dependent Reflectivity - Theory and Practice of AVO Analysis*, volume 8 of *Investigation in Geophysics*, pages 135–171. Society of Exploration Geophysicists, 1993.

L. Chabot, D. C. Henley, and R. J. Brown. Single-well imaging using the full waveform of an acoustic sonic. *CREWES Research Report*, 12, 2000.

A. Chaveste. Risk reduction in estimation of petrophysical properties from seismic data through well-log modeling, seismic modeling, and rock properties estimation. *The Leading Edge*, 22 (5):406–418, May 2003.

P. Chopra, E. Papp, and D. Gibson. Geophysical well logging. Technical report, CRCLEME, 2002.

R. A. Ensley. Analysis of compressional- and shear wave seismic data from the prudhoe bay field. *The Leading Edge*, 8(11):10–13, November 1989.

T. E. Ewing. Synthetic seismograms: Preparation, calibration, and associated issues. *Search and Discovery Article*, (40019), 2001.

J. Garat, M. Krief, J. Stellingwerf, and J. Ventre. A petrophysical interpretation using the velocities of P and S waves (full-waveform sonic). *Journal of the Acoustical Society of America*, 31(6):355–369, November 1990.

G. Gardner, L. Gardner, and A. Gregory. Formation velocity and density - the diagnostic basics for stratigraphic traps. *Geophysics*, 39:770–780, 1974.

F. Gassmann. Über die elastizität poroser medien: Veirteljahrsschrift der naturforschenden gesellschaft in zurich. 96:1–23, 1951.

J. Geertsma. Velocity-log interpretation: The effect of rock bulk compressibility. *Society of Petroleum Engineers Journal*, 1(4):235–248, December 1961.

P. Glover. Sonic (acoustic) log. *Petrophysics MSc Course Notes*, pages 172–197, 2008.

M. L. Greenberg and J. P. Castagna. Shear-wave estimation in porous rocks : Theoretical formulation, preliminary verification and applications. *Geophysical Prospecting*, 40:195–209, 1992.

D. Han, A. Nur, and D. Morgan. Effects of porosity and clay content on wave velocities in sandstones. *Geophysics*, 51(11):2093–2107, November 1986.

D.-H. Han. *Effects of Porosity and Clay Content on Acoustic Properties of Sandstones and Unconsolidated Sediments*. PhD thesis, Stanford University, 1986.

D. W. Hilchie. *Advanced Well Log Interpretation*. Douglas W. Hilchie, Inc. Golden Colorado, 1982.

D. L. Johnson. Theory of frequency dependent acoustics in patchy-saturated porous media. *Journal of the Acoustical Society of America*, 110(2):682–694, August 2001.

ldeo.columbia.edu. Sonic. http://www.ldeo.columbia.edu/BRG/ODP/LOGGING/TOOLS/sonic.html, May 2010.

G. Mavko, C. Chan, and T. Mukerji. Fluid substitution : Estimating changes in Vp without knowing Vs. *Geophysics*, 60(6):1750–1755, 1995.

G. Mavko, T. Mukerji, and J. Dvorkin. *THE ROCK PHYSICS HANDBOOK, Tools for seismic analysis in porous media*. Cambridge University Press, 2003.

C. P. Oden, J. J. LoCoco, and P. L. Staples. Sonic logging case histories using advanced equipment and data processing techniques. *Society of Professional Well Log Analysts, Minerals and Geotechnical Logging Society Chapter-at-Large, 8th International Symposium on Borehole Geophysics Proceedings CD-ROM*, (paper 13):1–14, 2002.

F. Oghenekohwo. A Comparison of Resistivity and Electromagnetics as Geophysical Techniques. AIMS PGD thesis, 2008.

A. Poupon and J. Leveaux. Evaluation of water saturations in shaley formations. *Trans. Soc. Prof. Well Log Analysts*, 12 Annual Logging Symposium:Paper O, 1971.

L. Raymer, E. Hunt, and J. Gardner. An improved sonic transit time-to-porosity transform. *Trans. Soc. Prof. Well Log Analysts*, 21st Annual Logging Symposium:Paper P, 1980.

J. M. Reilly. Wireline shear and AVO modeling: Application to AVO investigations of the Tertiary, U.K. Central North Sea. *Geophysics*, 59(8):1249–1260, August 1994.

M. Rider. *The Geological Interpretation of Well Logs*. Whittles Publishing, second edition, 2000.

R. Shuey. A simplification of the Zoeppritz equations. *Geophysics*, 50:609–614, 1985.

P. Simandoux. Dielectric measurements on porous media: Application to the measurement of water saturations: Study of the behaviour of argillaceous formations. *Revue de l'Institut Francais du Petrole*, 18:193–215, 1963.

J. Simmons and M. M. Backus. AVO modeling and the locally converted shear wave. *Geophysics*, 59(9):1237–1248, August 1994.

slb.com. DSI Dipole Shear Sonic Imager. http://www.slb.com/services/evaluation/wireline_open_hole/petrophysics/acoustic_wireline_tools/dipole_shear_sonic_imager.aspx, May 2010.

G. Smith and P. Gidlow. Weighted stacking for rock property estimation and detection of gas. *Geophysics*, 35(9):993–1014, 1987.

spwla.org. library info glossary reference. http://www.spwla.org/library_info/glossary/reference/glossp/glossp.htm, May 2010.

U. S. G. Survey. Introduction to borehole geophysics. http://ny.water.usgs.gov/projects/bgag/intro.text.html, .

T. Todorov, D. Hampson, and B. Russell. Sonic log predictions using seismic attributes. *CREWES Research Report - Volume 9*, 1997.

T. R. Tönsing. Using rock physics to determine uncertainties in pore-fluid and lithology-estimates from seismic attributes in the Bredasdorp basin, offshore South Africa. Master's thesis, University of Cape Town, January 2006.

C. Tosaya and A. Nur. Effects of diagenesis and clays on compressional velocities in rocks. *Geophys. Res. Lett.*, 9:5–8, 1982.

M. Turner. Near-surface velocity reconstruction using surface wave inversion. Master's thesis, University of Utah, May 1990.

G. Vasquez, L. Dillon, C. Varella, G. Neto, R. Velloso, and C. Nunes. Elastic log editing and alternative invasion correction methods. *The Leading Edge*, 23(1):20–25, 2004.

J. Walls and M. B. Carr. *The use of fluid substitution modeling for correction of mud filtrate invasion in sandstone reservoirs*. 71st Annual Meeting of Society of Economic Geophysicists, San Antonio, Texas, United States, September 2001.

W. well logging. Well logging. http://en.wikipedia.org/wiki/Well_logging, .

M. Wyllie. *The Fundamentals of Well Log Interpretation*. Academic Press Inc. (London) Ltd., third edition, 1963.

M. Wyllie, A. Gregory, and L. Gardner. Elastic wave velocities in heterogeneous and porous media. *Geophysics*, 21:41–70, 1956.

M. Wyllie, A. Gregory, and L. Gardner. An experimental investigation of factors affecting elastic wave velocities in porous media. *Geophysics*, 23:459–493, 1958.

M. Wyllie, G. Gardner, and A. Gregory. Studies of elastic wave attenuation in porous media. *Geophysics*, 27:569–589, 1963.

J. Xia, R. D. Miller, and C. B. Park. Estimation of near-surface shear-wave velocity by inversion of rayleigh waves. *Geophysics*, 64(3):691–700, May-June 1999.

S. Younis. Well log (the bore hole image). URL http://www.worldofteaching.com. http://www.worldofteaching.com.

M. Zahid. Little about basic petrophysics. *Specialization in Petrophysics, University of Azad Jammu and Kashmir, Muzaffarabad.*, 2008.